PhD THESIS

ABSORPTION AND LOCALIZATION OF LIGHT IN AMORPHOUS SEMICONDUCTOR THIN FILMS AND MULTILAYERS

by

ANTONIS KONDILIS

PHYSICS DEPARTMENT

UNIVERSITY OF CRETE

June, 1993

ΠΡΟΛΟΓΟΣ

Η διδακτορικη μου διατριβη αρχισε τον Σεπτεμβριο του 1987 και εκπονηθηκε εξ ολοκληρου στο πανεπιστημιο κρητης με επιβλεποντα καθηγητη τον κ. Παναγιωτη Τζανετακη.
Η πολυχρονη πειρα του και η εμβαθυνοη του στα θεματα της Φυσικης, σταθηκαν σημαντικοι καθοδηγητες στην αναπτυξη και ολοκληρωοη του δυσκολου εργου της διατριβης μου. Η βοηθεια του απο επιστημονικη αποψη και η ηθικη του υποστηριξη υπηρξαν ανεκτιμητες. Αισθανομαι βαθια ευγνωμοσυνη και τον ευχαριστω μεσα απο την καρδια μου.

Ο κ. Ε. Οικονομου αφιερωσε πολυ χρονο στην διεξοδικη συζητηοη των περισσοτερων απο τα θεματα στα οποια αναφερεται η διατριβη αυτη. Η εμπειρια του και η καθοδηγηοη που μου εδωσε, κυριως στο θεμα του εντοπισμου, ηταν πραγματικα πολυτιμες. Θελω να εκφρασω την ειλικρινη ευγνωμοσυνη μου για την βοηθεια του αυτη.

Ευχαριστω επισης την διοικηοη του Ι.Τ.Ε που με τη χορηγηοη υποτροφιας , μου εδωσε τη δυνατοτητα να εκπονησω τη διατριβη μου.

Ευχαριστω ιδιαιτερως τον Αργυρη Κασσιωτακη καθως και τον Γιωργο Παπαδακη, που σχεδιασαν και κατασκευασαν τον κρυοστατη. Η αψογη λειτουργια του δειχνει το μερακι και το ταλεντο των ανθρωπων που τον κατασκευασαν. Σε διαφορες κατασκευες συνεβαλλαν ο Μιχαλης Βισκαδουρακης και ο Μιχαλης Σμυρνακης τους οποιους ευχαριστω επισης.

Ευχαριστω θερμα τον φιλο και συναδελφο Γιαννη Φραγκιαδακη που μου παραχωρησε τα evaporating δειγματα που μετρηθηκαν. Τα καλα του λογια και το ενδιαφερον του με στηριξαν ηθικα στις δυσκολιες.

Ευχαριστω θερμα την συναδελφο Μαρια Ανδρουλιδακη για την πολυτιμη βοηθεια που μου προσφερε, ιδιαιτερα στην αρχη της διατριβης μου καθως και για την επιμελεια μερους των σχηματων.

Ευχαριστω πολυ τον κυριο Hellmut Mell που μου παραχωρησε τα δειγματα glow-discharge.

Ευχαριστω τους καθηγητες μου Πετρο Δητσα και Στεφανο Τραχανα απο τους οποιους σαν φοιτητης πηρα ξεκαθαρες γνωσεις πανω σε θεματα ηλεκτροδυναμικης και κβαντομηχανικης, που σταθηκαν θεμελιο στη στηριξη της εργασιας μου.

Ευχαριστω τους κυριους Στεργιο Λογοθετιδη, Σπυρο Ευαγγελου και τον κ. Π. Κελιρη που δεχτηκαν να ειναι μελη της επιτροπης.

Ανεκτιμητη υπηρξε η βοηθεια και η κατανοηση της μελλουσας συζυγου μου Μαριας Καγιαμπακη, που μου συμπαρασταθηκε σε ολα τα χρονια της διατριβης μου και επιμεληθηκε την επεξεργασια του κειμενου στον υπολογιστη. Την ευχαριστω θερμοτατα.

Chapter 1

THE ABSORPTION EDGE OF a-SI:H AND ITS TEMPERATURE VARIATION DETERMINED BY REFLECTANCE AND TRANSMITTANCE MEASUREMENTS

1.1 Introduction

In the last two decades the physics of amorphous solids has been raised into a topic of great importance, having accomplished so far and promising further, technological applications.

Amorphous semiconductors can be deposited in the form of thin films on various substrates and find nowadays very important applications taking advantage of the possibility to cover large surface areas with semiconducting material that serves as the base for devices. Without any doubt, the most important and better studied amorphous semiconductor is Hydrogenated Amorphous Silicon (a-Si:H).

Despite the sophistication of the deposition methods used to obtain thin a-Si:H films, one can see that a great potential exists for lowering the production cost of this

material. Cost reduction is important in photovoltaic applications but a-Si:H finds other important applications as well, with chief among them, thin film transistors and xerographic drums.

The electronic structure of amorphous semiconductors is more complex to apprehend theoretically and more difficult to study experimentally than that of the crystalline ones. a-Si:H is characterized by an energy gap of approximately 1.7 eV . Knowledge of the nature and density of electronic states near and within the gap is of great importance for understanding complex phenomena of technological interest, as are the transport and the recombination of carriers.

Light is as important of a tool to study a-Si:H, as it is for all semiconductors. The photon energy range of prime interest is the absorption edge of a-Si:H that is broad and extends from approximately from 1.2 to more than 2 eV. This chapter focuses on this particular energy range and aims at the establishment of the temperature dependence of the absorption edge. The nature of the effects measured, detailed in the following, gives the conclusions of this study a validity that extends beyond the particular samples and eventually beyond the material studied, amorphous silicon.

Electronic structure of amorphous solids

The comprehension of the behavior of amorphous solids or glasses has been proved to be difficult as opposed to the well known properties of crystalline solids or crystals. The key-property of translational periodicity of a crystal structure (long range order), greatly simplifies the problem of solving Schodinger's equation and getting all information necessary to understand the behavior of the solid.

Following a way briefly described below, Bloch, Pierls and Wilson, have developed the band theory of electrons in crystals. The atomic nuclei along with the electrons

tightly bound to each one of them, are assumed to be fixed in position on the sites of the crystalline lattice. The loosely connected electrons (these electrons participate in the formation of the bonds between atoms), are treated as independent particles moving inside a potential $V(\vec{r})$ having the translational periodicity of the crystal structure. This potential is intented to account for the interaction of one-electron with all the other particles in the crystal. Thus the Hamiltonian operator H, includes in addition to the electronic kinetic energy term $\frac{\vec{p}^2}{2m} = -\frac{\hbar^2}{2m}\vec{\nabla}^2$,
a crystal potential term $V(\vec{r})$. Since V (and therefore H) is periodic in space having the periodicity of the crystal structure, it follows that the solutions (wave functions) $\Psi_{n\vec{k}}(\vec{r})$ of Schrodinger equation

$$H\Psi_{n\vec{k}}(\vec{r}) = E_{n\vec{k}}\Psi_{n\vec{k}}(\vec{r}) \tag{1.1}$$

are Bloch functions of the form : $\exp(i\vec{k}\cdot\vec{r})u_{n\vec{k}}(\vec{r})$. The function $u_{n\vec{k}}(\vec{r})$ is periodic with the same periodicity as $V(\vec{r})$. The quandum numbers characterizing each wave function $\Psi_{n\vec{k}}(\vec{r})$ are : the wave vector $\vec{k}$, an integer band index n and the energy eigenvalue $E_{n\vec{k}}$ or $E_n(\vec{k})$. The electrons are distributed among the wave functions according to Fermi-Dirac statistics. The functional form of the dependence of $E_n(\vec{k})$ upon the crystal momentum $\hbar\vec{k}$ for each band n specifies the electronic band structure of a crystalline solid. The band stucture provides us with valuable information about the metallic , insulating, or semiconducting behavior of the crystal.
The above picture breaks down in the case of glasses. The reason for this is, that in contrast to crystalline solids, $\vec{k}$ is not a good quantum number for glasses, since the latter lack the structural property of translational periodicity. $E_n(\vec{k})$ energy band diagrams have no meaning for electronic states in amorphous solids.

As opposed to energy band diagrams, density of states n(E), diagrams do have meaning for both crystals and glasses. Provided that each wave function corresponds to exactly one state (able to accommodate two electrons with opposite spins), n(E) is defined as the number of electronic states per unit energy per unit volume. The

fact that n(E) is a meaningful quantity for both crystals and glasses, enables us to compare the density of states of a crystal with that of a glass. Typical n(E) diagrams are illustrated in Fig.1. Graph (a) corresponds to a crystal and graph (b) to a glass. As can be seen in (a), a crystal exhibits energy bands composed of *extended* states separated by a hiatus where no states exist. The valence band is the last completely or nearly filled with electrons band. The conduction band is the next, higher in energy, band. The difference between the lowest energy value of the conduction band E_c and the highest of the valence band E_v, is called the *energy gap*, $E_g = E_c - E_v$, of the crystal.

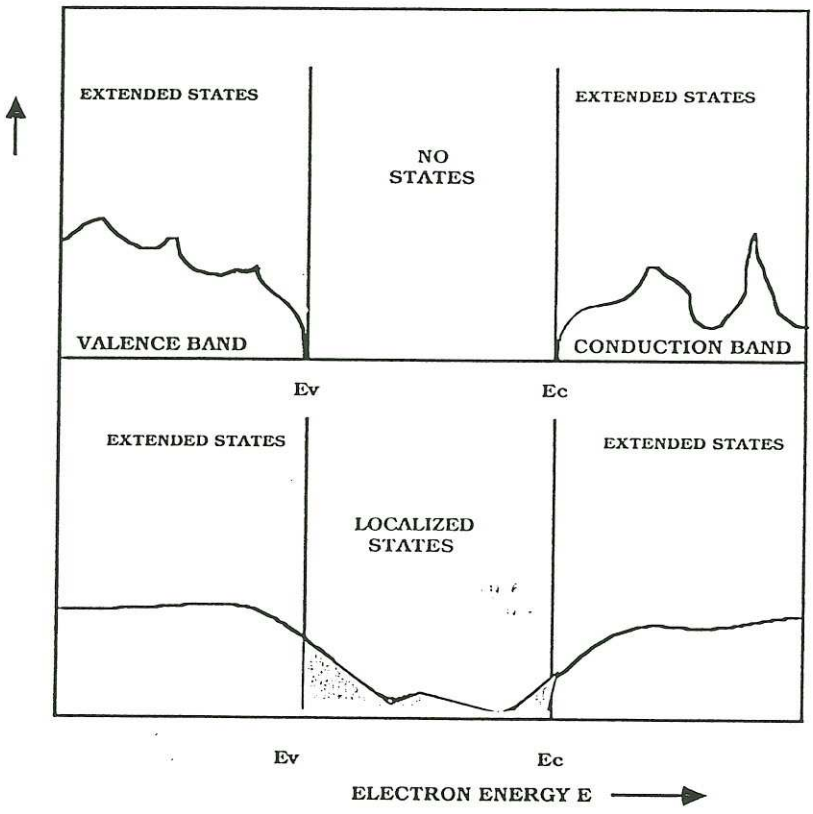

FIG.1. *Schematic density-of-states diagram for a crystalline and an amorphous semiconductor, in the vicinity of the highest occupied and lowest empty states. $\eta(E)dE$ is the number of electron states, per unit volume, with energies in the interval from E to E+dE.*

It is important to note that the creation of bands composed of extended states is not to be understood as a consequence of periodicity, but rather as the result of the overlapping orbitals among the atoms. Thus one expects bands of extended states to exist in the amorphous state also. The main difference between crystals and glasses appears in the region between bands. This is shown in graph (b) of Fig.1.
We first notice that the energy gap of the crystalline case disappears. Two high density energy bands composed of extended states , namely valence and conduction band, enclose a low density region (shaded area) composed of *localized* states. The demarcation energies separating localized and extended states are referred to as *mobility edges*. The region between mobility edges is called the *mobility gap*.
At this stage it is necessary to explain what is meant by the terms *extended/localized* states mentioned above. For this purpose Fig.2 is very helpful.

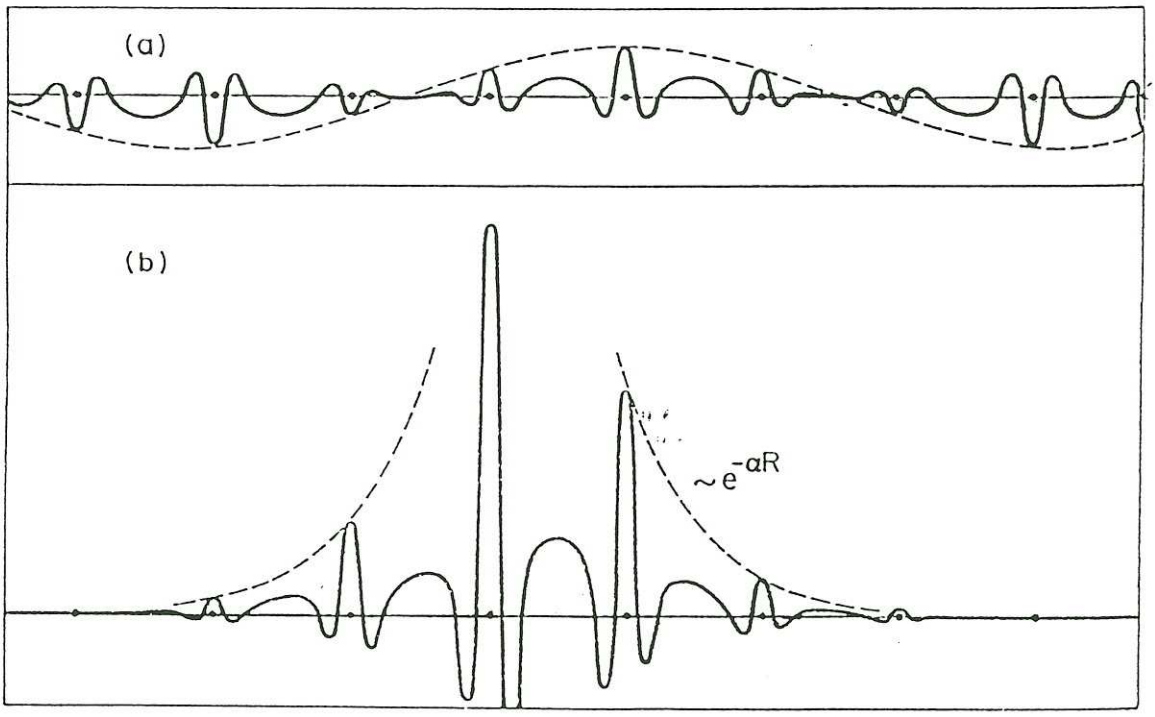

FIG. 2. *The distinction between extended and localized electron states. A Bloch-type extended-state wave function is illustrated in a; a localized-state wave function is illustrated in b.*

Graph (a) corresponds to an extended state. The wave function is spread throughout the solid. The amplitude of the envelope (dashed line) is sizeable everywhere. Graph (b) corresponds to a localized state. The wave function is concentrated near a center composed of just a few atoms and has negligible amplitude elsewhere in the solid. Away from a small region that contains essentially all of its integrated probability $\int |\Psi|^2 \, d\vec{r}$, the amplitude spatially decays *exponentially* with distance. This behavior is shown by the envelope (dashed line), which falls as $\exp(-\gamma R)$ at large distances R from the localization center. The inverse of γ is called the *localization lenght* of the state.

Semiconducting materials being intensively investigated so far, provide a lot of experimental evidence on the features illustrated in Fig.1. Interaction with light provides a powerful means for probing the properties of solids by measuring the absorption edge. Experimental and theoretical examination of the absorption edge of crystalline semiconductors, led to the distinction between two kinds of optical transitions occuring between valence and conduction band. They are termed *direct* and *indirect* transitions[1,2]. For the direct ones a photon of energy $h\nu$ and wave vector $\vec{k}_{photon}$ is absorbed by an electron in a state of energy E and crystal momentum $\vec{k}$. The electron is excited in a new state of energy $E' = E + h\nu$ and momentum $\vec{k}' = \vec{k} + \vec{k}_{photon} + \vec{G}$, where $\vec{G}$ is a reciprocal lattice vector. Since $|\vec{k}_{photon}|$ is very small compared to the linear dimensions of the Brillouin zone, it can be neglected and for the first Brillouin zone we obtain $\vec{k}' = \vec{k}$. For the indirect transitions momentum conservation is fulfilled by the participation of specific phonons. Then the energy of the transition is slightly modified by the characteristic energy of the emitted or absorbed phonon.

Many crystalline semiconductors exhibit direct optical transitions (e.g. c-GaAs). There is, however, an equally numerous class which exhibit indirect transitions (e.g. c-Si). For both transitions the sharp rise in the optical absorption at a characteristic

energy reflects the existence of an energy gap.

The absorption coefficient of amorphous semiconductors

In the case of an amorphous semiconductor the existence of a low density of states region instead of a gap, results in the creation of a broad absorption edge as compared to the sharp edge in crystalline semiconductors.

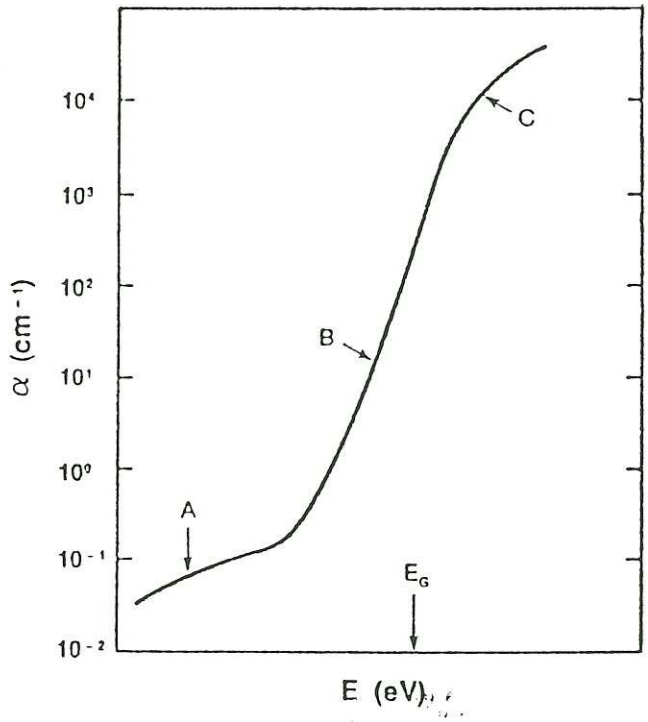

FIG. 3. *Typical energy dependence of the absorption coefficient of amorphous semiconductors*

As described by Tauc, and illustrated in Fig.3, by means of a typical plot of the absorption coefficient a versus photon energy, an amorphous semiconductor exhibits:

a shoulder for $a \lesssim 1cm^{-1}$ (region A)

an exponential rise for $1cm^{-1} \lesssim a \lesssim 10^3 cm^{-1}$ (region B)

and a slowly varying absorption regime for $a \gtrsim 10^4 cm^{-1}$ (region C).

In order to associate the absorption coefficient with the density of electronic states in an amorphous semiconductor, we focus on the imaginary part of the dielectric constant ϵ_2 , which bears a simple relationship to a:

$$\epsilon_2(E) = \hbar c \frac{n(E)a(E)}{E} \tag{1.2}$$

where c is the speed of light , E is the photon energy of the incident light and $n(E)$ is the real part of the complex refractive index of the illuminated sample.

At $T = 0°K$ and within the one electron approximation it holds that[3]

$$\epsilon_2(E) = (2\pi e)^2 \frac{2}{V} \sum_{i,f} |R_{if}|^2 \, \delta(E_f - E_i - E) \tag{1.3}$$

where

$$R_{if} = \int \Psi_i^*(\vec{R})(\vec{\tau} \cdot \vec{R})\Psi_f(\vec{R})d\vec{R} \tag{1.4}$$

The sum is over all initial (subscript i) and final (subscript f) electronic states. In the absorption process , electrons from the initial states are excited to the empty final states. V is the illuminated volume of the sample , $\vec{\tau}$ is the polarization vector of the light wave and $\vec{R}$ denotes the position of the electron. Assuming in addition to a constant dipole matrix element R_{if}, that any transition between initial and final states differing in energy by E is allowed, we obtain

$$\epsilon_2(E) \propto \int N_i(\xi)N_f(\xi + E)d\xi \tag{1.5}$$

where $N_i(E), N_f(E)$ are the densities of the initial and final states respectively. In eq.(1.5) only energy conservation is taken into account, in contrast to the crystalline case where both energy and momentum conservation are required. Even though eq.(1.5) lacks a rigorous theoretical basis , it is a widely accepted formula

usefull in interpreting experimental data.

Optical absorption in region C of Fig.3, often referred to as Tauc region, is associated with transitions from the extended states of the valence band to those of the conduction band. Assuming parabolic densities of the form

$$N_f \propto (E - E_c^\tau)^{1/2} \quad \text{and} \quad \mathrm{N_i} \propto (\mathrm{E_v^\tau - E})^{1/2} \tag{1.6}$$

we get

$$\epsilon_2(E) = K_{BB}(E - E_g^\tau)^2 \tag{1.7}$$

where $E_g^\tau = E_c^\tau - E_v^\tau$ and K_{BB} is a constant.

The energy dependence, given by eq.(1.7), has been verified experimentaly in many amorphous semiconductors[3,4,5]. This relationship implies that $(a(E)/E)^{1/2}$ versus E is a straight line. The so called *Tauc gap* E_g^τ is determined by extrapolating this line down to zero absorption and taking the intersection with the energy axis. E_g^τ lies in the transition region between A and B.

Region B or Urbach region, can be considered as resulting mainly from transitions between extended band states near the mobility edges and localized tail states. The term *tail states* is used to denote states which lie inside the mobility gap close to the mobility edges. (see Fig.1) We take parabolic densities for the bands (see eqs.(1.6)). For simplicity, let the mobility edges coincide with the characteristic energies E_v^τ, E_c^τ of eqs.(1.6).

Assuming an exponential energy dependence for the density of tail states we obtain:

$$\epsilon_2(E) = K_{TB}^v \exp\left(\frac{E - E_g^m}{E_0^v}\right) + K_{TB}^c \exp\left(\frac{E - E_g^m}{E_0^c}\right) \quad , \qquad E < E_g^m \tag{1.8}$$

K_{TB}^v and K_{TB}^c are constants, E_0^v, E_0^c are the widths of the exponential densities of

the tail states which lie close to the valence and conduction band respectively and E_g^m is the mobility gap. In the limit $E_0^v \to 0$ or $E_0^c \to 0$ the corresponding tail disappears giving a zero contribution to ϵ_2. We expect a greater contribution with increasing tail width. In other words, we expect the energy dependence of the dielectric constant to be established by the broader tail[6]. The above remark along with (1.2),(1.8) lead to the relationship

$$a(E) = a_0 \exp(E/E_0) \tag{1.9}$$

where E_0 equals the width of the broader tail. E_0 is often referred to as the Urbach parameter. The weak energy dependence of a_0 is of no importance against the exponential factor $\exp(E/E_0)$. Such a behavior is observed on the absorption edge of crystalline semiconductors as well [7]. In this case the effect is due to thermal disorder. The values of E_0 , however, are much smaller ($\sim 10\ meV$) than those in amorphous semiconductors ($\sim 60\ meV$).

Regarding a-Si:H, the analysis of many experimental data is compatible with the exponential character of the density of states near the mobility edges. In addition to that, the width of the tail near the valence band is approximately twice the width of the tail near the conduction band. Thus it is expected that the transitions from the localized states of the valence band tail to the extended states of the conduction band dominate the energy dependence of a . Region A in Fig.3 relates to transitions from defect states around the middle of the mobility gap to states in the conduction band.

The effect of temperature on the absorption edge

Having introduced the above simple picture for the absorption edge of amorphous semiconductors we proceed considering the effect of temperature , an interesting as well as difficult topic in solid state physics. Experimental evidence shows that the

shifts towards lower energies and the so called Urbach parameter E_0 (see eq.(1.9)) increases with increasing temperature.

Both effects are present in crystalline as well as in amorphous semiconductors. In the former, the disorder is due to temperature (thermal disorder) that causes random deviations of the atoms from their equilibrium positions. In the latter, along with thermal, static disorder is also present, due to the absence of long range order in the amorphous state. It is useful to discuss the effects of temperature starting from the crystalline case, since it provides the physical basis for understanding the more complicated amorphous case.

Crystalline case ; Energy gap

The temperature variation of the energy gap of a crystal can be decomposed into two parts: one associated with the dilation of the lattice and an other due to the interaction of electrons with the vibrating lattice.
The first part can be obtained theoretically by calculating the band structure as a function of lattice constant. The second part has attracted the attention of several workers[7] since 1951, when *Fan*[8] presented a calculation taking into account electron-phonon interaction in second order perturbation theory.
He considers the Hamiltonian term ΔU associated with the electron-phonon interaction, as a perturbation to the host Hamiltonian H_0 : $H_0 = \left[\frac{p^2}{2m} + V(\vec{r})\right] + H_L$.
H_0 is the sum of two independent terms. The first, enclosed in brackets, equals the Hamiltonian of eq.(1.1).
The second, H_L, is the vibrational energy of the crystal and can be written in the harmonic approximation , as the sum of independent one dimensional oscillators.
The total Hamiltonian is equal to $H = H_0 + \Delta U$.
In the interaction term ΔU, only the acoustic modes are taken into account since the optical modes give a negligible contribution in the case of Silicon and Germanium,the

materials of interest in Fan's paper.

ΔU taken in the first approximation with respect to the displacement of the atoms, contains only first order creation/annihilation operators (one phonon emission/absorption). The energy correction at the top/bottom of the valence/conduction band leads to a correction in the energy gap. The temperature T, enters the calculation through the mean occupation number of acoustic modes : $n_{\vec{q}} = \exp\left(\frac{\hbar w_{\vec{q}}}{kT} - 1\right)^{-1}$.

For $kT \gg \hbar w_{\vec{q}}$ the leading term is proportional to T. Thus differentiating with respect to T, Fan gets the variation of the gap with temperature, due to electron-phonon interaction. He gives an estimation for Silicon $\left(\frac{\partial E_g}{\partial T}\right) \approx -1.8 \times 10^{-4}\ eV/^\circ K$, a value almost identical to the variation due to the dilation of the lattice. The total effect i.e the sum of the two contributions equals to $-3.6 \times 10^{-4}\ eV/^\circ K$, a value which is in good agreement with experiment. As regards Ge , the corresponding value is very different from the experimental one.

Allen and *Cardona*[9] have found that the explicit temperature dependence of the energy gap in crystalline semiconductors can be written in the form:

$$E_g(T) = E_g(0) - D(< u^2 >_T - < u^2 >_0) \tag{1.10}$$

D, is a second order deformation potential.

$< u^2 >_T$ and $< u^2 >_0$ are ensemble averages of the squares of the displacements of the atoms from their equilibrioum positions , taken at T and zero temperature respectively. In the Einstein approximation

$$< u^2 >_T = \frac{\hbar w_0}{w_0^2 M}(< n_{1-d} > + \frac{1}{2}) = \frac{\hbar w_o}{w_0^2 M}\frac{1}{2} coth(\frac{\hbar w_0}{2K_B T}) \tag{1.11}$$

$$< n_{1-d} > = \left[exp(\frac{\hbar w_0}{K_B T}) - 1\right]^{-1} \tag{1.12}$$

where M is the atomic mass and $< n_{1-d} >$ is the average occupation number for a single one-dimensional harmonic oscillator of frequency w_0 . For $K_B T \gg \hbar w_0$, $< u^2 >_T$ and therefore $E_g(T)$, is proportional to T, in agreement with Fan's work.

Crystalline case ; Urbach parameter

Proceeding to the second thermal effect, that is the variation of the Urbach parameter E_0 with temperature, we focus on the Urbach region of the absorption edge. The typical dependence of a on E for defferent temperatures is shown in Fig.4.

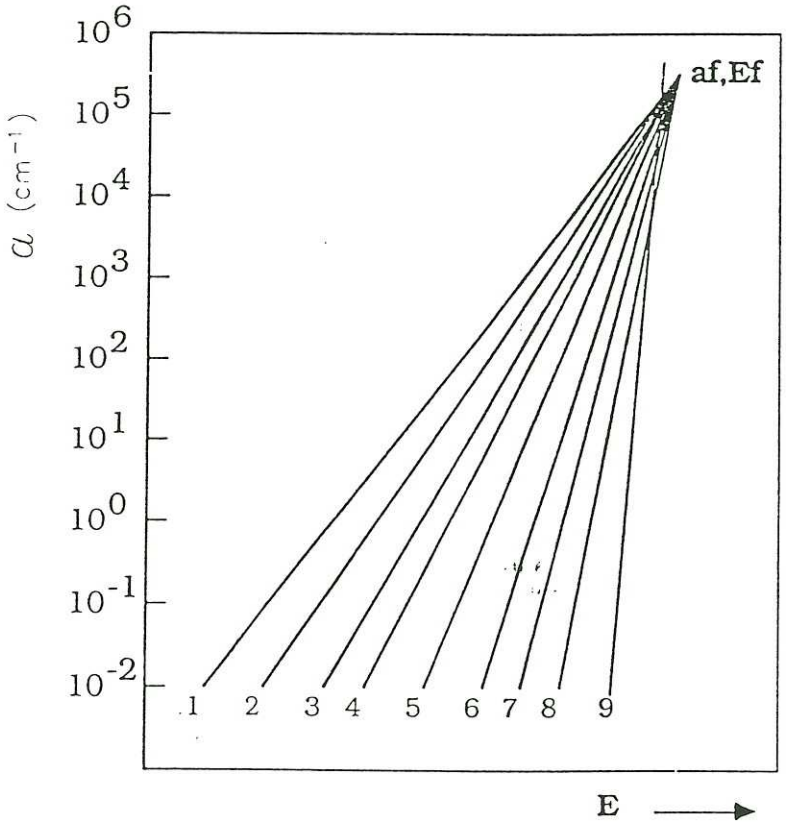

FIG. 4. *Absorption edge of crystalline semiconductors at different temperatures. The denoting each curve increases as the temperature decreases.*

It can be seen that the absorption curves plotted semilogarithmically give a convergent bundle . The point of convergence has coordinates a_f, E_f. The temperature region of such a behaviour lies, as a rule, above the Debye temperature of a given material. At lower temperatures the absorption edge maintains the same form but the curves may deviate from point a_f, E_f. The temperature dependence of E_0 is the same as that of the energy gap

$$E_0(T) \propto < u^2 >_T \tag{1.13}$$

Many workers[7] explain this behaviour of E_0 by a mechanism involving exitons or electrons interacting with thermal phonons. *Skettrup*[10] bypasses the specific mechanism and interprets this effect in terms of thermal fluctuations in the band-gap energy. It can be easily proved by combining (1.10),(1.11) , that the temperature dependence of E_g due to electron-phonon interaction can be written as:

$$E_g(T) = E_g(0) - A < n_{3-d} > \tag{1.14}$$

$$n_{3-d} = n_x + n_y + n_z \tag{1.15}$$

where A is a constant

$$A = \frac{D}{3} \frac{\hbar w_0}{w_0^2 M} \tag{1.16}$$

and n_x, n_y, n_z are the occupation numbers for a three-dimentional, isotropic harmonic oscillator of frequency w_0. The isotropy assumption requires:

$$< n_x > = < n_y > = < n_z > = < n_{1-d} > \tag{1.17}$$

where n_{1-d} is defined in equation (1.12).

Skettrup incorporates the effect of lattice dilation in eq.(1.14) through a change in the constant A. Thus he keeps eq.(1.4) valid, adopting a new constant that includes

contributions from both electron-phonon interaction and dilation.

The transitions between valence and conduction band take place in time intervals much shorter than the atomic motions due to thermal phonons. Consequently the relevant gap is not the time and spatial average given by (1.4) but rather a local and instantaneous gap which is obtained when $< n_{3-d} >$ is replaced by a particular occupation number n_{3-d} :

$$E_{g,n_{3-d}} = E_g(0) - An_{3-d} \tag{1.18}$$

The standard deviation of n_{3-d} is comparable to $< n_{3-d} >$ as can be seen from the expression :

$$\sigma_{n_j} =< n_j > (1+ < n_j >^{-1})^{1/2} \quad , \qquad j = x, y, z \tag{1.19}$$

Thus $E_{g,n_{3-d}}$ is a fluctuating quantity. Since the typical duration of a measurement is much longer than any other characteristic time relevant to the microscopic events (atomic motions, electronic transitions) in the crystal and the illuminated regions are much larger than a phonon coherence length, the measured absorption coefficient at temperature T, is a space-time averaged quantity given by:

$$< a(E) >_T = \sum_{n_{3-d}} P_{n_{3-d}} a(E - E_{g,n_{3-d}}) \tag{1.20}$$

$$P_m = \frac{exp(-m\frac{\hbar w_0}{K_B T})}{(1 - exp(\frac{-\hbar w_0}{K_B T}))^3} \tag{1.21}$$

Considering $a(E - E_{g,n_{3-d}})$ a step function:

$$a(E - E_{g,n_{3-d}}) = \begin{bmatrix} constant, & E_{g,n_{3-d}} < E \\ 0, & E_{g,n_{3-d}} > E \end{bmatrix} \tag{1.22}$$

it follows that

$$< a(E) >_T = a_0 \exp\left[-\frac{E_g(0) - E}{AK_B T}\right] \tag{1.23}$$

where a_0 is a weakly temperature dependent prefactor.
Relation (1.23) implies that

$$E_0 = AK_B T \tag{1.24}$$

This is the temperature dependence we expect for $K_B T \gg \hbar w_0$. Skettrup does not restrict his calculations only on the simple arguments given above. Adopting a more rigorous approach he obtains the correct temperature dependence of E_0 (see eqs.(1.11),(1.13)).

We summarize the crystalline case in the following:

1) In the Urbach region of the absorption edge of a crystalline semiconductor , the curves of $ln a$ versus E are straight lines. They converge for different temperatures, smaller than the Debye temperature of the material under consideration, on a focal point a_f,E_f (see Fig.4).

2) The disorder parameter $E_0(T)$ bears a linear relationship to the gap $E_g(T)$ as it is seen from eqs.(1.10),(1.13). E_0 increases, in contrast to E_g that decreases with increasing temperature.

Amorphous case ; Energy gap and Urbach parameter

Experimental evidence[11] shows that the above characteristics are observed in amorphous semiconductors too. In proceeding to the presentation of the effect of temperature on the absorption edge of amorphous semiconductors we remind the reader that in this case, static disorder is present along with thermal. A convenient

way to think of static disorder resides in the concept of the *frozen in* phonons, first indroduced by Tauc[12]. Based on this concept, he suggested the following modification of eq.(1.13) in order to account for static disorder as well:

$$E_0(T,x) \propto (< u^2 >_T + < u^2 >_x) \tag{1.25}$$

where $< u^2 >_x$ is the average displacement of the atoms due to the *frozen in* phonons. It is usual to think of the parameter x as the glass transition temperature T_g. Since most of the amorphous semiconductors are not fabricated by quenching, T_g is not a well defined parameter. It is more realistic to think of x as parameters depending on the specific technique used to construct the semiconductor under consideration.

Cody et al.[11] measured the temperature dependence of the Urbach absorption edge of a-Si:H films and found a focal point at $a_f = 1.5 \times 10^6 cm^{-1}$, $E_f = 2.2eV$. Seeking for the interdependence between the Tauc gap defined in eq.(1.6) and the Urbach parameter, he took measurements at varius temperatures before annealing and at $300°K$ after annealing. Annealing affects static disorder by indroducing dangling bonds through thermal evolution of hydrogen. In a plot of the Tauc gap versus Urbach parameter, measured for various thermal and static disorder grades, a straight line was drawn suggesting a linear dependence. Based on the above experimental evidence Cody et al. extended the idea of equivalence of static $< u^2 >_x$ and thermal $< u^2 >_T$ disorder in the gap and modified (1.10) in the same way Tauc modified (1.13) into (1.25) :

$$E_g(T,x) = E_{g_0} - D(< u^2 >_T + < u^2 >_x - < u^2 >_0) \tag{1.26}$$

where E_{g_0} is the zero-temperature, zero static disorder gap.

The behavior of the absorption edge in amorphous semiconductors found theoretical support on the work of Grein and John[13] . In this model the combined effect of static and thermal disorder, the latter in the form of electron phonon interaction, is examined.

A more complete than the usual[8] treatment of electron-phonon interaction gives rise to multiple phonon emission and absorption processes which accompany the optically induced electronic transitions. These processes dominate the absorption in the Urbach regime.

It is not necessary to deal with such detailed physical mechanisms in order to understand the exponential behavior in the Urbach absorption edge.

Economou[14] based on simple arguments interprets this behavior through exponential tails in the density of states (DOS). Based on the idea that an amorphous semiconductor can be considered as resulting from an ideal (periodic) lattice by a disordering procedure, Economou suggests the following form for the Hamiltonian operator:

$$H = H_0 + H_1 \ , \ < H_1 >= 0 \tag{1.27}$$

H_0 is the Hamiltonian of the ideal lattice and H_1 incorporates the disorder, thermal and static, in the form of a fluctuating potential. The first effect, the narrowing of the energy band gap, is obtained as a second order perturbation result for the energy levels. The absolute value of the energy displacement of either the conduction or valence band edge is given by :

$$| E_b - E_b^0 | \ = \ w^2 \int \frac{\rho_0(E')dE'}{E_b^0 - E'} \tag{1.28}$$

The quantity $\rho_0(E)$ is the density of states of the ideal lattice. The symbol E denotes the energy level, the subscript b , either the conduction or valence band edge and the superscript 0 stands for the ideal lattice. The quantity w^2 is the standard deviation of the disorder related part H_1, of the Hamiltonian. The second effect of disorder in the DOS is the development of tails extending beyond E_b. One can distin-

guish three regions in the tail : the near tail (NT) or Halperin-Lax which lies around E_b, the deep tail (DT) or Urbach region and the very deep tail (VDT) or deep defect region. As far as Fig.3 is concerned, NT in the DOS, relates to the small transition region between C and B in the absorption domain. DT and VDT correspond to eigenstates bound around a single potential well or potential bump and relate to regions B and A of Fig.3, respectively. Potential wells create localized states at the bottom of the conduction band, whereas potential bumps, at the top of the valence band. The larger the deviations from the periodic potential of the ideal lattice are and the greater the spatial concentration of such potential deviations is, the stronger the effect of tail states in the DOS.

Let us remind the reader the main results concerning the elementary problem of the bound ground state in a three dimensional local (i.e. short range) potential well. We denote by ϵ the depth of the potential well and by r its linear extent; E is the ground bound state energy and λ is its decay length.

For very deep potential wells ($|\epsilon| >> \epsilon_0 = \vec{\hbar}^2/2mr^2$) , the bound ground state is essentially inside the well ($\lambda < 0.1r$) and $|E|$ is proportional to $|\epsilon|$, i.e.

$$|E| = |\epsilon| - \epsilon_0 \tag{1.29}$$

There is an intermediate regime, where the wavefunction is, roughly speaking , half in and half out of the potential well ($0.4 \lesssim \lambda/r \lesssim 1.4$) . In this regime the ground bound state energy is approximately proportional to the square of the potential well depth

$$|E| = A\,\epsilon^2 - B \qquad E_1 \leq |E| \leq E_2 \tag{1.30}$$

Finally, there is a critical value of ϵ, ϵ_c, such that for $|\epsilon| < |\epsilon_c|$ there is no

bound state in a 3-d potential well. For $|\epsilon|$ just above the critical value ϵ_c , λ tends to blow up $(\lambda \sim |\epsilon - \epsilon_c|^{-1/2}$, which means that the bound eigenfunction is essentially outside the potential well) and

$$E \sim |\epsilon - \epsilon_c|^2 \qquad \epsilon \to \epsilon_c \tag{1.31}$$

The VDT region corresponds to states bound inside deep fluctuations, where eq.(1.29) is approximately valid.

The NT or Halperin-Lax region may be associated to loosely bound states for which eq.(1.31) holds.

The DT or Urbach region corresponds to the intermediate regime of bound states in isolated local potential wells for which eq.(1.30) is valid. Hence the DOS in the Urbach regime is given by

$$\rho(E) = p \left(\sqrt{\frac{|E| + B}{A}} \right) \tag{1.32}$$

A Gaussian distribution of ϵ (which is expected to be very common in this intermediate regime), $p(\epsilon) \sim exp(-\epsilon^2/2w^2)$, gives for the DOS

$$\rho(E) \sim exp(-|E|/2w^2 A) \tag{1.33}$$

Eq.(1.33) provides a simple explanation for many features observed in the optical absorption of ionic crystals (where the disorder is of thermal nature) and of amorphous semiconductors. The most recent theoretical developments on the subject of the Urbach absorption edge can be found in references [15], [16].

Review of experimental methods used to probe the Urbach region of a-*Si:H*

One can find in the literature many experimental investigations of the optical parameters of a-Si:H, in the absorption edge region. The most interesting part of the absorption edge, is the low energy end where the absorption coefficient a has values below $10^3\,cm^{-1}$. It relates to the tails of the density of states inside the gap of this semiconductor, often called pseudo-gap because of the non null DOS in it. Since the typical thickness of a-Si:H films is only 10^{-4} cm (1 $micron$), very careful measurements are needed to determine $a(E)$. Many investigations use two alternative techniques: the Constant Photocurrent Metchod (CPM) and Photo-Deflection Spectroscopy (PDS). Both have excellent sensitivity to low absorption but present significant drawbacks, discussed in the following, when one is interested in the temperature variation of the absorption spectra.

In PDS, optical absorption is detected by measuring the heat absorbed in the film, near its free surface. The film is illuminated with a chopped monochromatic light beam. This induces slight temperature variations at the free surface of the film, which in turn change the refractive index of a special transparent liquid into which the sample is immeresed. The amplitude of these effects depends on the absorption of light in the film. A liquid having refractive index stronly dependent on temperature is selected. Index variations are detected, in synchronization with the chopper, using lock-in techniques, through the deflection of a laser beam which crosses the liquid almost side by side to the surface of the film. A gas (eg. He) , can be used instead of the liquid with significantly lower precision and stability in the measurement.

Although PDS is able to measure extremely low $a\,d$, of the order of 10^{-5}, it is inapplicable at temperatures much different from ambient's temperature if a liquid is used. One could use He instead. However, in addition to the low accuracy in mea-

surement, it is very problematic to obtain the necessary absence of any turbulence in a cryostat.

The CPM measures absorption by measuring photoconductivity spectra. It is also very sensitive to low absorption and in contrast to PDS, probes the entire film. The photocurrent must be proportional to the generation rate of carriers due to the illumination. In order to ensure this, a constant photocurrent is maintained at every photon energy. This may not be sufficient especially when the temperature, and as a consequence the recombination mechanism, changes. The CPM is widely used for low absorption measurements, especially in order to probe the defect absorption shoulder below the Urbach region. However, its basic assumptions and results have recently come under attack[17]. We believe both methods are inadequate to accurately determine the temperature variation of the absorption edge.

We have performed only transmittance and reflectance measurements and have developed data-analysis techniques, that enable us to extract the absorption spectra with good accuracy down to $a \approx 10^2\ cm^{-1}$. In the following, we present first the design and implementation of the experimental setup, considering the systematic error sources related to it. Systematic errors in the extraction of $a(E)$ can result as well from neglecting inherent characteristics of actual samples, as the thickness non-uniformity[18], index inhomogeneity[19] and surface roughness[20]. These imperfections can be successfully accounted for in the analysis, yielding useful information about the sample in study.

1.2 Experimental Setup

Accurate determination of weak optical absorption through reflectance (R) and transmittance (T) measurements cannot be attained using standard spectrometers. All measurements presented in this section, were performed using a specially built setup that has evolved during the progress of the experiment, in order to improve its accuracy and capabilities. A schematic representation of the arrangement on the optical bench is given in Fig.5. The sample is located in a cryostat and is illuminated by a monochromatic beam through one window. Light reflected from the sample passes through the same window while the transmitted beam emerges through the second window opposite to the first. With the help of a set of mirrors both the reflected and transmitted beams are collected and focussed onto the same detector and are measured alternately by switching back and forth a shutter. The use of a single detector is dictated by the need to provide identical measurement for the two beams.

R and T spectra are obtained by measuring first the transmitted light intesity $I_{t0}(E)$ in the absence of sample. Without sample, R is zero. All subsequent measurements, with a sample, of transmitted $I_t(E)$ and reflected $I_r(E)$ light intensity, are divided by $I_{t0}(E)$ to obtain T and R respectively. Since I_t and I_{t0} follow identical paths, they undergo the same relative attenuation because of the response of the detection system. Taking the ratio of the two quantities, the common factor that accounts for the response of detection system is eliminated and thus the correct T is obtained:

$$\mathsf{T} = \frac{I_t(E)}{I_{t0}(E)} \tag{1.34}$$

However, as regards I_r and I_{t0}, the detection paths are different. Then

$$\mathsf{R} = f(E)\,\frac{I_r(E)}{I_{t0}(E)} \tag{1.35}$$

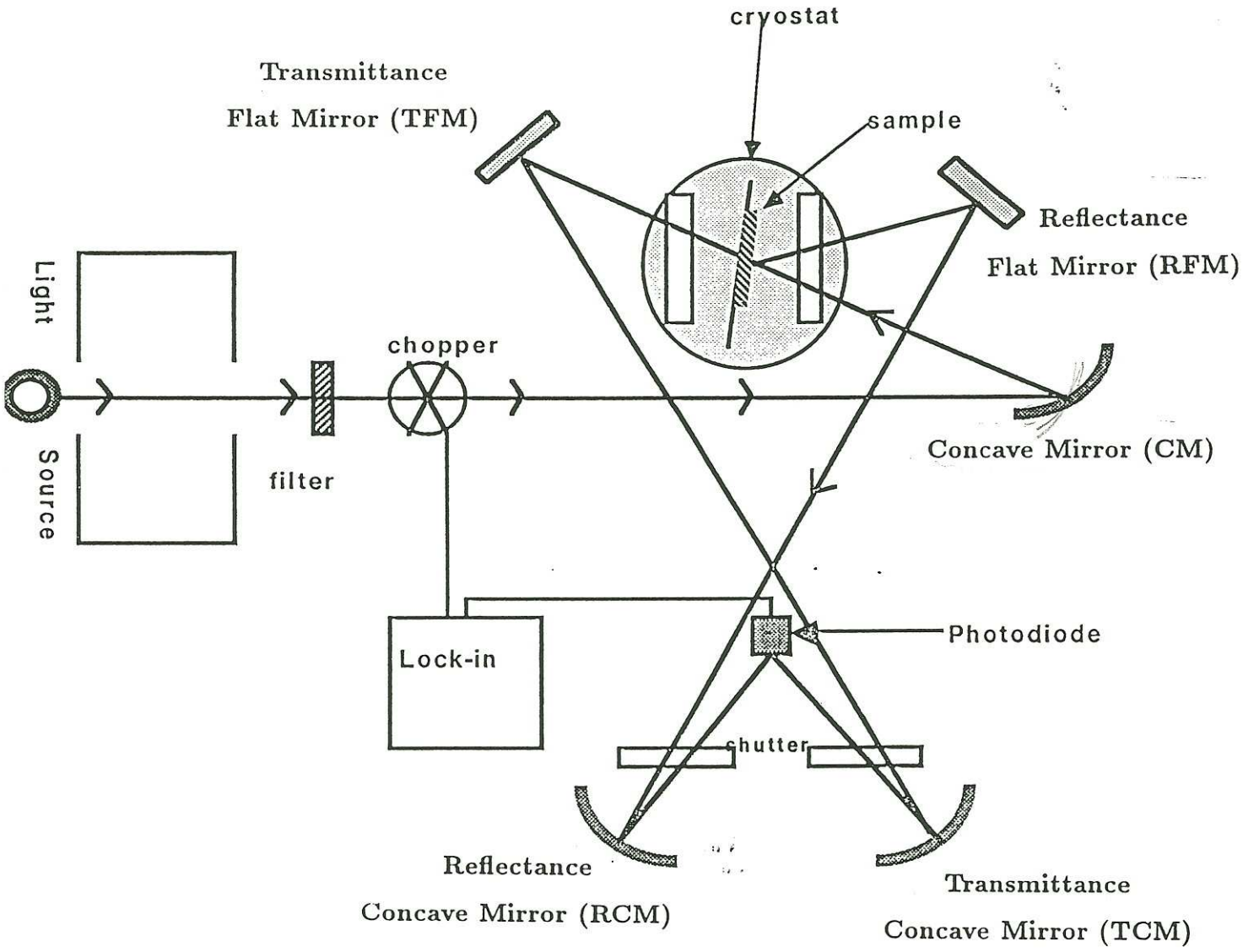

FIG. 5. *Schematic diagram of the optical set-up*

where $f(E)$ is a correction factor for small differences between the mirrors of R and T detection paths. The factor $f(E)$ can be measured once, by swapping TFM with RFM and RCM with TCM (see Fig.5). The method of mesuring $f(E)$ is given in Appendix A.

For successful R and T measurements, excellent long term stability of both the illumination intensity and the detection system are necessary. At the end of the series of experiments, performed at different temperatures and requiring many hours of run, a second $I_{t0}(E)$ calibration spectrum is taken and is compared to the first one. We achieve deviations between the two of less than 0.3 %.

Optics

No lenses are used in the optical setup to ensure absence of chromatic aberrations. This is a key feature of our measurement since, any systematic wavelength dependent error can distort the $a(E)$ spectra. Chromatic aberrations in lenses, may cause a spot of different size at different wavelengths. Given that the measured spectra are strongly affected by the size of the spot on the sample, in the presence of thickness or index non uniformity[18] , we exclude lenses from the setup. Focussing of the beam is achieved by high reflectivity concave mirrors. In order to minimize the effects related to thickness or index non uniformity, we focus the incident beam on the surface of the sample in a small spot whose larger dimension is less that 1mm. The spot, that is the image of the exit slit of the monochromator limited by knife edges, is formed on the sample with the help of the concave mirror CM (see Fig.5). The relative positions of the monochromator, CM and the sample are chosen in order to diminish spherical aberrations of CM and create a reduced image of the exit slit on the sample. Collimators are used to limit the angular dispersion of the incident beam. The transmitted and reflected beams are not collimated. This ensures complete collection of the R and T beams. Reflected and transmitted light is focussed on the photodiode, well within

its active surface.

The glass windows of the cryostat cause reflections which must be deviated away from the photodiode to avoid erroneous measurements. This is achieved by providing for non parallel windows on the cryostat. Care is taken, to have a small angle of incidence on the windows ($\lesssim 20\,deg$), as well as symmetrical (with respect to the plane of the film) T and R detection paths, as to minimize errors in the measured R , due to polarization effects.

The analysis of the data is based on the assumption of normal incidence. In our experiment, all rays in the convergent, incident on the sample , beam, are within 15 *deg* from the normal on the sample's surface. Both, calculations and experimental results indicate that one can safely use the assumption of normal incidence for angles of this magnitude.

Illumination

The light source is a 100 W halogen lamp operated at regulated voltage, below maximum power, for better stability. We use a SPEX $0.25\,m$ monochromator with a 1200 $grooves/mm$ grating, blased at 500 nm. Slits are adjusted to 0.3 mm which corresponds to a bandwidth $\delta\lambda$ around $1\,nm$ in the range of the experiments. This resolution is high enough to avoid any rounding[18,21] of fringe peaks even for the thickest samples used.

Detection

Since long term stability is of paramount importance in this experiment, we use a temperature regulated Si-photodiode in the photovoltaic mode. In order to achieve

good signal to noise ratio we use a high quality Lock-in amplifier (EG&G 5206) and a chopper operated at about $28\,Hz$. DC (Picoammeter) detection may have better signal amplitude resolution that a lock-in amplifier, but requires total darkness over the whole optical bench which is impractical. The resolution of the AC detection is greatly improved by using multiple ranges (autoranging feature) of the lock-in amplifier. The experiment is fully controlled by a personal computer. This includes scanning of wavelengths and measurement by the lock-in as well as switching between R and T by the shutter. Data collection is automatic. It takes about half to one hour for each R / T spectrum.

Cryostat

Our first experiments at temperatures below ambient's, have been performed using a commercially available cryostat (OXFORD Cryogenics) specially designed for optical measurements. It soon became evident that it was inadequate for two principal reasons: the limited temperature range (it could exceed room temperature by only a few tens of degrees) and the poor vacuum in the sample chamber. Poor vacuum has a detrimental consequence on optical measurements performed at low temperature : water vapor and eventually oil from the mechanical pump condenses on the surface of the sample in the form of a very thin film. Its thickness increases with time, creating serious problems to a measurement requiring very good long term stability.
The pumping ports of the commercial cryostat were too small for secondary vacuum.

We have designed and built a special, liquid nitrogen (LN_2) circulation cryostat for optical measurements, that permit us to cover a wide range of temperatures:
80 to 900 $^{\circ}K$. It is also designed for in-situ annealing of the samples performed in a movable isothermal space inside the vacuum chamber. Precision optical measurements at low temperatures require a good, oil vapor free, secondary vacuum. We use a turbomolecular pump that enables us to create a vacuum $\lesssim 10^{-5}$ $mbar$ inside the

chamber of the cryostat.

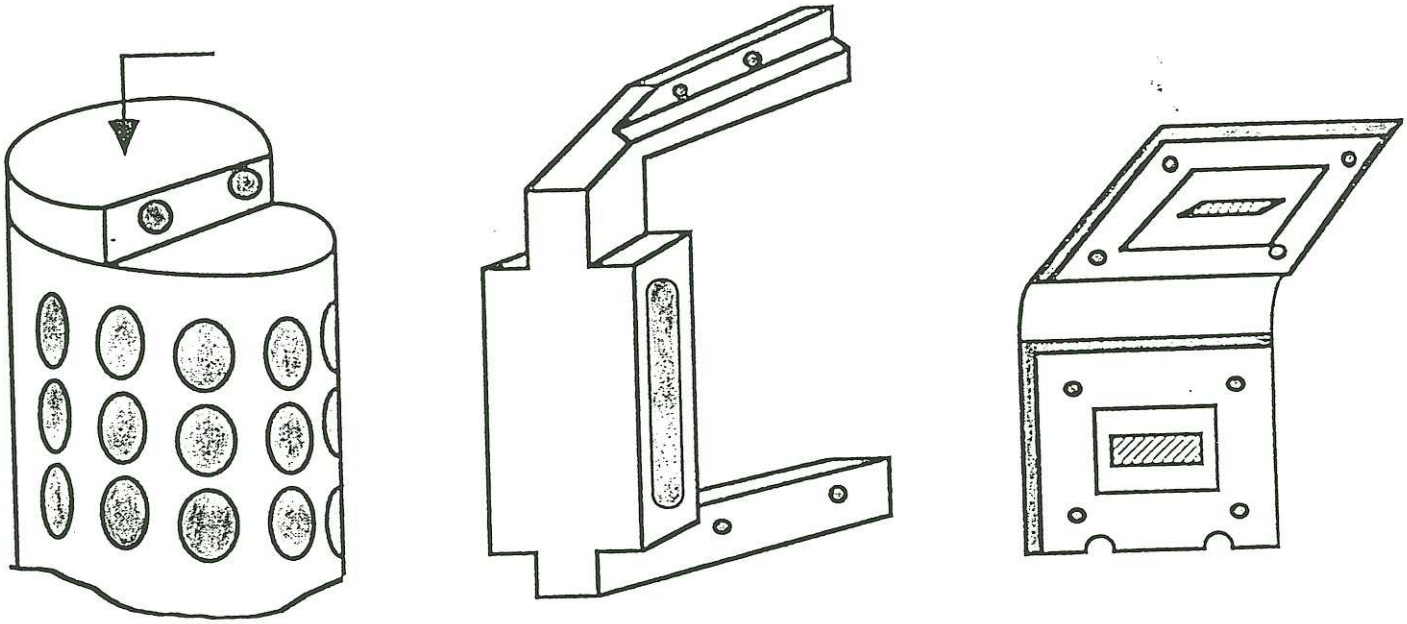

part a part b part c

FIG. 6. *Sample holder assembly.*

The cryostat is vertically mounted and is composed of two sections. The head containing the sample, emerges through a hole in the optical table. It has a cap that bears the optical windows and is removable for easy installation of the sample. The body, located entirely below the optical bench, provides for the vacuum ports, all electrical feed-throughs and the cryogenic (LN_2) tubing feed-throughs.

The sample holder is mounted on the top of a long, thin walled stainless steel tube that has a diameter of $3cm$. This tube serves the dual purpose to provide for rigid support of the sample required for optical measurements and at the same time, isolate thermally the sample holder from the base of the cryostat on which the stainless tube is mounted. The stainless tube is perforated to further increase thermal resistance

without loss of rigidity. The upper end of the tube (Fig.6, part a) is closed by a solid stainless plug onto which the sample holder is attached (Fig.6, parts b and c). The plug is cooled by circulating LN_2 through a thin conduit inside it. $1/4 - inch$ cryogenic stainless tubing, fed through the base plate, and running inside the perforated tube, is used to bring LN_2 to the plug.

Details of the sample holder are shown in Fig.6 (parts b and c). The heating element is a 100 W quartz halogen incandescent lamp, located in a specially provided cavity inside part b. Two main thermocouples are used. One is located near the lamp and serves regulation, the other is attached with good thermal contact onto the sample mounting plate (part c) and is used for measurement. Parts b and c are made out of copper. In order to ensure good thermal conductivity between parts a and b we use Indium pressed between the two parts by applying a relatively large torque to the attaching screws.

The main cause of long term drift of the sample's temperature and of errors in its measurement, is heat exchange between the sample and the walls of the cryostat, the latter always being at room temperature. We take care to expose the minimum of sample's surface, necessary for the optical measurements, by opening a small window on each of the two plates of part c between which the sample is clamped.

Both, good regulation of the sample's temperature and accuracy in the reading, depend on the relative importance of the heat radiated to/from it to that conducted to/from it through the means of attaching it onto the sample holder. Here also we use Indium in the form of a gasket placed inside a special groove, machined around the windows of part c. Use of springs in pressing the sample in sandwich between the two halves of part c is necessary, in order to avoid breaking the glass substrate by uneven stress. Good thermal contact between the two halves of part c is obtained by a Cu foil welded between them. We have avoided gluing the sample onto the holder

for many reasons:

i) The difference in thermal expansion coefficients between copper and glass (the thin film's substrate) can cause bending of the substrate and result in misalignment of the beam.

ii) If no glue is used, several locations on the surface of one film can be measured by sliding the sample inside part c and clamping it tight again.

iii) The same sample can be removed, remounted again at will and serve for other measurements as well.

Temperature regulation within better than one degree is achieved by a digital PID controller. A combination of LN_2 flow control and heater (lamp) control is necessary at T below ambient. For higher temperatures, only the heater is necessary.

1.3 Data Analysis. The Role Of Sample Imperfections

1.3.1 The ideal case

As we have already mentioned, actual samples present various, more or less important, deviations from a constant thickness, uniform index and plane interfaces. These imperfections complicate the analysis of the experimental data and the interpretation of the results. In order to indicate the effects of these characteristics on the optical measurements, we have used and developed specific models that are presented below.

Let us start with the ideal case. We consider a film having constant thickness, deposited on a perfectly flat, non absorbing substrate. Both the substrate and the film have uniform and isotropic dielectric constants. The film has a complex refractive index n :

$$n = \eta - ik \tag{1.36}$$

The index of the (non-absorbing) substrate is η_s. Generally, both indices depend on the wavelength of light, but since η_s varies very little in the range of interest to our measurements, it is assumed to be a constant in the following. Since the thickness of the substrate is orders of magnitude larger than the wavelength, it is perfectly justified to treat it incoherently.

Assuming normal incidence of light, we calculate R/T spectra of ideal films, in the photon energy range of the experiments, using for the optical parameters realistic values of a-Si:H. The details of the derivation of transmittance[21] and reflectance are given in Appendix B. The results are given in Fig.7. The solid and dashed curves

correspond to T and R respectively. Both curves oscillate with wavelength. These oscillations (fringes) are interference effects due to reflections on the surfaces that bound the film. As absorption increases, the interference fringes for both R and T shrink gradually till they disappear altogether. It is evident that T-maxima are most sensitive to absorption.

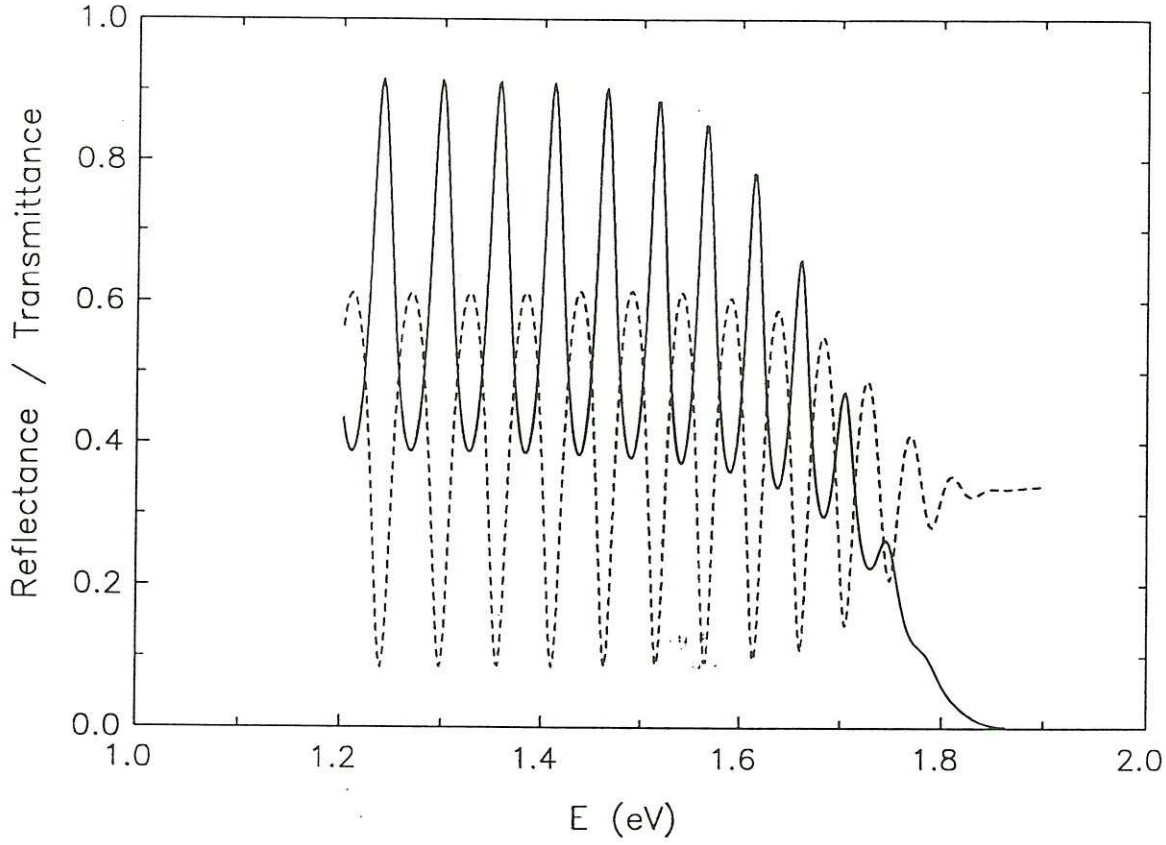

FIG. 7 *Calculated reflectance (dashed line) and transmittance (solid line) of an ideal sample. The thickness of the film is* $3\mu m$. *The substrate index* η_s *equals 1.53. The absorption coefficient a(E) and the refractive index* $\eta(E)$ *used as input to the calculation, are plotted by dashed lines in Figs.11 and 12, respectively.*

The experimental energy range extends in the infrared region well inside the optical

gap of a-Si:H. One is certain that between 1.2 and 1.4 eV, light absorption is so weak in a-Si:H that we can use this region to determine the low energy limit of the index of the film. We refer to this energy range as the transparent region. In this region, the maximum transmittance, T_{max}, is equal to the transmittance T_s of the substrate alone[21] :

$$T_{max} = T_s = \frac{2\eta_s}{\eta_s^2 + 1} \tag{1.37}$$

The T-minimum values are given by:

$$T_{min} = \frac{4\eta^2\eta_s}{\eta^4 + \eta^2(\eta_s^2 + 1) + \eta_s^2} \tag{1.38}$$

The basic equation for interference fringes is

$$2\eta d = m\lambda \tag{1.39}$$

m is an integer for maxima and half integer for minima, in the case of transmittance, and vice-versa for reflectance. Equation (1.39) holds strictly in absence of absorption. Nevertheless one can verify numerically that it can also be used in the absorption regime, if fringes are visible, without significant error.

Both R and T are functions of η_s, d, η, k. Given these, it is easy to calculate R and T. On the contrary it is difficult to perform the inverse procedure which is necessary for the analysis of the experimental data. Many techniques have been proposed[21–26]. The analysis of the transmittance spectrum alone is sufficient for the determination of all four quantities : η_s, d, η, k . The reflectance data are not indispensable, but they can still serve to cross-check the results of the analysis.

We have used for the analysis, the following method given below : According to eq.(1.37), the substrate's index can be found by measuring, either the transmittance T_s of the naked substrate, or the value T_{max} in the transparent region, which

practically extends over one or two fringes in most of our experiments. Since our experimental spectra and consequently T_{max} , are affected by various types of imperfections (discussed in the following), it is safe to measure directly T_s in order to find η_s .

Once η_s is known, one can calculate the long wavelength value of the film's index η_0 using eq.(1.38).

Let us now denote by the integer m_0 the order of the fringe of the extremum appearing at the lowest energy in the transmittance spectrum.(see Fig.7). We label consecutive extrema by the index $j = 0, 1, 2, \ldots$. The value $j = 0$ corresponds to the extremum of order m_0. One can prove, taking into account (1.39) that:

$$\eta_j = \frac{\eta_0 \Delta E}{E_j} \left(fo + \frac{j}{2} \right) \tag{1.40}$$

If m_0 corresponds to a maximum then:

$$fo = m_0 \tag{1.41}$$

Otherwise, if it corresponds to a minimum then:

$$fo = m_0 - \frac{1}{2} \tag{1.42}$$

η_j , is the value of the real part of the refractive index at photon energy E_j . ΔE is the energy difference between two consecutive maxima/minima at the long wavelength limit. We obtain ΔE through

$$\Delta E = 2 (E_1 - E_0) \tag{1.43}$$

Using (1.40) it is easy to verify that

$$fo = \frac{E_0}{\Delta E} \tag{1.44}$$

According to eqs (1.41) and (1.42) the vaue of fo must be integer of half integer. However in analysing data, one finds that the ratio in (1.44) deviates from this condition. This is expected, if one keeps in mind that the order of the fringes appearing in our experimental spectra is larger than 10 even for the thinner of the samples used. Therefore, we correct ΔE found, to bring fo to the nearest integer or half integer. Following the way we just mentioned, we calculate the values η_j at the energy-positions of T-extrema. Intermediate values for η are obtained by linear interpolation.

One can show, from (1.39) that the thickness of the film relates to ΔE through:

$$\Delta E = \frac{hc}{2\,\eta_0\,d} \tag{1.45}$$

Finally, the extinction constant is calculated as a function of energy from the envelope of T-maxima. The theoretical expression for the envelope of T-maxima, $T^{th}_{env}(\eta_s, d, \eta(E), k(E))$, in the form of a continuous function of wavelength[27], can be obtained by taking, in the expression for the transmittance, the phase shift inside the film equal to a multiple integer of π. This condition corresponds to the interference fringe maxima of the transmittance. Experimentally, we can obtain the envelope of interference maxima, $T^{exp}_{env}(E)$ by SPLINE interpolation of the experimental T-maxima. Since all other parameters except k are known, one can solve numerically, at any E, the equation:

$$T^{th}_{env}(\eta_s, d, \eta(E), k(E)) \; - \; T^{exp}_{env} \; = \; 0 \tag{1.46}$$

and find $k(E)$. The absorption coefficient $a(E)$, is obtained through :

$$k(E) \; = \; \frac{h\,c\,a(E)}{4\,\pi\,E}$$

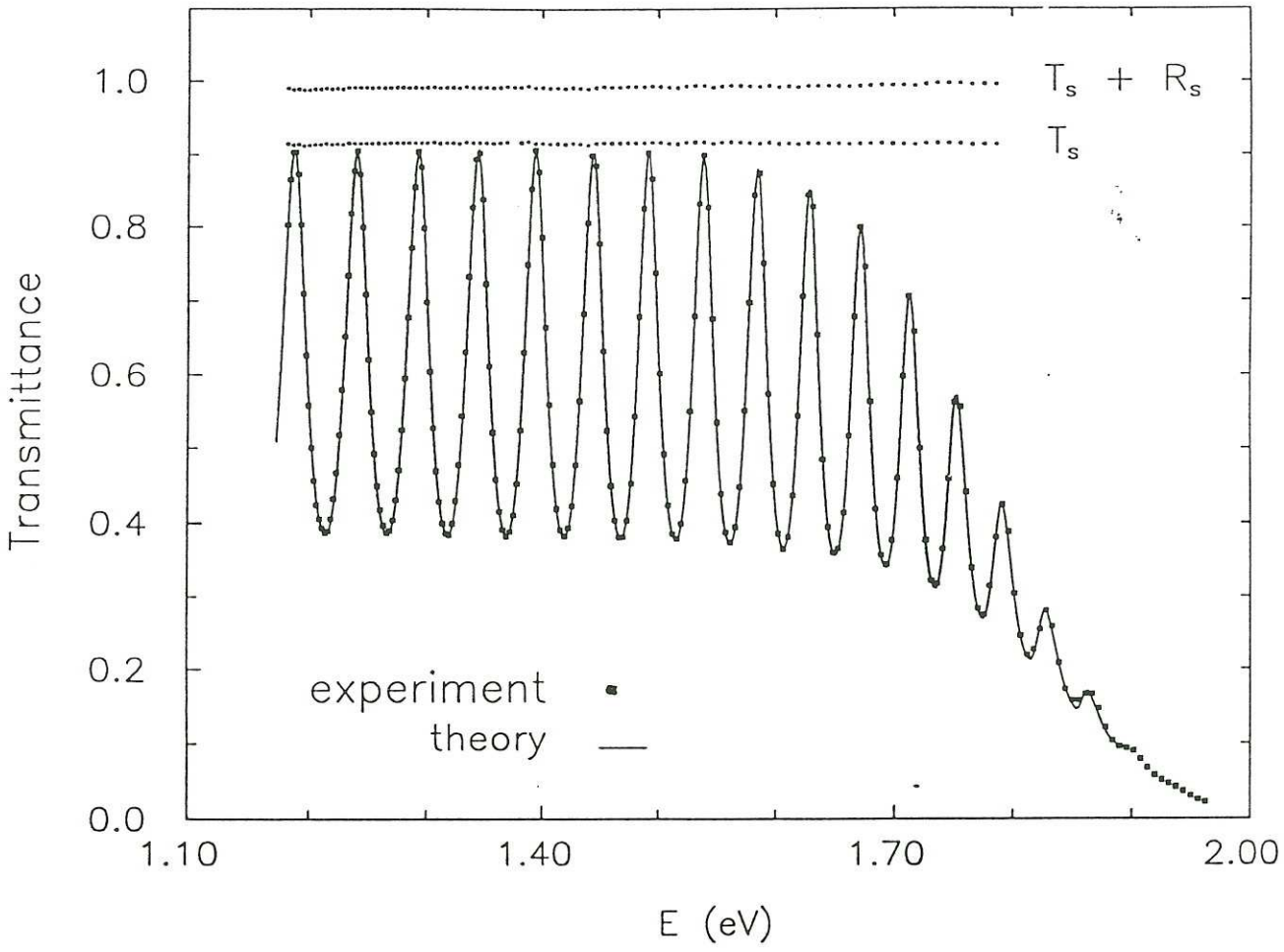

FIG. 8 *Example of experimental transmittance spectrum (solid squares) for sample RFS250 measured at* $89°K$. *As an indication of the quality of our analysis, we plot the transmittance (solid line) calculated using as input, the parameters derived from analyzing the experimental spectrum (solid squares). The data a(E) for this particular sample are shown in Fig. 17. The measured transmittance of the naked substrate* T_s *and the sum of its transmittance and reflectance* $T_s + R_s$ *are also plotted.*

Fig.8 shows an experimental transmittance spectrum (solid squares) obtained for sample RFS250 at $89°K$. The solid line is calculated from the $\eta(E)$, $a(E)$ data deduced from the analysis of this spectrum using the ideal sample approximation. The agreement is excellent. As an indication of the experimental accuracy we plot on

the same graph the measured transmittance T_s and the sum of the measured transmittance and reflectance, $T_s + R_s$ of the naked substrate (Corning 7059 glass). One notices that the experimental values of this sum are equal to 1 within 1% over the entire wavelength range of the spectra.

Additionally, one can observe that the transmittance maxima in the long wavelength limit are very close to the measured transmittance T_s of the naked substrate, in agreement with relation (1.37).

1.3.2 Sample imperfections

The analysis of the spectrum detailed above, assumes an ideal sample. Actual samples have imperfections that influence the optical spectra rendering the foregoing analysis generally invalid. In spite of that it remains a very good approximation for many actual samples, as effectively shown through Fig.8. In the following we present specific models for the most probable imperfections and we indicate their effect on transmittance. If one does not take into account sample imperfections and analyses the spectra in the ideal sample approximation, the deduced $a(E)$ curves show more or less important deviations from the true ones.

In order to understand qualitatively the role of various types of imperfection and obtain a quantitative estimate of their magnitude we have adopted the following procedure:

1) T-spectra are calculated using realistic $a(E)$, $\eta(E)$ input numerical functions and particular models of imperfection.

2) The calculated spectra are analysed in the ideal sample approximation.

3) We adjust the values of parameters that characterize the imperfections as to obtain $a(E)$ curves similar to the experimental ones.

This provide us with an approximate knowledge of the magnitude of sample imperfections and of the error one may make in estimating E_0.
Based on the understanding of the role of specific types of imperfections, we reach interesting conclusions from the data on the temperature variation of the absorption edge.

Variable thickness

The simplest case is a variable thickness throughout the illuminated area of the film. Swanepoel[18] suggests that the effect of thickness non-uniformity on the optical spectra is similar to that of more complex imperfections. Accounting for it, presents a more general interest.

The transmittance $\mathsf{T}_{\Delta d}$ at a specific photon energy is obtained by integrating the ideal transmittance T over a range of phase shifts determined by the average thickness $\bar{d}$ and the thickness deviation Δd

$$\mathsf{T}_{\Delta d} = \frac{1}{\phi_2 - \phi_1} \int_{\phi_1}^{\phi_2} \mathsf{T}\, d\phi \tag{1.47}$$

where

$$\phi_1 = 4\pi\eta\,(\bar{d} - \Delta d)/\lambda \tag{1.48}$$

$$\phi_2 = 4\pi\eta(\bar{d} + \Delta d)/\lambda \tag{1.49}$$

Examples of thickness deviation Δd are shown in Fig.9 for various particular forms of the illuminated surface.

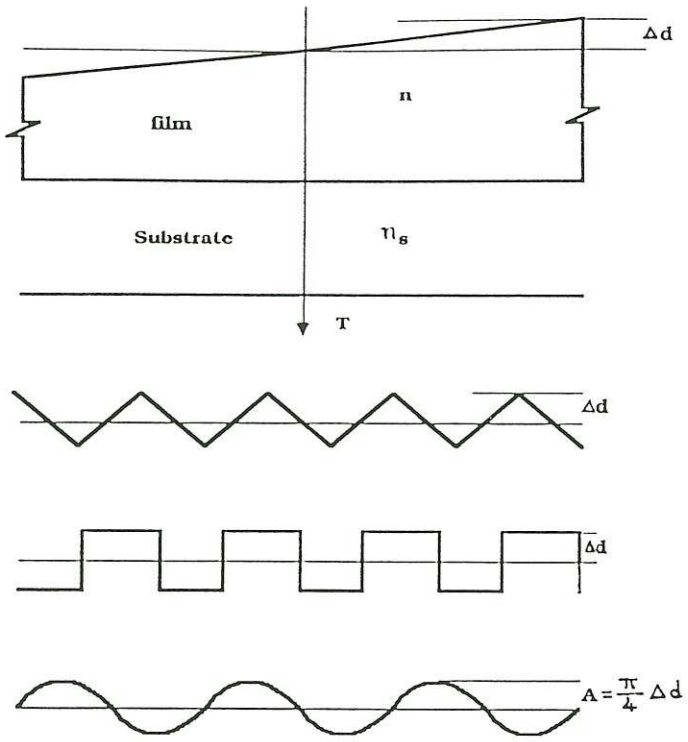

FIG. 9 *Schematic representation of various forms of thickness variations.*

Integration over a range of phases can, more generally, account for optical path variations within the illuminated area of the film whether these come from thickness or index non-uniformity. For the latter case we can write:

$$n = \bar{\eta} \pm \Delta\eta \tag{1.50}$$

Equation (1.47) is still valid if we modify the integration limits to

$$\phi_1 = 4\pi\,(\bar{\eta} - \Delta\eta)\,d\,/\,\lambda \tag{1.51}$$

$$\phi_2 = 4\pi\,(\bar{\eta} + \Delta\eta)\,d\,/\,\lambda \tag{1.52}$$

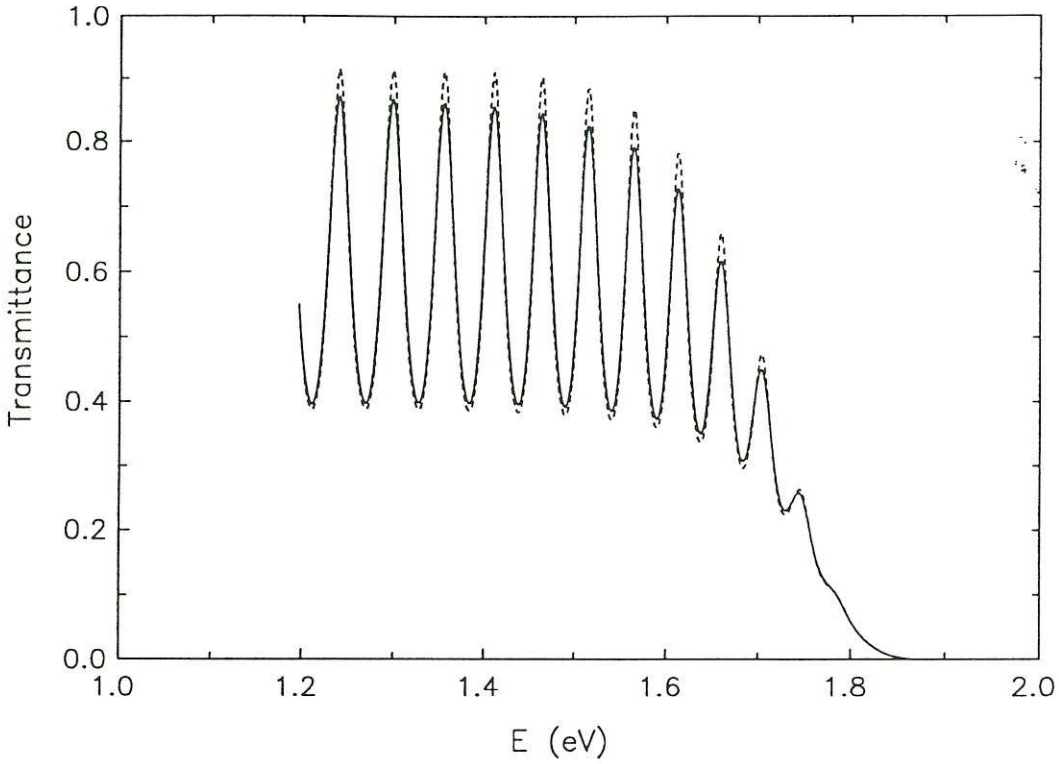

FIG. 10. *Calculated transmittance (solid line) of a film having thickness variations within ± 15 nm from an average thickness of 3 μm. The transmittance of an ideal film of 3 μm thickness is plotted for comparison (dashed line). a(E) and η(E) are identical for both cases and are plotted by dashed lines in Figs. 11 and 12 respectively.*

The combined effect of non-uniformity in the optical path and of absorption is shown in Fig.10. The transmittance of a non-uniform film, the solid line, is compared to that of the ideal film, the dashed line. The fringes shrink. Their amplitude is smaller for non-uniform film with higher T-values for minima and lower T- values for maxima. Figs.11 and 12 show the effect on $a(E)$ and $\eta(E)$ respectively, deduced from the T-spectra using the analysis presented in the beginning of this section. The lowering of T-maxima, which are used to calculate $a(E)$, creates an apparent absorption tail in the long wavelength limit (see Fig.11) and influences the slope at higher energy. The film property of interest to this study is precisely this slope, expressed as the Urbach parameter E_0. In the particular case plotted, one would calculate a value

for E_0 , higher by about 10% than the actual one corresponding to the dotted curve. Fig.12 shows the effect on the refractive index. The dashed line corresponds to the actual index. The agreement here is better. A slight apparent decrease of about 1% is observed. It is almost independent of energy.

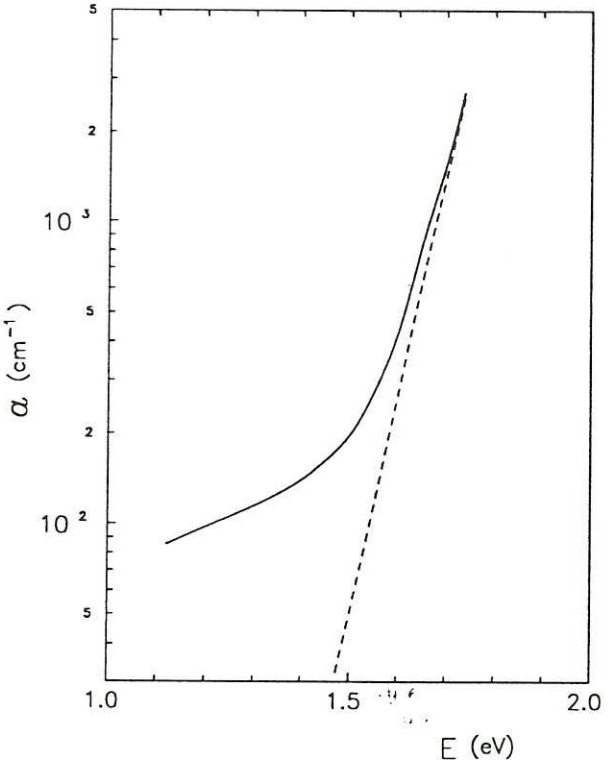

FIG. 11. *The absorption coefficient a(E) deduced in the ideal sample approximation, from the calculated spectrum of a non-uniform film, plotted in Fig.10. The actual absorption curve is plotted by a dashed line in orded to indicate the systematic error introduced by failing to take into account this particular type of imperfection.*

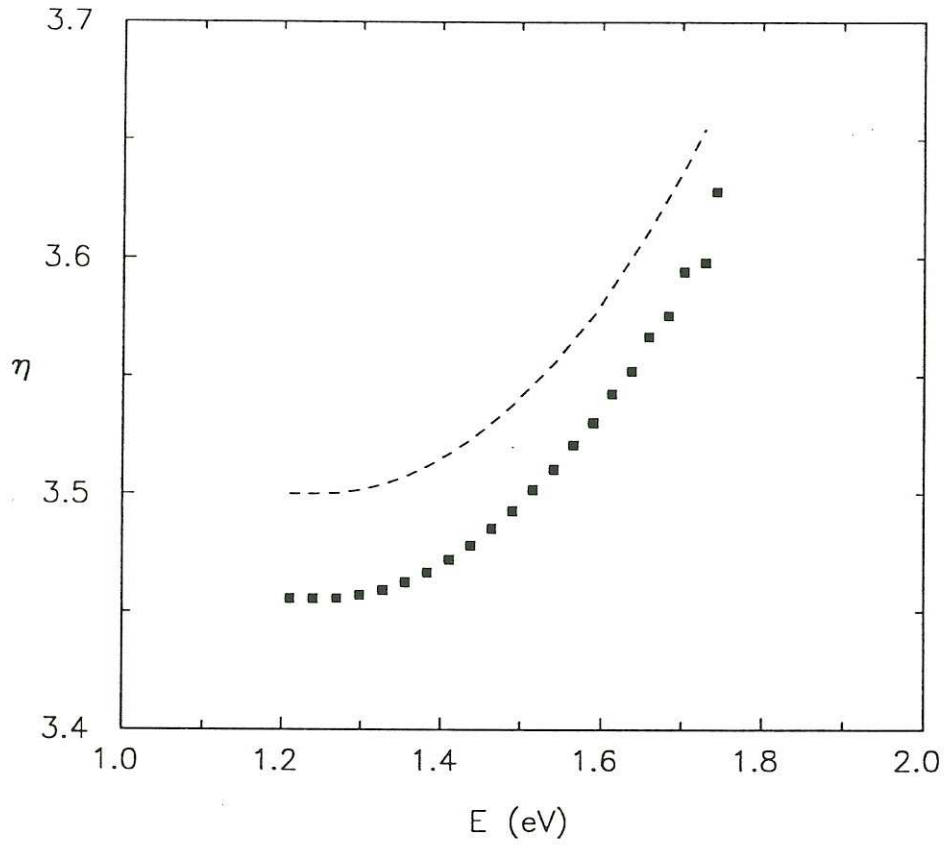

FIG 12. Refractive index (solid squares) extracted from transmittance spectrum of a sample with thickness variations within ±15 nm from an average thickness of 3 μm. In extracting η(E) (squares) we don't take into account the thickness variations. The dashed line is the actual index η(E). The actual absorption curve is the dashed line in Fig.11.

Surface roughness

Surface roughness is another common type of imperfection, present in actual samples. It characterizes interfaces with irregularities of various size and shape (Fig.13). Roughness scatters a plane wave. We have then to deal with specular and diffuse reflectance as well as direct (also referred to as specular by some authors) and diffuse transmittance. The specular reflectance is defined as the component of the scattered flux that obeys the laws of classical optics formulated for plane interfaces. It is directional and has the important property that it's phase is coherent. A similar definition applies to the direct transmittance. All remaining energy flux that is neither specularly reflected nor directly transmitted is said to be diffusely scattered. The diffuse reflectance is the component of the diffusely scattered flux contained in the 2π steradians above the free surface of the film (Fig.13). The diffuse flux contained in the 2π steradians below the free surface of the substrate (Fig.13), is the diffuse transmittance. The phase of both the diffuse reflectance and transmittance are incoherent.

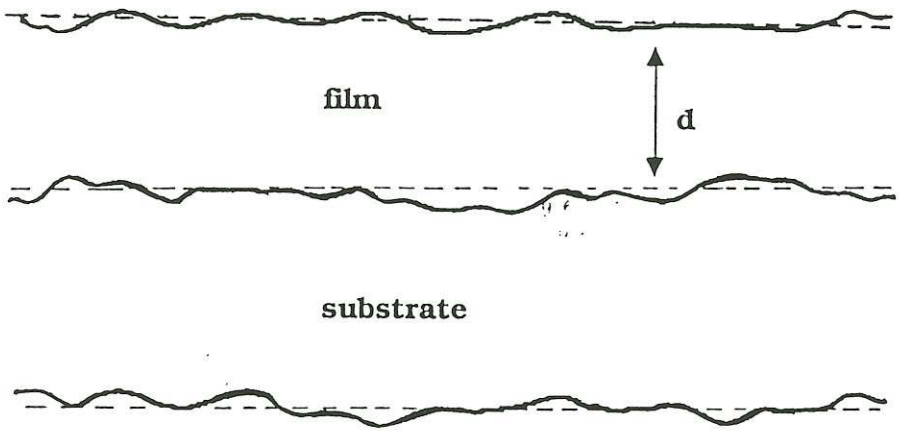

FIG 13. *Schematic representation of uncorrelated surface roughness on both free surfaces and at the interface between film and substrate. If present, surface roughness causes loss of light in diffuse scattering.*

A telltale sign of important surface roughness is a lower than 1 sum of R and T in the low energy, very low absorption, end of the spectrum caused by significant loss of light in diffuse scattering. The measured light loss for all the samples presented here, is so close to the experimental error limit ($< 1\%$) that one cannot speak of measurable roughness effect.

In order to evaluate the effect of surface roughness on the transmittance spectra, we have adopted the transfer matrix formalism[20] . The method does not require exact knowledge of the form of interfaces. A statistical description of their characteristics is sufficient. It assumes a fictitious mean plane, at each interface, around which the rough surface is distributed with zero mean value and standard deviation σ that is a measure of roughness. The calculation is performed at normal incidence in the limit of small σ ($\sigma \ll \lambda$).

All interfaces are assumed to be random in form, statistically independent and uncorrelated, obeying a Gaussian distribution. The distance between successive mean planes determines an average thickness for the embedded layer. Details on the formalism and assumptions of the method are given in Appendix C.

We have verified numerically that the effect of surface roughness on the trasmittance spectra cannot be qualitatively distinguished from the previously treated case of lack of uniformity in the optical path. If no significant loss of light is observed experimentally, one can safely use an apparent optical path variation within the illuminated area to account for roughness as well. This is convenient since actual films present both irregularities to some extend.

Index variation with depth

Index variations in the plane of the film can be accounted for by the non-uniformity optical path integration. On the other hand one expects significant variations of index along the direction of film's growth[19], especially in the vicinity of the substrate where both the structure and even the chemical composition may be different from those of the film's bulk. Even in the absence of any structural or chemical inhomogeneities, non relaxed stresses near the substrate-film interface can result in index variations along an axis perpendicular to the substrate's surface: the z axis.

We model this type of imperfection assuming a continuous function for the index $\eta(z)$ (Fig.14). We have used a realistic form of $\eta(z)$ with the bulk of the film characterized by a constant index η_0 and a transition layer near the substrate-film interface having a z dependent refractive index of the form:

$$\eta_{tl}(z) = \frac{\eta_0}{1 - b\,\eta_0\,z} \quad , \qquad 0 < z < \Delta d \tag{1.53}$$

where

$$b = \frac{\eta_{\Delta d} - \eta_0}{\eta_0\,\eta_{\Delta d}\,\Delta d} \tag{1.54}$$

$\eta_{\Delta d}$ is the index at the interface with the substrate. The sign of b denotes whether the variable index increases or decreases with z, near the interface with the substrate.

This particular form is chosen because of its convenience in solving exactly the wave equation for the system. It is representative of a near-linear variation of index between η_0 and $\eta_{\Delta d}$ in the transition layer. We expect very similar results for other functions with the same feature that would require numerical solution.

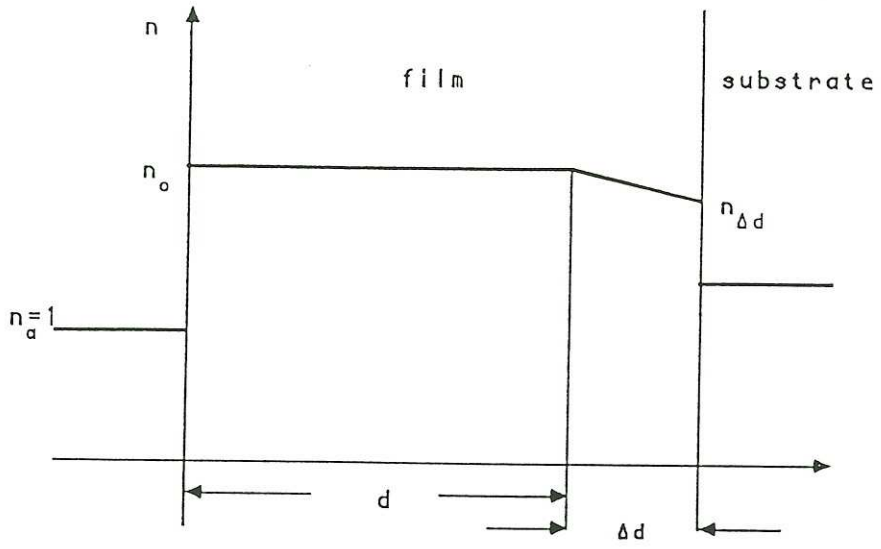

FIG 14. *Spatial dependence of the refractive, index assumed to interpret spectra of samples with interface stresses. The index is continuous. It is constant outside a transition layer having thickness Δd near the interface and may increase or decrease in the transition layer as well as we approach the substrate.*

Our calculation is not restricted to real indices. Absorption is taken into account through the imaginary counterparts of η_0 and $\eta_{\Delta d}$. Again with the transfer matrix formalism (Appendix D) we calculate transmittance at normal incidence. The effect of index variation with depth, on T-spectra, is shown in Fig.15. Squares and dots, correspond to interface index $\eta_{\Delta d}$ that is lower and higher respectively, than that of the bulk, η_0 . We adopt here a presentation different from the previous types of imperfections in order to better illustrate the effects observed on the spectra. We plot the envelope of transmittance in the absence of absorption. For reference the corresponding envelope (solid line) for uniform index is shown.

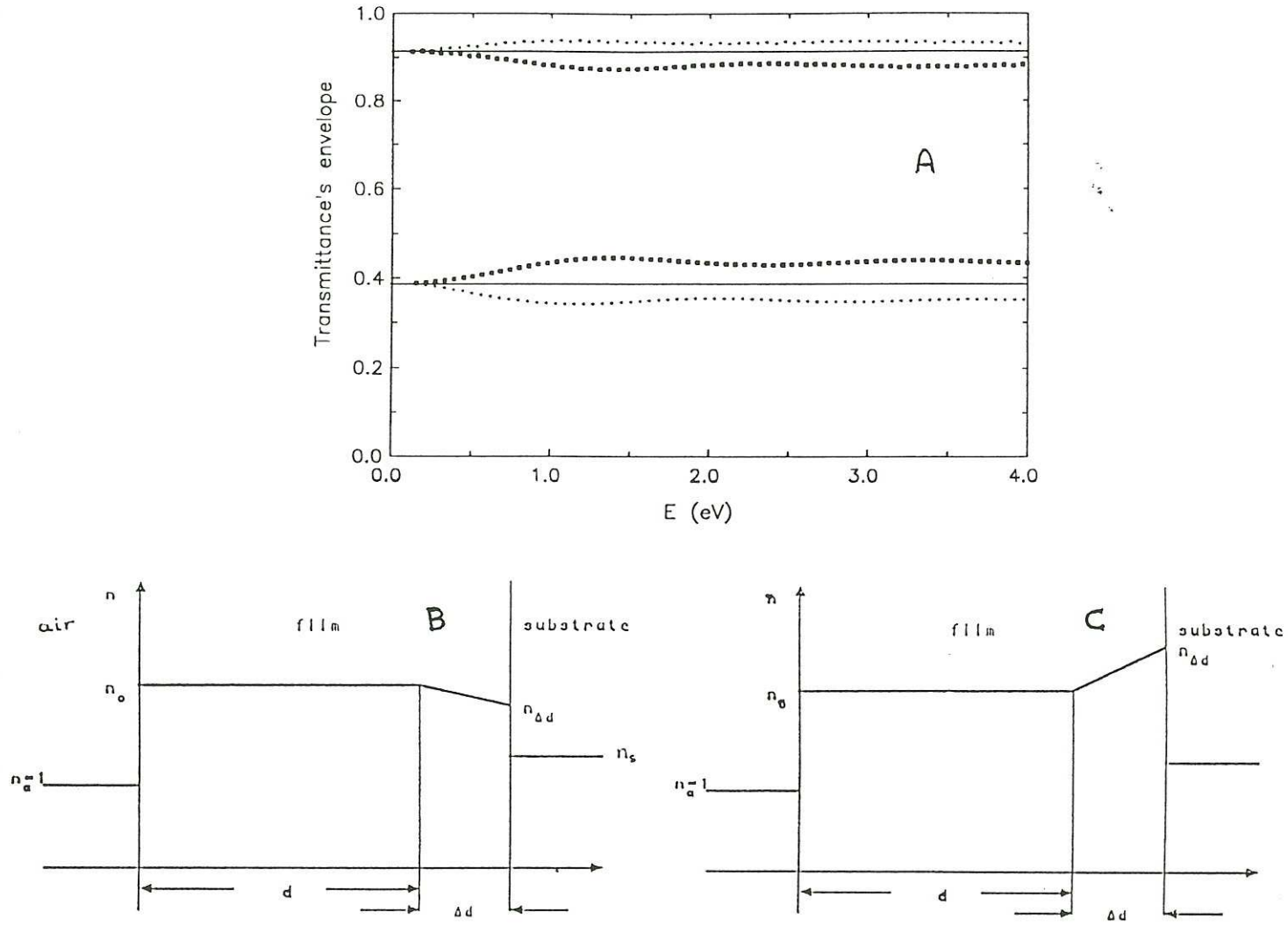

FIG. 15. *Calculated envelopes of the transmittance (graph A, squares and dots) of samples having index variation along the axis of growth (z-axis). The solid line corresponds to a uniform sample having constant index* η_0 *(see graphs B and C). The particular form of* $\eta(z)$ *assumed for each case is indicated in graphs B and C. The squares of graph A correspond to the index of graph B and the dots of graph A correspond to the index of C.* η_0*=3.5,* d*=2.9*μ*m,* Δd*=0.1*μ*m.* $\eta_{\Delta d} = 3$ *for graph B and* $\eta_{\Delta d} = 4$ *for C.*

One can verify numerically that successive fringes are equidistant in energy and

that the basic equation (1.45) holds provided that we substitute the integral: $\int_0^{d+\Delta d} \eta(z)dz$ for the optical path ηd.

The fringe-envelopes corresponding to z- dependent index exhibit oscillations (fringes) that are "slow", i.e. vary less rapidly with energy, in comparison to the "rapid" main fringes of the film. This is a pattern reminding beats. It has actually a similar origin, since we can think of it as resulting from interference of waves in two similar films differing only by the interface layer. We adopt the term beats for convenience. The beat amplitude is larger at long wavelength and decreases as E increases. The envelope value it tends to, at short λ, is significantly different from that of the uniform film.

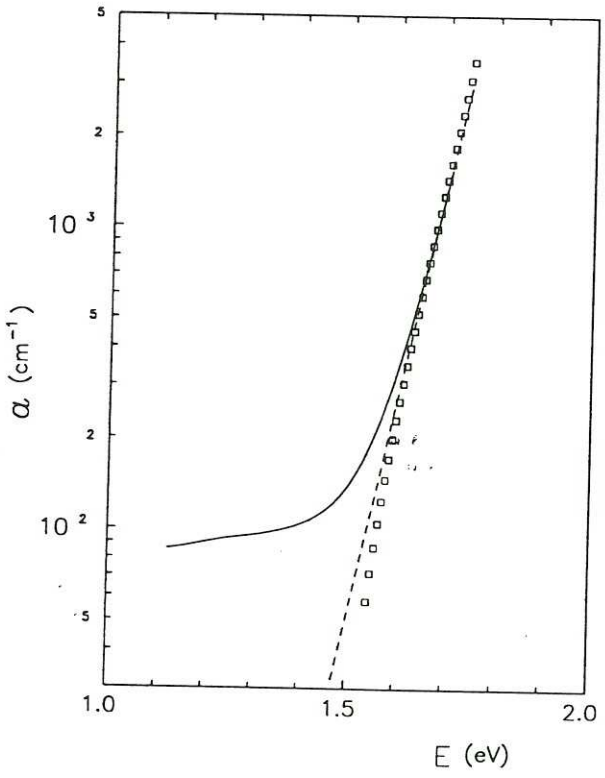

FIG 16. *Absorption spectra calculated in the ideal sample approximation for non-uniform index films. The solid line corresponds to increasing index near the interface and the squares to decreasing index. The functions $\eta(z)$ indicated on graphs B and C of Fig. 15 are used. The dashed line shows the actual absorption curve a(E).*

One observes a remarkable difference between the two cases. In the case of decreasing index near the substrate-film interface, (squares), the beat envelope is always contained within the uniform index envelope. The dotted line corresponds to an increasing index at the interface. In this case the beat envelope is always outside the envelope of the uniform film. When combined with energy dependent absorption, this particular index anomaly results in an apparent low energy dependence of the absorption coefficient, opposite to the tails caused by all other types of non-uniformity. This effect is illustrated by squares in Fig.16. Since this effect has never been observed in the analysis of the films we have measured, we conclude that the index at the interface with the substrate is lower than that of the bulk, by a smaller or larger amount, depending on the deposition technique and conditions.

1.4 Measurements of the Absorption and it's Temperature dependence in a-Si:H samples. Results and Discussion

In this section we present the results we have obtained on the temperature variation of optical parameters of a-Si:H films, derived from the analysis of experimental spectra. The method adopted for the analysis has been already discussed in section 1.3.1. The films measured, have been prepared by the RF-sputtering, reactive evaporation and glow-discharge deposition techniques. Table 1 gives the preparation conditions and thicknesses of four of them.

Sample	Deposition Technique	A_r / H_2 (mtorr/mtorr)	Substrate Temperature ($^{\circ}C$)	Thickness (μm)
RFS250	RF-sputtering	5.0/0.5	220	3.3
RFS220	RF-sputtering	5.0/1.0	250	3.4
RE79	Reactive evaporation	see ref.[33]	275	1.6
GD11	Glow discharge		250	

Table 1

In Figs.17,18,19 and 20, we show the absorption spectra that correspond to the four samples of table 1. Each figure illustrates absorption spectra obtained for different measurement temperatures. As shown by the curves of Figs.17,18 and 19, reactive evaporation and RF-sputtering samples (RFS250, RFS220, RE79) exhibit similar absorption spectra. For each specific temperature the common feature of the exponential rise of $a(E)$ is obvious for a - values between $\sim 10^2\, cm^{-1}$ and $\sim 10^3\, cm^{-1}$.

In the high absorption end, a slight bending of the curves denotes the onset of the Tauc region.

The apparent absorbtion tails in the low absorption end, originate from films' imperfections (see section 1.3.2). For a given sample, the absorption curve shifts, with increasing temperature, to lower energies (red shift) implying narrowing of the gap. However, the slope in the exponential region which is associated with the disorder, is little affected by temperature.

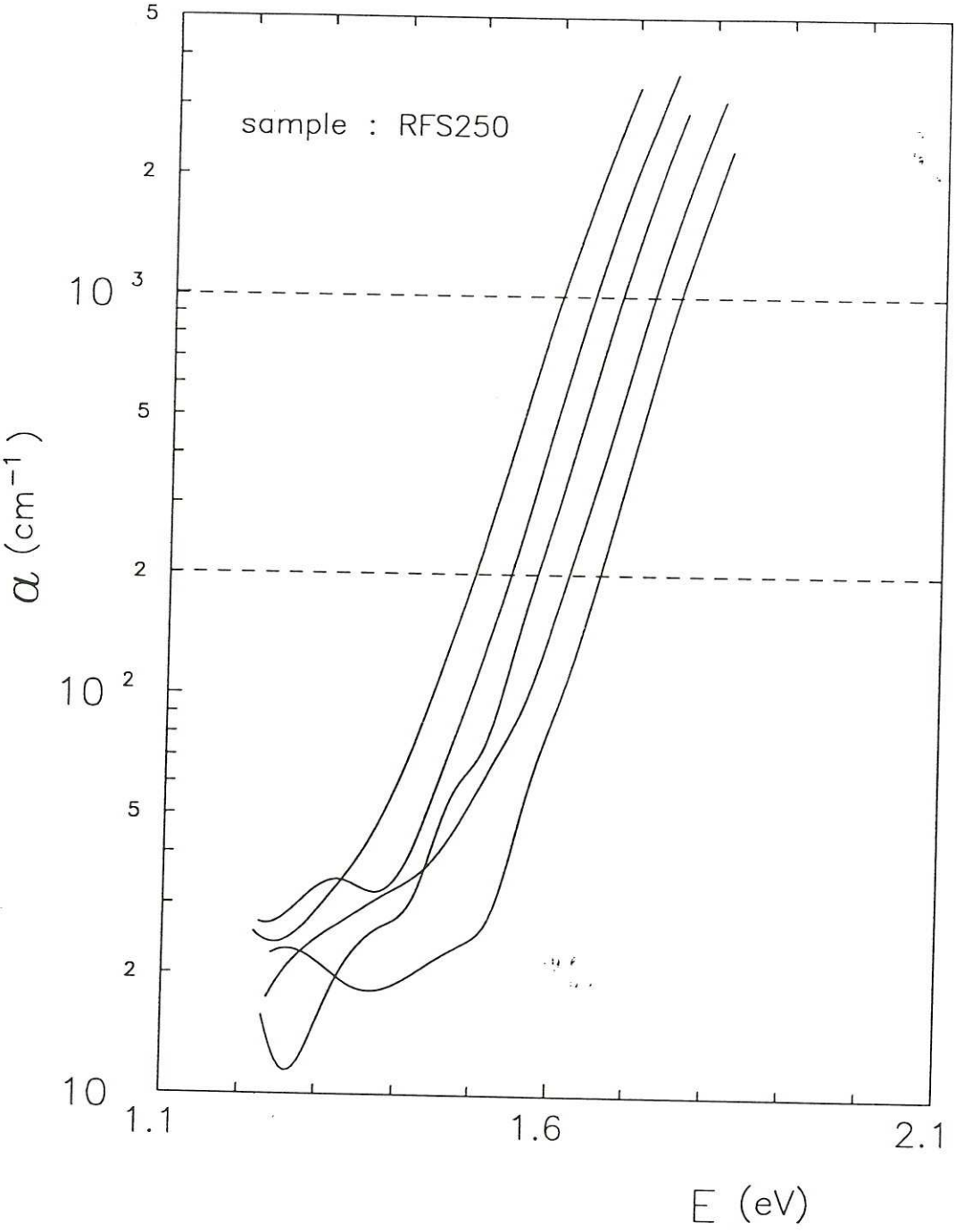

FIG. 17. *The absorption coefficient of sample RFS250 plotted versus photon energy for different measurement temperatures. From right to left: 89 °K, 189° K, 293° K, 374° K and 460° K. The dashed lines indicate the limits of absorption values used to determine* E_0.

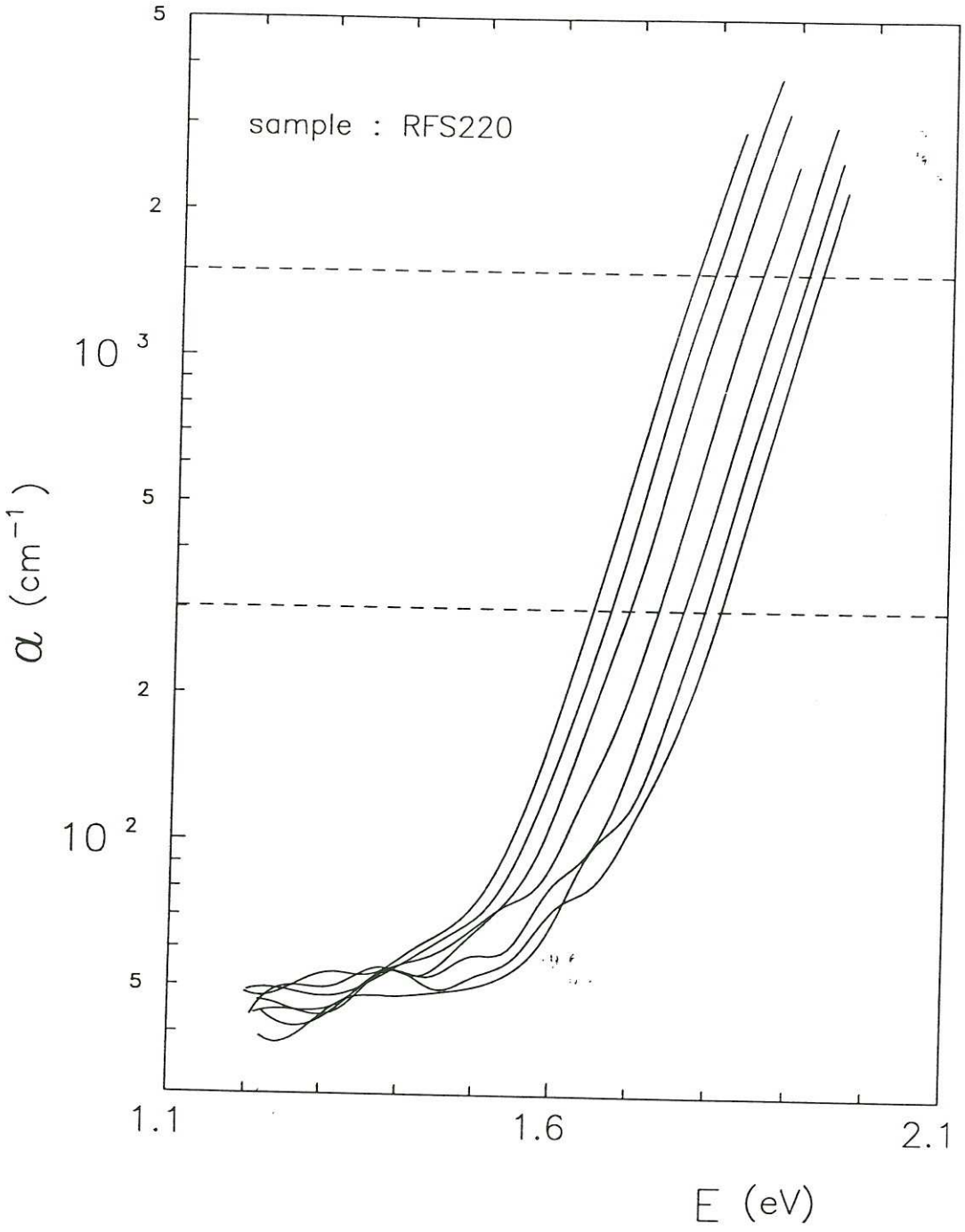

FIG. 18. *The absorption coefficient of sample RFS220 plotted versus photon energy for different measurement temperatures. From right to left: 88° K, 154° K, 219° K, 291° K, 368° K, 421 °K and 460° K.The dashed lines indicate the limits of absorption values used to determine* E_0.

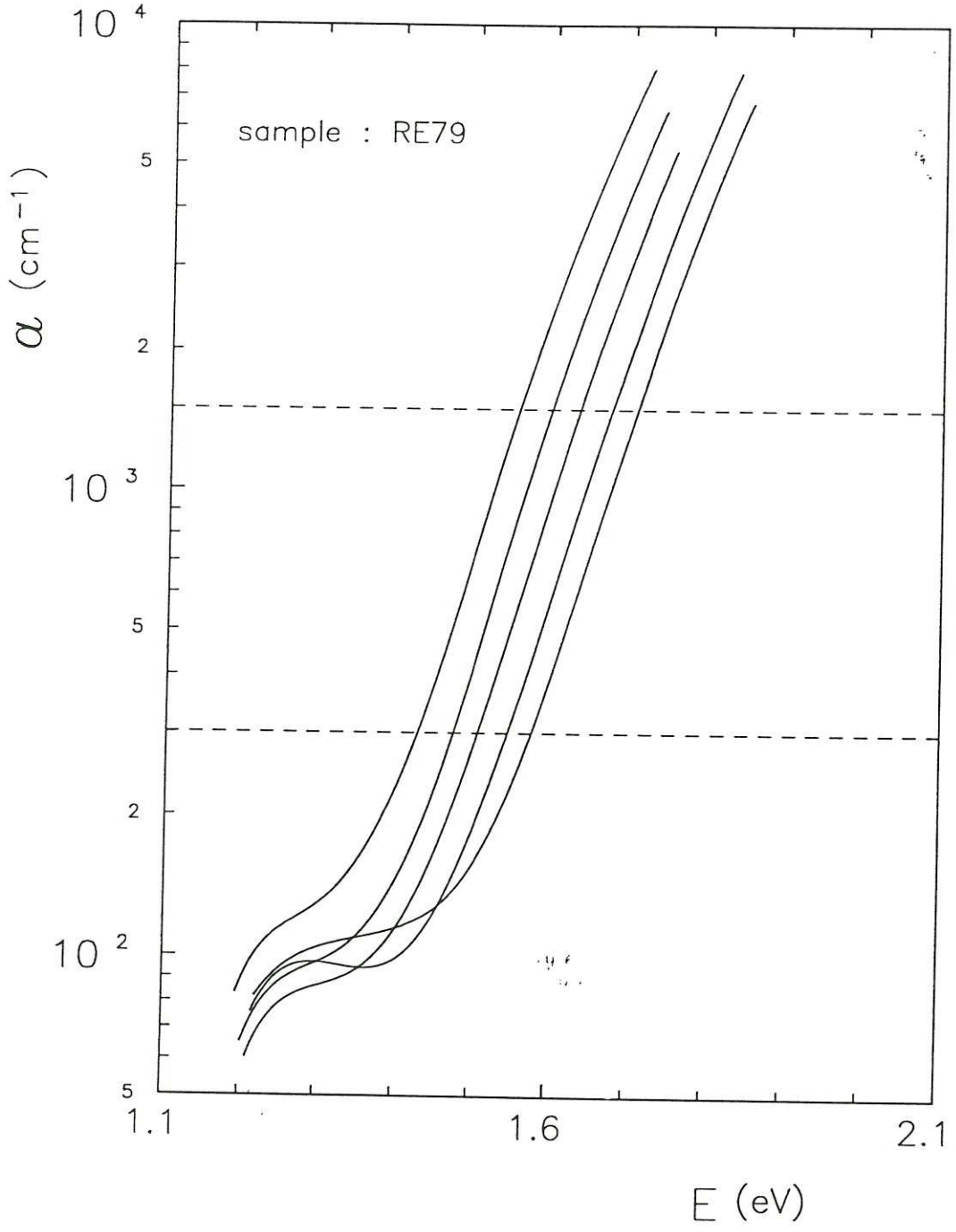

FIG. 19. *The absorption coefficient of sample RE79 plotted versus photon energy for different measurement temperatures. From right to left: 89° K, 195° K, 293° K, 378° K and 461° K. The dashed lines indicate the limits of absorption values used to determine* E_0.

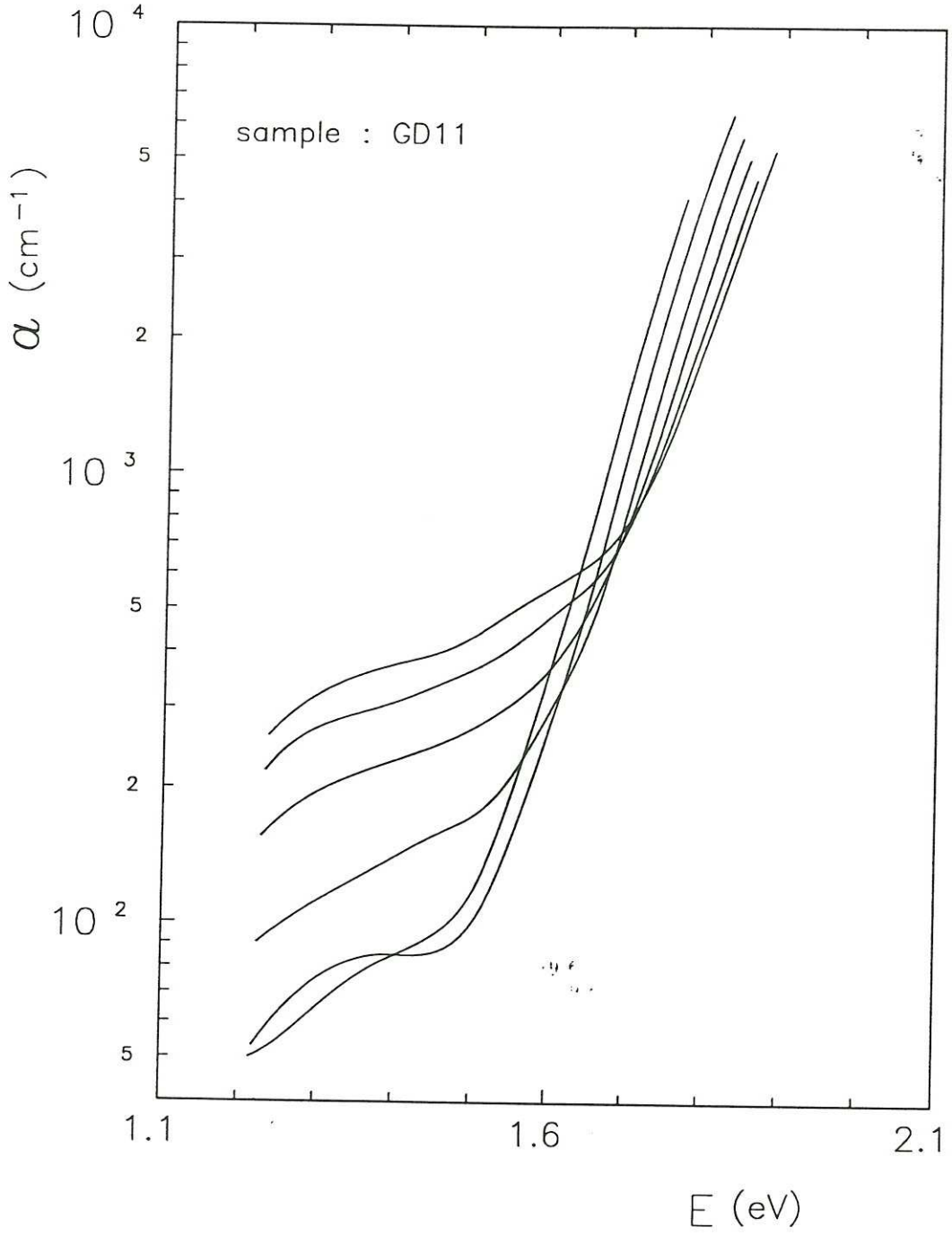

FIG. 20. *The absorption coefficient of sample GD11 plotted versus photon energy for different measurement temperatures. From right to left: 88° K, 152° K, 224° K, 294° K 369 °K and 426° K.*

In comparing the curves of Fig.17,18 and 19 with that of Fig.20, which corresponds to the glow-discharge sample GD11, we observe remarkable differences. The absorption spectra for GD11 are significantly distorted. Gradually, as temperature decreases, the characteristic feature of the exponential rise of $a(E)$ is hidden by large apparent absorption tails that grow at the low energy end of the curves. The tails become very long for curves at low T and cross the curves corresponding to higher T. The key-remark for the explanation of this behavior is that the effects become stronger as we move to temperatures away from $T_s = 250\,°C$ (the substrate's temperature during deposition).

It is well established that films deposited by glow-discharge have lower defect density than those produced by any other technique. By defects we denote here both dangling bonds and other types of structural inhomogenities as microvoids. An indication of the presence of the second type of defects in sputtered and evaporated films is a large IR absorption peak related to "di-hydride" sites i.e. two H atoms bonded to a single Si atom. GD films axhibit also the best properties from the point of view of device applications related to carrier transport and recompination.

It is also known that GD films contain large unrelaxed stresses. As these films are cooled from the deposition temperature, usually around 250 $°C$, to room temperature, relatively large stresses built at the interface with the substrate due to the difference in thermal expansion coefficients. The relatively low disorder and low defect density of GD films prevents stresses from being relaxed on the contrary to the sputerred or evaporated ones. Stresses near the film-substrate interface affect locally the refractive index of the films resulting in the reversible, temperature dependent, phenomena illustrated in Fig.20.

We plot in Fig. 21 (graph A) two $a(E)$ curves derived from calculated spectra, in order to show that realistic assumptions about the spatial and temperature

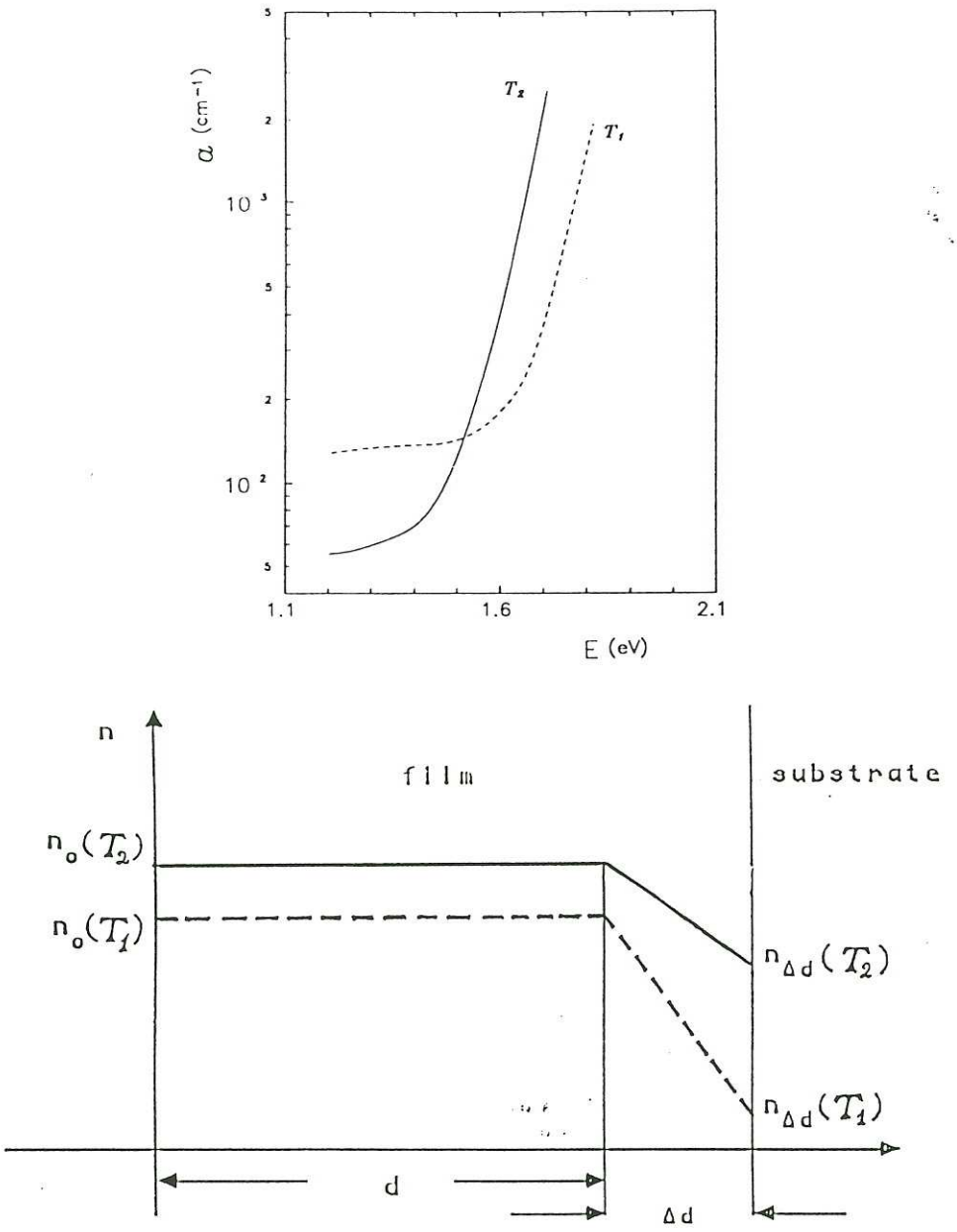

FIG. 21. *Calculated absorption curves (graph A) for the interpretation of the distortion of a(E) in the case of sample GD11 (Fig. 20) The basic assumption is that the difference between the index at the interface and that in the bulk, decreases as the measurement temperature approaches the deposition temperature of the film. In graph B we plot the $\eta(z)$ functions used to derive the corresponding type of curve (solid/dashed) of graph A.*

dependence of the refractive index in GD films, can produce curves similar to the experimental ones. We assume that, at two different arbitrary temperatures T_1 , T_2, $(T_1 < T_2)$, $\eta(z)$ obeys the curves plotted in graph B of Fig. 21 by dashed and solid lines respectively. We calculate the coresponding transmittance spectra and we analyze them in the usual manner. The curves of graph A are obtained. They have all the qualitative features of the experimental ones (Fig. 20).

Temperature variation of the gap

The gap E_g of amorphous semiconductors is not uniquely defined either theoretically or experimentally. Most common among the experimental definitions of E_g are the Tauc gap (section 1.1) and E_{03} .

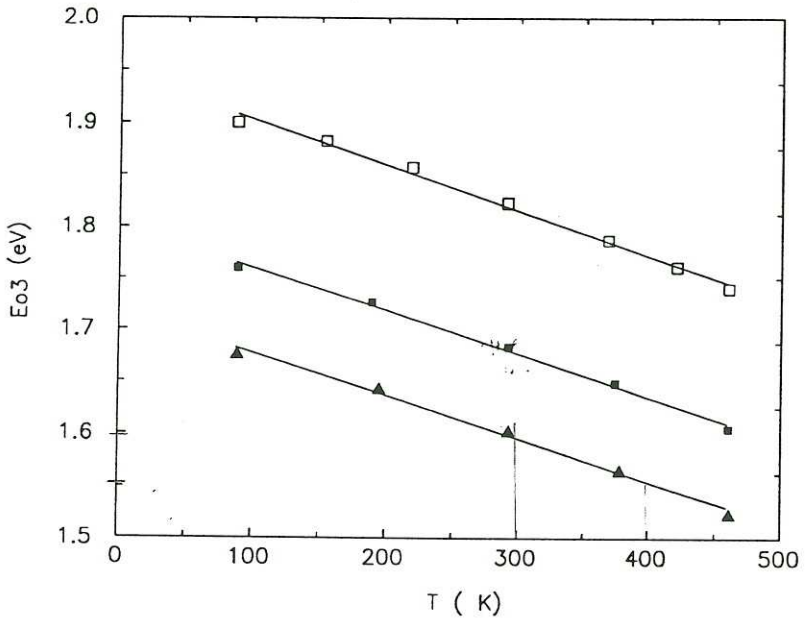

FIG. 22. *The temperature variation of the gap (E_{03}) of samples: RFS250(solid squares), RFS220(open squares) and RE79(solid triangles). The solid lines are linear least square fits to the experimental points. The corresponding temperature coefficients are:* -4.17×10^{-4} *eV/°K for RFS250,* -4.39×10^{-4} *eV/°K for RFS220 and* $-4.09\times10^{-4}eV/°K$ *for RE79.*

E_{03} is merily the energy at which the absorption coefficient becomes equal to $10^3\ cm^{-1}$. Whithin experimental error, both gaps change by the same amount ΔE with varying temperature. We have adopted E_{03} to indicate the temperature variation of the gap.

In Fig.22 the temperature dependence of E_{03} is illustrated. In all cases E_{03} decreases with increasing temperature. In the range of the measurements, $E_{03}(T)$ curves can be fitted by straight lines. The values for the slopes, $\frac{dE_{03}}{dT}$, are almost identical for all cases and agree very well with those measured by other workers[11,28] in a-Si:H films.

Temperature variation of the Urbach parameter

The Urbach parameter E_0 is a measure of disorder present in the film as discussed in section 1.1 . E_0 is derived by taking the inverse slope of $lna(E)$. On the graphs of Figs.17 through 19, we mark by dotted lines, parallel to the E-axis, the limits that bound the absorption data used for the determination of E_0 by linear regression.

In Fig.23, we plot E_0 values for various measurement temperatures for all samples of table 1 with the exception of GD11, since interfacial stress-related distortions of $a(E)$ in this sample would introduce large errors in E_0. Interface stress related distortions of the $a(E)$ curves prevent us from deducing E_0 . In all cases the temperature variation of E_0, if any, is very weak compared to that of the gap.

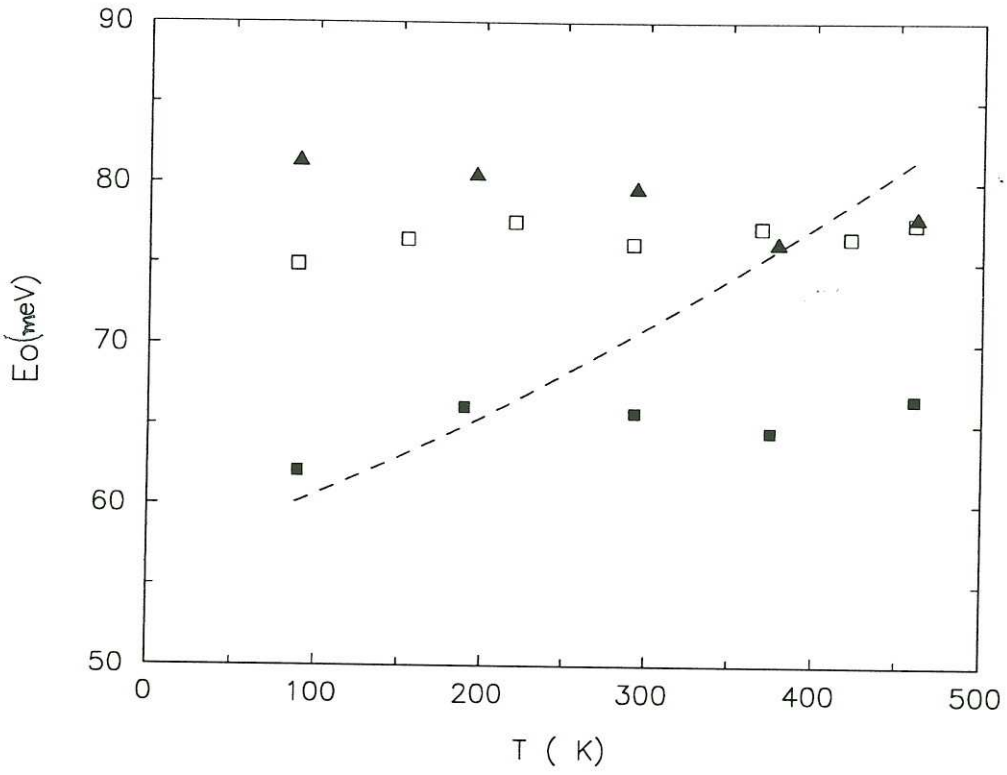

FIG 23. *The Urbach parameter E_0 for the samples of Fig. 22. The same symbols of Fig. 22 are used to indicate the data for the three samples. The dashed curve indicates the variation of E_0 that should be observed for sample RFS250 according to the correlation between the gap and the Urbach parameter proposed by Cody (see text).*

The best known and largely cited experimental study of the temperature variation of the Urbach parameter E_0 has been published by Cody and his coworkers [29]. Cody, using also optical transmission measurements, he obtained the thermal evolution of E_0 in a-Si:H films. Cody has tried to establish a common origin and manifestation of static and thermal disorder in a-Si:H. He has presented a family of absorption curves obtained at various measurment temperatures before annealing together with curves measured at $300\,°K$ after annealing at different stages. Annealing changes static disorder by releasing hydrogen from the a-Si:H network. He suggested that since, either static or thermal disorder are described through a single

family of curves, it is evident that they cause similar effects on the absorption. With increasing disorder, the band gap, E_g, decreases and the slope of the Urbach edge, E_0, increases. The latter varies in such a way as to cause all the absorption curves to converge on a single focal point $a_f = 1.5 \times 10^6\, cm^{-1}$, $E_f = 2.2\, eV$. In this way, Cody has extended the Urbach focus concept in amorphous semiconductors and has proposed a common phenomenological treatment of static and thermal disorder. Another way of presenting the data in support of his argument of common focus for both static and thermal disorder is a correlation plot between E_0 and E_g. Again he has used data taken at various measurement temperatures as well as after annealing at progressivety higher temperature. His plot indicates a strong correlation described by:

$$E_g = -6.2\, E_0 + 2.0\, eV \tag{1.55}$$

In order to compare our results with Cody's we use our experimental values $E_{03}(T)$ and we calculate the corresponding $E_0(T)$ assuming an Urbach focus at $2.2\, eV$, $1.5 \times 10^{-6}\, cm^{-1}$. In Fig.23, the dashed line corresponds to $E_0(T)$ calculated for sample RFS250. As can be seen, there is complete disagreement between the temperature dependence of E_0 proposed by Cody and our results. It is worth noticing that, in contrast to $E_0(T)$, our results conserning the temperature dependence of the gap *do agree well* with Cody's. This discrepancy is discussed in the light of the arguments presented below.

First of all, Cody's curves, taken before annealing, show no trend for converging on a single point. The supposed common Urbach focus for various measurement temperatures and various state of annealing derived, is stressed. On the other hand, our results are in agreement with those of other workers[30,31] who similarly do not observe such a strong effect in the temperature variation of E_0, as Cody does. Furthermore, our results are supported by resent experimental evidence based on a new technique

used for probing the density of electronic states (DOS), namely Total-Yield Electron Spectroscopy (TYES).

In TYES, incident UV illumination excites electrons from occupied states below the Fermi level E_f to energies above the vacuum level. As the optical excitation energy is scanned, the total number of photoemitted electrons within a window of kinetic energy is counted, yielding information on the DOS. The method makes it feasible to probe separetely the DOS of valence and conduction band-tail states. This is advantageous in comparison to optical absorption measurements which represent the convolution of both tails.

Aljishi *et al.*[32], using TYES , measured the energy and temperature dependence of both the conduction and valence band tails in a-Si:H films in order to deduce the role of thermal and static disorder on the tails. Their results clearly show that the broader of the two tails, the valence-band tail (VBT), is very little sensitive to temperature. In the range between $100\,°K$ and $500\,°K$, which is also the range of our measurements, the width of the VBT E_{0v} varies by less than $3meV$. Since in optical absorption measurements, the Urbach parameter E_0 reflects the width E_{0v} of the VBT (see section 1), we conclude that E_0 must change by the same magnitude as E_{0v} does.

The main conclusion of our experimental study is that the Urbach parameter E_0 of a-Si:H varies by less than 5 meV in the temperature range between $100°K$ and $500°K$. The same conclusion has been reached recently by Alishi *et. al.* using a completely different experimental method. This is certainly a much weaker temperature dependance of E_0 than that found by Cody, although we obtain very similar results on the temperature variation of the gap.

These results challenge the commonly accepted view based on Cody's work about the existence of a, so called, Urbach focus at around 2.2 eV for a-Si:H common for state and thermal disorder. In the light of our results, static disorder dominates by far thermal disorder in a-Si:H. In contrast to Cody's conclusion, we believe that the effect of temperature on the gap of a-Si:H cannot be attributed axclusively to a change of disorder. The magnitude of the temperature induced broadening of the absorption edge is comparable to that present in crystalline semiconductors although hidden by the large static disorder in the material.

Bibliography

[1] Pankove,J.:"OpticalProcesses in Semiconductors," p.34. Prentice-Hall,Englewood Cliffs,New Jersey.(1971)

[2] Wooten,F.:"Optical Properties of Solids."Academic Press,New York.(1972)

[3] J.Tauc: In optical Properties of Solids, ed. by F.Abeles (North-Holland, Amsterdam 1972)p.277

[4] F.Demichelis,E.Minetti-Mezzetti,A.Tagliaferro,E.Tresso,P.Rava,N.M.Ravindra: J.Appl.Phys. **59**(2),611 (1986)

[5] J.Bullot,P.Cordier,O.Gallais,M.Gauthier,F.Babonneau:J.Non-Cryst.Solids **68**,135-146, (1984)

[6] D.Redfield: Solid State Commun. **44**,1347,(1982)

[7] M.V.Kurik: Phys.Stat.Sol.(a) **8**,9,(1971)

[8] H.Y.Fan: Phys.Rev. **82**,6,900,(1951)

[9] P.B.Allen,M.Cardona: Phys.Rev.B **23**,1495(1981);B**24**,7479,(E)(1981)

[10] T.Skettrup:Phys.Rev.B **18**,2622 (1978)

[11] G.D.Cody,T.Tiedje,B.Abeles,B.Brooks,Y.Goldstein:Phys.Rev.Lett.**47**,1480 (1981)

[12] J.Tauc: Mat.Res.Bull. **5**,721 (1970)

[13] C.H.Grein,Sajeev John: Phys.Rev.B **39**,1140 (1989)

[14] E.N.Economou: 1stInt.Symp. on Phys.&Applic. of Amorphous Semic., ed. by F.Demichelis,(1987)

[15] John,S.,M.Y.Chou,M.H.Cohen,C.M.Soukoulis: Phys.Rev.B **37**,6963 (1988)

[16] John,S.,C.H.Grein: Rev.Solid State Sci. **4**, 1-59 (1990)

[17] M.Tran,H.Fritjsche,P.Stradins:MRS 1993 Spring Meeting, San Francisco

[18] R.Swanepoel:J.Phys.E:Sci.Instrum.**17**,896 (1984)

[19] R.Jacobsson in Physics of Thin Films,vol.8,Academic Press (1975)

[20] J.M.Edstman in Physics of Thin Films,vol.10,Academic Press (1978)

[21] R.Swanepoel:J.Phys.E:Sci.Instrum.,**16** ,(1983)

[22] O.Stenzel,V.Hopfe,P.Klobes:J.Phys.D:Appl.Phys.,**24**,2088 (1991)

[23] T.C.Poulick:Appl.Opt.,**25**,562 (1986)

[24] D.A.Minkov,P.H.Drashkova:Thin Solid Films,**191**,193 (1990)

[25] Y.Hishikawa,N.Nakamura,S.Tsuda,S.Nakano,Y.Kishi,Y.Kuwano: Jap.J.Appl.Phys.,**30**,1008,(1991)

[26] D.Ritter,K.Weiser:Opt.Commin.,**57**,336 (1986)

[27] J.C.Manifacier,J.Casiot,J.P.Fillard:J.Phys.E:Sci.Intstrum.,**9**,1002 (1976)

[28] L.Ley:Review

[29] G.Cody:"Semiconductors and semimetals"vol.21,ed.by J.Pankove,Academic Press (1984)

[30] E.Freeman,W.Paul:Phys.Rev.B **20**,716 (1979)

[31] S.Yamasaki:Phil.Mag.B **56**,79 (1987)

[32] S.Aljishi,J.Cohen,S.Jin,L.Ley:Phys.Rev.Lett.,**64**(23),2811 (1990)

[33] Y.Franghiadakis,P.Tzanetakis:J.Vac.Sci.Technol.A **7**(2),136 (1989)

Chapter 2

RANDOM MULTILAYER FILMS. TRANSFER MATRIX CALCULATION OF REFLECTANCE, TRANSMITTANCE AND LIGHT LOCALIZATION.

PHILOSOPHICAL MAGAZINE LETTERS, 1990, VOL. 62, NO. 4, 299–304

Reflectance of multilayer amorphous semiconductor films with random thickness layers

By A. KONDILIS and P. TZANETAKIS

Physics Department, University of Crete and
Institute of Electronic Structure and Laser,
Foundation for Research and Technology Hellas,
P.O. Box 1527, GR-71110 Heraklion, Greece

[*Received in present form 7 June 1990 and accepted 5 July 1990*]

ABSTRACT

Reflectance and transmittance spectra of amorphous semiconductor multilayer films were computed for layers of random thickness. This choice was prompted by the experimental results recently reported on hydrogenated amorphous silicon/silicon-nitride films in which the thickness of the lower bandgap material layers is randomly chosen. The calculation clearly elucidates the origin of a peculiar behaviour of the reflectivity observed in the spectral region of strong absorption.

§ 1. INTRODUCTION

A novel form of multilayered thin-film structure has been prepared and studied by Nitta, Itoh, Nonomura, Ohta and Morigaki (1989 and references therein). Two amorphous semiconductor materials with different optical band gap have been used: hydrogenated amorphous silicon (a-Si : H) and silicon nitride (a-$Si_{0.6}N_{0.4}$: H). The samples consisted of about 200 layers of the higher bandgap material, the nitride, referred to as the barrier layers, alternating with another 200 'well' layers of the lower bandgap semiconductor. The thickness of the barrier layers was constant at 40 Å. The well layers had a thickness randomly chosen, but obeying a Gaussian distribution, according to the above authors, with a central value of 20 Å and a standard deviation of 12 or 20 Å. These are denoted by 20 ± 12 Å and 20 ± 20 Å in the following. A reference sample with well and barrier layers of constant thickness, the regular superlattice, was also measured.

The scope of these experimental investigations seems to be the establishment of the effects that this form of one-dimensional disorder has on the gap states of films. Both amorphous and epitaxial random superlattices are very interesting systems for the study of the effects of disorder on classical and quantum mechanical wave propagation. In one study (Yamaguchi *et al.* 1987), the photoluminescence spectra and the optical gap of the random superlattice was compared to that of the regular one. Nitta *et al.* (1989) have reported two effects on the spectra of the reflection and transmission coefficients of these films. These are the distortion of the normal interference fringe pattern, in the longer wavelength region of the spectrum and a reflectance peak, in the shorter wavelength region. This peak seems to increase with increasing disorder according to these authors.

The fact that the well and barrier thicknesses are much smaller than the wavelength of the light in the spectral region studied, makes one sceptical about interpreting these effects as interference phenomena.

§2. Calculation method and assumptions

Our calculation is based on the matrix treatment of the reflection and transmission of a classical electromagnetic wave incident on a layered system (Knittl 1976). We have assumed that each layer has uniform and isotropic optical properties and is characterized by a different thickness and a different complex index of refraction n. Two components of the plane wave, travelling in opposite directions are considered. Let e_i be the electrical component of the incident wave and e_r that of the reflected wave, both at the film's free surface, and let e_t be the electrical component of the wave emerging from the substrate's free surface. At each wavelength, a system transfer matrix $\mathbf{S}$ is evaluated. $\mathbf{S}$ is defined by

$$\begin{bmatrix} e_i \\ e_r \end{bmatrix} = \mathbf{S} \begin{bmatrix} e_t \\ 0 \end{bmatrix}. \tag{1}$$

$\mathbf{S}$ is constructed from the phase matrices of the individual layers (i.e. the operators giving the phase shift and the attenuation of the waves upon traversal of the layer), and from the boundary conditions at the interfaces, in the form of admittance matrices.

The calculation is simplified by the assumption of normal incidence of the light. In most of the experimental set-ups for measuring reflection and transmission, the beams involved have small angles with respect to the normal and the results agree very well with calculations made for normal incidence.

Since the thickness of the substrate is usually orders of magnitude larger than that of the film, the corresponding interference fringes cannot, and need not, be resolved in any experiment. In the calculation of the spectra presented below we have taken this into account by treating the substrate incoherently. This is done by separating the thin film's contribution from that of the substrate in the system transfer matrix and by averaging over a substrate fringe in the energy domain. For this integration we made the justified assumption that all quantities concerning the thin film remain constant over one substrate fringe. The calculation data are shown for the reflectance r and the transmittance t defined by the relations

$$r = \langle |e_r/e_i|^2 \rangle, \tag{2}$$

$$t = \langle |e_t/e_i|^2 \rangle, \tag{3}$$

where the average, $\langle\ \rangle$, is computed over one substrate fringe in energy.

In order to calculate the reflectance and transmittance spectra over a given photon energy range, one must know the dependence of the complex refractive index (i.e. including the extinction coefficient), for both a-Si:H and a-$Si_{0.6}N_{0.4}$:H. For the purpose of qualitative comparison with the experimental results, $n(E)$ need not be known with great accuracy. Only the important features must be reproduced. The exact values can vary even from one sample to another, depending on the deposition conditions. For amorphous silicon we have taken as representative the data given by Cody (1984). The experimental spectra (Nitta *et al.* 1989) cover approximately the region from 1 to 4 eV. Our calculation was also limited to this region, since all the essential information is contained in it.

The absorption coefficient against energy data for the nitride were taken from the results of Morimoto, Tsujimura, Kumeda and Shimizu (1985). We have used for the real part of the nitride's index, $n_b(E)$, an analytical formula for a smooth transition between a low n value at the long-wavelength limit and a high one at higher energies.

This function gives an approximation for the index variation over the absorption edge of the nitride that is satisfactory for the purpose of this calculation. Thus

$$n_b^2(E) = \frac{n_{b,\min}^2 + n_{b,\max}^2}{2} + \frac{n_{b,\max}^2 - n_{b,\min}^2}{2} \tanh\left[\frac{(E - E_{1b}) - E_{2b}/2}{E_{2b}/2}\right], \tag{4}$$

where E_{1b} and E_{2b} are two parameters for the nitride that correspond approximately to the onset and the width, respectively, of the transition from a low to a high value of the refractive index, according to relation eqn. (4). We have taken the value of 2·2 eV for E_{1b}, which is the optical gap deduced from experimental data on the optical absorption of amorphous silicon nitride films (Morimoto *et al.* 1985). $n_{b,\min}$ is the long-wavelength limit of the refractive index of the nitride. Its value was estimated with the assumption that, at this limit, the average index of the entire film is a weighted average of the indices of the barrier and well layers according to the formula

$$n_{\min} = \frac{\sum d_w n_{w,\min} + \sum d_b n_{b,\min}}{\sum d_w + \sum d_b}, \tag{5}$$

where $\sum d_b$ and $\sum d_w$ are the sums of the thicknesses of all the barrier and well layers respectively.

The average index at the long-wavelength limit, $n_{\min}$ was deduced from the energy difference of two consecutive fringe minima of the experimental data (Nitta *et al.* 1989, fig. 4). The validity of eqn. (5) was confirmed by computing spectra of superlattices, both regular and random, with given values for the two indices and calculating from fringe extrema the average index in the same way as is done for the experimental spectra. $n_{w,\min}$ was taken equal to 3·5 (Cody 1984). Finally, we have chosen the values of $n_{b,\max} = 4$ and $E_{2b} = 4$ eV by an approximate fitting of the calculated spectra of regular periodic Si/SiN multilayers to the corresponding experimental data (Nitta *et al.* 1989). Concerning the substrate, we have assumed that it does not absorb light in the spectral region studied and that its refractive index is 1·5, an approximate value for fused silica, the substrate material used for the experiments.

The method of random selection of well layer thickness obeying a Gaussian distribution is not explicitly stated by Nitta *et al.* (1989). They mention that the minimum and maximum thickness of the well layers was 1 and 39 Å respectively (truncation). We have adopted the following procedure. A random number is selected in the 0 to 1 interval of the normalized derivative of a Gaussian probability distribution function for the thickness, having mean and standard deviation values of 20 Å and 12 or 20 Å respectively. The corresponding thickness is accepted if its value lies in the interval between 1 and 39 Å. If it does not, two cases have been examined. In the first, the layer thickness is rejected and selections continue until the total number of desired layers is obtained. In the second, all layers having thicknesses outside the 1 to 39 Å range are given the thickness of the respective limit. Both methods yielded very similar results.

§ 3. Results obtained and discussion

We have plotted in fig. 1 the calculated reflectance (solid lines) and transmittance (dashed lines) spectra for two superlattices. Figure 1 (*a*) corresponds to a regular superlattice of 205 a-Si : H layers, 20 Å thick, alternating with 206 a-$Si_{0.6}N_{0.4}$: H layers with a thickness of 40 Å. The spectra of fig. 1 (*b*) correspond to a superlattice with all the characteristics of the previous one except for the thickness of the well (a-Si : H) layers which is randomly chosen at 20 ± 12 Å.

Fig. 1

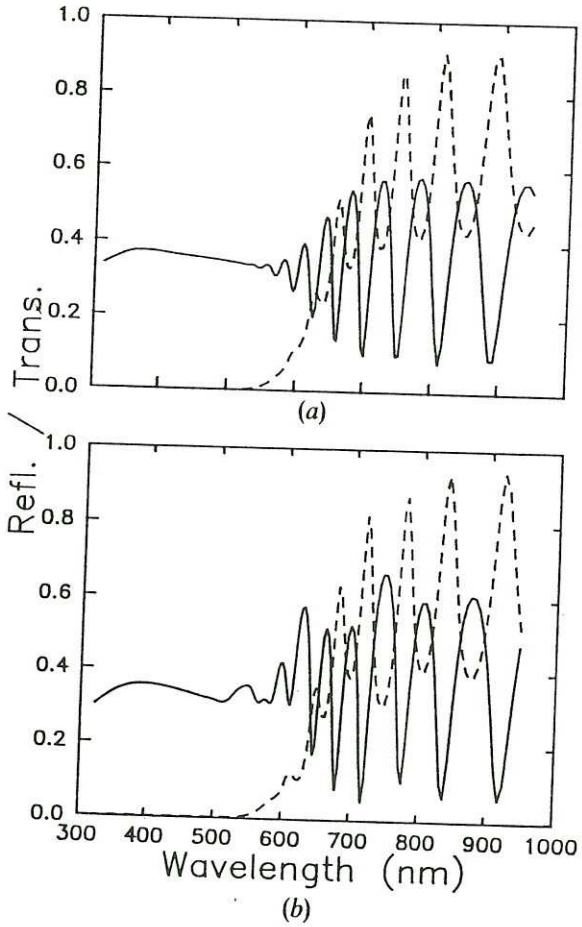

Reflectance (solid lines) and transmittance (dashed lines) spectra of a-Si:H/a-$Si_{0.6}N_{0.4}$:H multilayer films. (*a*) Constant thickness layers; (*b*) random thickness of a-Si:H layers.

The agreement of the calculated spectra with the experimental ones is surprisingly good. Both effects observed experimentally are present: a significant distortion of the interference fringe pattern as well as the rather broad reflectance maximum, in the strong absorption region of the spectrum.

We have plotted in fig. 2 the calculated reflectance spectra obtained for random multilayers 20 ± 12 Å for I and II and 20 ± 20 Å for III and IV. The only difference between I and II and between III and IV is a different random number sequence for the well layer thickness. The amplitude of the 'disorder' peak increases on the average with increasing standard deviation, but the variation from one sample to the other is also very important.

The assumptions of our calculation and the striking similarity of the experimental and calculated spectra do not leave any doubt that all the effects observed by Nitta *et al.* (1989) are due to interference phenomena. We believe that the probability of significant clustering of thin and thick layers in the film can give variations of the average index that will correspond to much thicker layers than the 20 or 40 Å building blocks of the superlattice. The probability of 'thickness clustering' is non-negligible in the systems studied experimentally and reproduced in this calculation. The large standard

Fig. 2

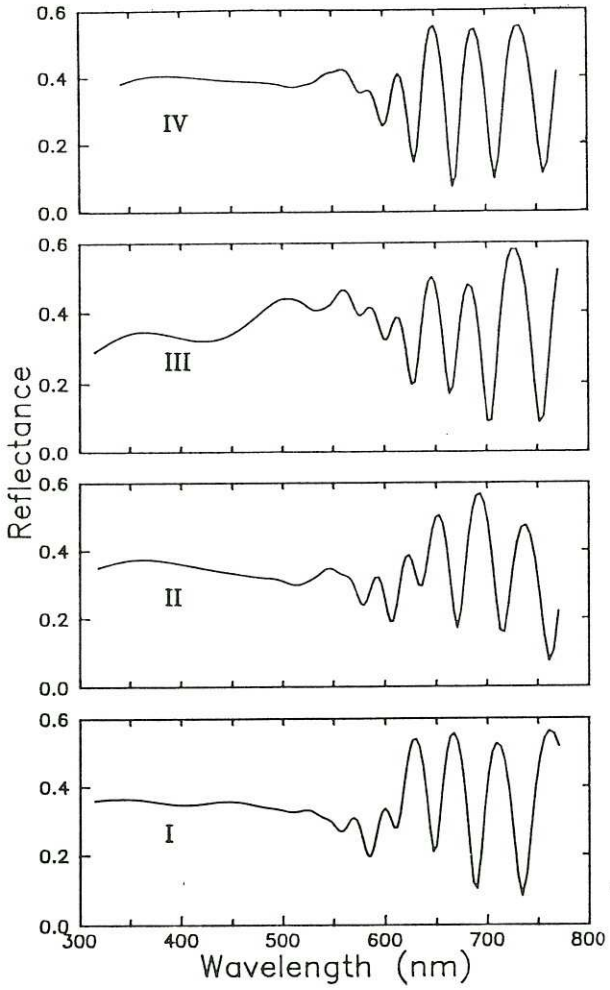

Reflectance spectra of random superlattices with well layer thickness of 20 ± 12 Å (I and II) and 20 ± 20 Å (III and IV). Spectra with the same standard deviation differ in the random thickness sequence.

deviations, the truncation of the layer thickness between 1 and 40 Å and a limited total number of layers, cannot yield a distribution even vaguely resembling a Gaussian. A surprising fact remains. Both the experiment and the calculation show that the interference structures on the reflectance spectra of this type of multilayered films can extend very far into the high-absorption-energy region. The reader is referred, more specifically, to spectrum III of fig. 2 for this effect. In our opinion, the observation of a difference in the optical bandgap (Tauc gap) in the random multilayer film relative to the regular one, reported by Yamaguchi *et al.* (1987) is probably due to the fact that, for the random superlattice, one cannot make the usual assumption that the light reflected by the film is constant over the wavelength range of a typical Tauc plot.

§4. Conclusion

The reflectance spectra of random thickness amorphous multilayer films obtained by a classical wave-propagation calculation in these media, show the effects observed

experimentally (Nitta *et al.* 1989). Among these the most interesting seems to be the structure, often manifested as a broad maximum, in the strong-absorption region, at wavelengths at which no interference fringes appear in regular superlattices with the same layer types. In interpreting experimental data on the absorption edge of random multilayer films one must take into account these effects.

References

CODY, G. D., 1984, *Semiconductors and Semimetals*, vol. 21, edited by J. Pankove (New York: Academic), chap. 2.

KNITTL, Z., 1976, *Optics of Thin Films* (New York: Wiley).

MORIMOTO, A., TSUJIMURA, Y., KUMEDA, M., and SHIMIZU, T., 1985, *Jap. J. appl. Phys.*, **24**, 1394.

NITTA, S., ITOH, T., NONOMURA, S., OHTA, H., and MORIGAKI, K., 1989, *Phil. Mag.* B, **60**, 119.

YAMAGUCHI, M., OHTA, H., OGIHARA, C., YOKOMICHI, H., MORIGAKI, K., NONOMURA, S., and NITTA, S., 1987, *J. non-crystalline Solids*, **97/98**, 931.

Numerical calculations on optical localization in multilayer structures with random-thickness layers

A. Kondilis and P. Tzanetakis
Physics Department, University of Crete, Crete, Greece
and Institute of Electronic Structure and Laser, Foundation for Research and Technology, Hellas, P.O. Box 1527, GR-71110 Heraklion, Greece

(Received 24 February 1992; revised manuscript received 25 June 1992)

A study of localization effects in random, one-dimensional optical systems is presented, based on calculations in superlattices with random-thickness layers. A numerical treatment of the problem of electromagnetic wave propagation in these systems is employed with a transfer-matrix formalism. A localization length l is determined numerically in each case. In order to ensure that the computation results have more general validity in as wide a range of wavelengths as possible, there was no restriction imposed on the number of layers necessary to obtain the value of l with a given accuracy. Appropriate dimensionless variables have been used that greatly simplify the presentation of results. The numerical calculation gives interesting hints about the dependence of the localization length on the gap structure of the corresponding regular superlattice, i.e., the one formed by reducing to zero the standard deviation of layer thickness. This dependence is more intricate than a simple broadening of the regular's gaps, a creation of band tails, induced by disorder.

I. INTRODUCTION

The propagation of light in random media is a topic that has recently received considerable attention.[1–7] The work presented here is the continuation and generalization of calculations we have performed[8] that have successfully accounted for features observed experimentally on the reflection spectra of amorphous multilayer structures, consisting of alternating "well" (w) layers of a-Si:H and "barrier" (b) layers of a-$Si_{1-x}N_x$:H.[9,10] In the previously mentioned studies, the well layers had thicknesses chosen randomly from a Gaussian distribution. In this case, the randomness parameter is the standard deviation σ_{dw} of the well layer thickness distribution.

The study mentioned above[8] and subsequent publications[11] have raised several important questions regarding the effect of electromagnetic wave *localization* in random superlattices. We use the term localization to denote an exponential attenuation of wave amplitude versus depth that is not due to absorption. This effect is often referred to as *strong localization*. In the first place, it is not clear when this term can be used to describe phenomena observed in the reflectance and transmittance spectra of random multilayer structures. In this respect, the number of layers in the superlattice may not be the only relevant parameter that sets a border line, even a vague one, between microscopic and macroscopic systems. In the former, it is more appropriate to speak about random interference effects, whereas, in the latter, localization can be detected unambiguously.

A second group of questions concerns the dependence of the localization length on the frequency of light. Does this dependence follow a predictable pattern? What are the energy regions that are most affected by disorder? Are there particular energies at which, for a given random sequence, the localization length is much lower or much higher than that of neighboring energies?

A third question is related to the interplay of three different effects resulting in exponential attenuation of the wave in the superlattice, namely, Bragg reflection (optical band gaps), disorder, and absorption.

II. ASSUMPTIONS AND METHODS OF CALCULATION

The multilayer structures or superlattices studied consist of alternating layers of lower and higher index material termed "barrier" and "well" layers, respectively. In order to make the numerical calculations more realistic, we have considered a superlattice (SL) deposited on a dielectric substrate. In each case, we have been interested in three SL's related to each other: the *regular* that has well and barrier layers with constant thickness d_w and d_b, the *random well* that has constant thickness d_b for all the barrier layers and well layers with thickness $d_{w,k}$ (k is the layer pair index) chosen randomly from a Gaussian distribution around d_w and, finally, the *all random* that has random thicknesses, around the values of the corresponding regular, for both types of layers.

In the absence of absorption, regular superlattices exhibit frequency spectra with regions of free propagation for the wave interrupted by photonic gaps. Within the gaps, the mean value of amplitude envelope of the wave decays exponentially with depth. This is not an exact statement since the mean envelope in the same layer is constant. Nevertheless, if we plot it versus the distance from the free surface of any given position within the superlattice period, we find an exponential variation.

The mean amplitude envelope decays exponentially with depth at any frequency in all the random superlattices studied. Since we are interested in the effect of ran-

domness on wave propagation both outside and within the gaps of the corresponding regular SL, we use the term localization length to denote the decay constant for both random and regular SL's.

All calculations presented assume normal incidence of light. We start from the "exit" surface: the interface between the SL and the substrate. This interface is the origin of an axis z having direction opposite to that of the incident wave.

We follow the evolution of the electric field inside the medium using *refraction* and *phase matrices*.[12] A phase matrix is defined by

$$\begin{bmatrix} E_m'^{+} \\ E_m'^{-} \end{bmatrix} = U_m \begin{bmatrix} E_m^{+} \\ E_m^{-} \end{bmatrix} , \tag{1}$$

where m denotes a layer of either well or barrier type, the E's are the electric field components at one end of the layer, the one that is closer to the substrate, and the E''s are the components at the other end. The plus/minus signs designate waves traveling in opposite directions. The plus sign labels the wave component traveling in the direction of incidence.

A refraction matrix at the interface between layers $m-1$ and m is defined by

$$\begin{bmatrix} E_m^{+} \\ E_m^{-} \end{bmatrix} = W_{m-1/m} \begin{bmatrix} E_{m-1}'^{+} \\ E_{m-1}'^{-} \end{bmatrix} . \tag{2}$$

In most of the calculations, we have assumed inside the substrate a zero value for the reflected component (superscript minus) of the electric field and unity value for the transmitted. It was verified that neither this assumption nor the substrate index affect in any significant way the results obtained for l.

The refraction matrix has the form

$$W_{m-1/m} = \frac{1}{2} \begin{bmatrix} 1+n_{m-1}/n_m & 1-n_{m-1}/n_m \\ 1-n_{m-1}/n_m & 1+n_{m-1}/n_m \end{bmatrix} \tag{3}$$

and the phase matrix is

$$U_m = \begin{bmatrix} e^{i\varphi_m} & 0 \\ 0 & e^{-i\varphi_m} \end{bmatrix} , \tag{4}$$

where n_m and φ_m are, respectively, the refractive index and phase shift inside layer m.

The electric-field amplitude oscillates with z inside the SL. In order to determine the localization length, we first find the positions and values of the extrema of the electric-field amplitude. Next, we compute the mean envelope amplitude E_0. It is defined as the mean value between one maximum or minimum and the linear interpolation between its adjacent minima or maxima, respectively. This value is attributed to the z position of the central extremum. l is obtained from linear regression on $\log_e(E_0)$ versus z, in a range of 8 orders of magnitude of E_0. This range may, *a priori*, seem excessively large for the determination of an average exponential decay length. It becomes evident in the analysis of the computation results that follows that it is not.

In the case of random SL's, the results may depend on the particular random sequence (RS) used for the calculation. Nevertheless, in plotting and comparing results for different RS's, convenient combinations of the average thicknesses $\langle d_w \rangle$, $\langle d_b \rangle$, the standard deviations δd_w, δd_b of the layers and the refractive indices n_w, n_b can be used. As can be seen from (3) and (4), it is the phase shifts and the ratio of indices that enter the calculation. Based on the above remarks, we have chosen the following set of variables: Z, σ_w, σ_b, c_n, φ, c_φ, where

$$Z = z/(\langle d_w \rangle + \langle d_b \rangle) , \tag{5}$$

$$\sigma_w = \delta d_w/(\langle d_w \rangle + \langle d_b \rangle) \tag{6a}$$

and

$$\sigma_b = \delta d_b/(\langle d_w \rangle + \langle d_b \rangle) , \tag{6b}$$

i.e., Z, σ_w, and σ_b are measured in units of the average SL period

$$c_n = n_w/n_b , \tag{7}$$

$$\langle \varphi_b \rangle = \frac{2\pi n_b \langle d_b \rangle}{\lambda} , \tag{8a}$$

and

$$\langle \varphi_w \rangle = \frac{2\pi n_w \langle d_w \rangle}{\lambda} , \tag{8b}$$

where λ is the vacuum wavelength of light.

$$c_\varphi = \langle \varphi_w \rangle / \langle \varphi_b \rangle \tag{9}$$

Finally, in order to simplify the notation we take

$$\varphi = \langle \varphi_b \rangle . \tag{10}$$

The localization length l is also expressed in units of the average SL period. A value of 2 for c_n is used in all calculations presented here.

III. COMPUTATION RESULTS FOR THE LOCALIZATION LENGTH

Figure 1 shows a typical semilogarithmic plot of $E_0(z)$ in a case of relatively weak localization. Despite the large fluctuations observed, the overall exponential variation with depth is apparent. A linear fit on these data yields a localization length of 3250 average SL periods. There are regions in the random-thickness sequence where the wave propagates more freely than in others. The size of these regions can be large compared to l. In the lower left part of Fig. 1, one such region extends over about 15 000 SL periods. The extent of and average wave attenuation in these regions depend on the particular random sequence used.

We have found that the best way to identify, unambiguously, an exponential decay and to determine with confidence l is not to restrict the number of layers that enter the calculation, but to stop when the ratio of entrance to exit amplitudes has reached a given value. We have chosen 10^8 as a sensible compromise between accuracy and computation length. In the case of large σ_w, near the gap edges, l is of the order of 10. The number of

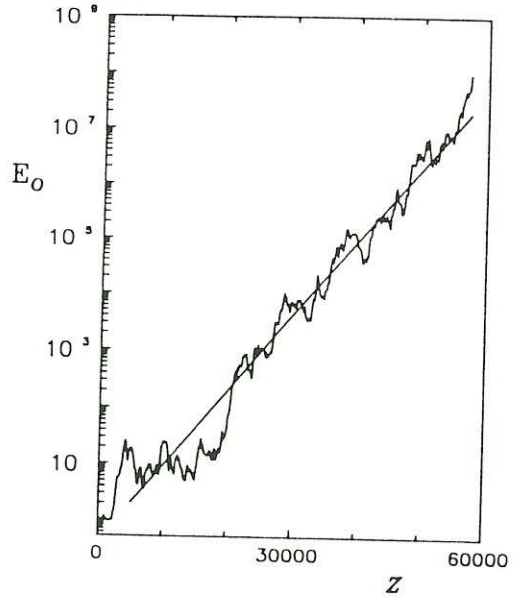

FIG. 1. Mean amplitude envelope E_0 vs distance from the substrate-superlattice interface, for a random-well superlattice. $c_n=2$, $c_\varphi=1$, $\varphi=0.05\pi$, $\sigma_w=10/60$ (see text for symbols). The localization length, calculated by linear regression on this curve, is 3250 average SL periods. Z is expressed in average SL periods.

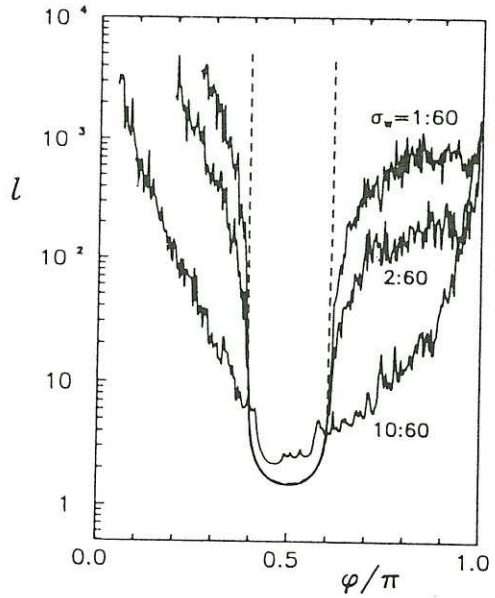

FIG. 2. Localization length l in units of the average SL period, vs φ in the first zone ($0<\varphi<\pi$), for three random-well SL's with different normalized thickness standard deviation σ_w shown with each curve. $c_\varphi=1$ and $c_n=2$. The dashed curve is the plot of $l(\varphi)$ for the corresponding regular SL.

layers that correspond to a ratio of 10^8 decreases significantly and l obtained may be strongly dependent on the particular sequence. We have verified, then, that ratios of 10^{16} and 10^8 yield similar values for l.

It is expected that $l(h\nu)$ or $l(\varphi)$ in the units we have defined above depends strongly on the proximity of a photonic gap. In a regular SL with two types of layers, one can distinguish between *tuned* and *detuned* structures.[12] Tuned SL's have a ratio c_φ that is the quotient of two small integers. We have studied the effect of disorder in random well SL's with corresponding regulars that belong to two representative cases: (i) the simplest tuned with $c_\varphi=1$ and (ii) a detuned SL with $c_\varphi=0.63$. In the following, we refer to the φ ranges: 0 to π and π to 2π as the first and second zone, respectively. The tuned SL with $c_\varphi=1$ has the simplest gap structure with one gap centered in each zone. This holds for higher-order zones also. On the contrary, the detuned SL does not have the same gap structure in each zone. A periodicity in this φ space may appear for much larger φ's if the ratio c_φ is a rational number. For disordered SL's, the dependence of $l(\varphi)$ from the proximity of gaps can be illustrated very well in the first two zones. We restrict the presentation of results within this range.

Figure 2 shows the computed l in the first zone for three random-well SL's with standard deviations: $\sigma_w=1/60$, $\sigma_w=2/60$, and $\sigma_w=10/60$. The average SL period is tuned with $c_\varphi=1$. The dashed curve is the plot of l values calculated for the corresponding regular SL. The photonic gap has very sharp edges. Outside the gap l is infinite. For the random SL's, l follows a regular pattern despite fluctuations. The strongest localization appears in the gap and its immediate vicinity with the formation of tails on the gap edges. Inside the gap, disorder induces a small increase of l. Between gaps, very small disorder induces relatively strong localization. l appears to reach a plateau (for $\sigma_w=1/60$ and $\sigma_w=2/60$), interrupted by a singularity at $\varphi=\pi$. The existence of this plateau is discussed below, along with the presentation of the results obtained for the detuned SL's.

At the boundary between zones, where φ is an integer multiple of π, l goes to infinity. This is a photon energy at which light propagates freely in a random-well superlattice of any number of layers. The explanation of this singularity is very simple: When the barrier layer thickness is constant and the phase shift inside it is equal to an integer multiple of π, the barrier layer phase matrices become unit matrices times ±1. Consequently, in the layer matrix product, that is, the system transfer matrix, two consecutive well layer phase matrices are separated by a unit phase matrix and two refraction matrices which are inverse to each other. The result is that their product is equivalent to the phase matrix of one well layer having thickness equal to the sum of the two-well-layer thicknesses. One can then consider the medium as consisting entirely of well material. A ±1 factor for the whole is of no importance to the determination of the electric-field amplitude. For convenience, in the following, we refer to the singularity at $\varphi=k\pi$, where k is an integer, as an *antigap*. An interesting observation is that the width of the antigap broadens significantly with increasing disorder.

As mentioned above, it is expected that l does depend on the particular sequence used in the calculation. This is especially true if the number of layers entering a calculation is necessarily limited, as is the case when l has a value of the order of 10. We have plotted in Fig. 3 l

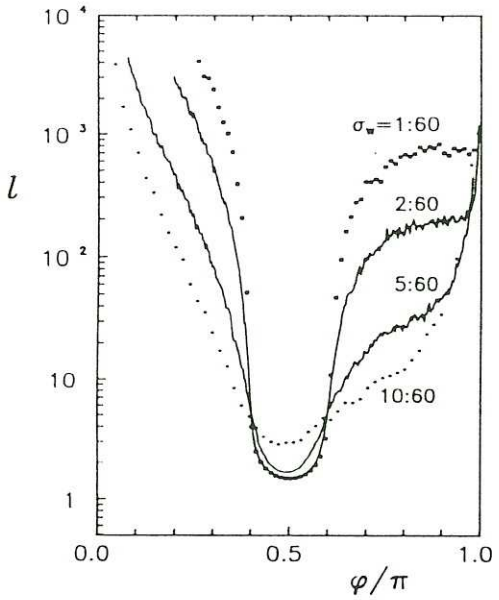

FIG. 3. Average localization length l in the first zone. Each data point is obtained by averaging over 20 different random-well SL's all having the same σ_w. Other parameters are identical to those of Fig. 2. The normalized standard deviation σ_w of the well layer thickness is shown with each curve.

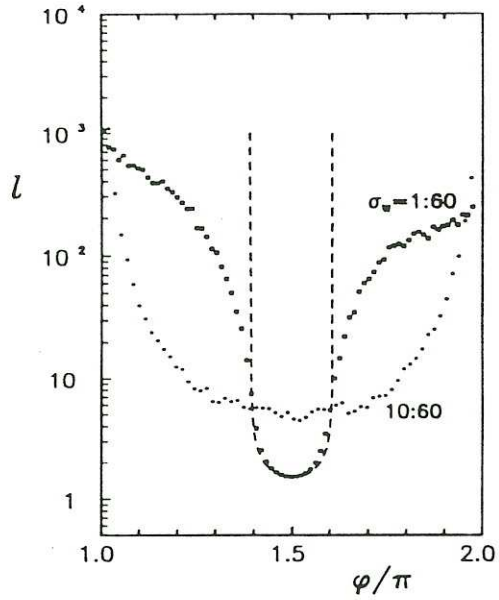

FIG. 4. Average localization length l, over 20 different sequences, in the second zone for two values of σ_w. All other parameters are identical to those of Figs. 2 and 3. The dashed line shows $l(\varphi)$ for the corresponding regular SL.

values that are the average of those computed for 20 different random sequences with all other conditions identical. In comparing the curves of Fig. 3 to those of Fig. 2, one observes much lower fluctuations in the average l plots. On the other hand, all the general features of $l(\varphi)$ are the same for a single random sequence and for the average curves.

IV. DISORDER AND PHASE SHIFTS OF THE WAVE INSIDE THE LAYERS

The behavior of l in the second zone, as can be seen in Fig. 4, is qualitatively similar to that in the first one. The effect of a given randomness is stronger. This is expected if one considers that the important parameter is not σ_w but $\sigma_{\varphi w}$, the standard deviation of phase shifts φ_w. One expects an increasing effect as a wider range of *well layer phases* enters the calculation, either by increasing σ_w or by increasing φ_w. Indeed, the curve for $\sigma_w=2/60$ of Fig. 3 in the upper half of the first zone is almost identical to that for $\sigma_w=1/60$ in Fig. 4 in the upper half of the second zone. In this respect, for a given σ_w, there should be a saturation in the localization effect at photon energies large enough to give $\sigma_{\varphi w}$ of the order of π.

There is a more general relationship between l computed in different zones with different standard-thickness deviations. The following derivation is valid even when both layers have thickness varying randomly. It assumes that c_n is constant. Let us separate the phase shift, e.g., inside a barrier layer m, into two parts:

$$\varphi_m=\langle\varphi_m\rangle+\Delta\varphi_m\ , \tag{11a}$$

with mth barrier layer thickness

$$d_m=\langle d_m\rangle+\Delta d_m\ . \tag{11b}$$

We observe that phase matrices remain invariant or are multiplied by -1 (which has no effect on l) if we change the average barrier phase by an integer multiple of π, without affecting the $\Delta\varphi_m$'s. It can be easily verified that the localization length computed for a given SL for $\langle\varphi_m\rangle$ is identical to that computed for $\langle\varphi'_m\rangle=\langle\varphi_m\rangle+k\pi$ in another SL whose barrier layers have thickness deviations $\Delta d'_m$ given by

$$\Delta d'_m=\begin{bmatrix}\dfrac{\langle\varphi_m\rangle/\pi}{\langle\varphi_m\rangle/\pi+k} & \dfrac{\langle d'_m\rangle}{\langle d_m\rangle}\end{bmatrix}\Delta d_m\ ,$$

hence,

$$\delta d'=\begin{bmatrix}\dfrac{\langle\varphi_m\rangle/\pi}{\langle\varphi_m\rangle/\pi+k} & \dfrac{\langle d'_m\rangle}{\langle d_m\rangle}\end{bmatrix}\delta d\ , \tag{13}$$

where δd's are the standard deviations of Δd_m's. Identical relations hold for the well layers.

Since, as we have pointed out above, the general behavior of l does not depend on the particular sequence, we expect it to depend only on the distribution parameters. In conclusion, using the set of dimensionless variables define by relations (5)–(10), we expect l to be invariant under the transformations

$$\varphi'=\varphi+k\pi\ , \tag{14}$$

$$\sigma'_b=A\sigma_b\ , \tag{15a}$$

$$\sigma'_w=A\sigma_w\ , \tag{15b}$$

where

$$A=\frac{\varphi/\pi(c_n+c_\varphi)}{(\varphi/\pi+k)(c_n+c'_\varphi)} \tag{16}$$

and

$$c'_\varphi=\frac{\varphi/\pi}{\varphi/\pi+k}c_\varphi+\frac{\mu}{\varphi/\pi+k}\,, \tag{17}$$

k,μ are integers.

As we have pointed out above, the curve for $\sigma_w=2/60$ (Fig. 3) at the end of the first zone and the curve for $\sigma_w=1/60$ (Fig. 4) at the end of the second zone are similar. This is one example of l invariance under the above transformations with $c_\varphi=c'_\varphi=1$ and $\mu=k=1$.

In the case of all random SL's with tuned regular, we have obtained results that are similar to those presented in Figs. 3 and 4 with the exception of the antigap singularities at $\varphi=\pi,2\pi$. When σ_b is low, one can still observe small peaks that are the remnants of the antigaps of the *random-well* case. These peaks disappear with increasing σ_b. If disorder is strong, the variation of l with energy shows two distinct regimes: the low-frequency end, characterized by a rapid decrease of l with increasing $h\nu$, followed, at higher frequencies by a region where $l(\varphi)$ depends on the underlying gap structure of the corresponding regular SL but remains close to 10 SL periods. This value is very close to those found for large disorder, for two different random SL models, by Sheng.[7]

Figure 5 shows the results obtained for detuned SL's. One can observe a qualitative difference in the behavior of l when comparing the curve for the random SL in Fig. 5 to those with $\sigma_w=1/60$ in Figs. 3 and 4. The disorder parameter is almost identical, but the clear plateau and the very narrow antigap of the tuned case are absent. l values in the vicinity of $\varphi=\pi$ are much higher for $c_\varphi=0.63$ (Fig. 5) than for $c_\varphi=1$ (Figs. 3 and 4). At first sight, one is surprised by the difference in the behavior of

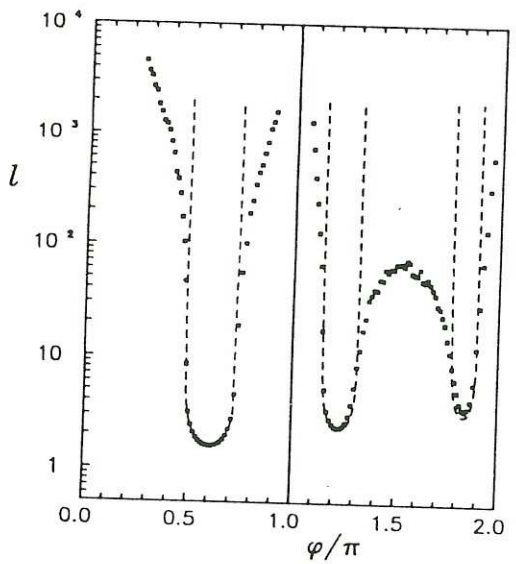

FIG. 5. Average l, over 20 sequences, vs average barrier layer phase shift φ in the first two zones, for random-well SL's with detuned equivalent regular. $\sigma_w=0.019$, $c_\varphi=0.63$, $c_n=2$. The dashed line is the plot of $l(\varphi)$ for the regular SL.

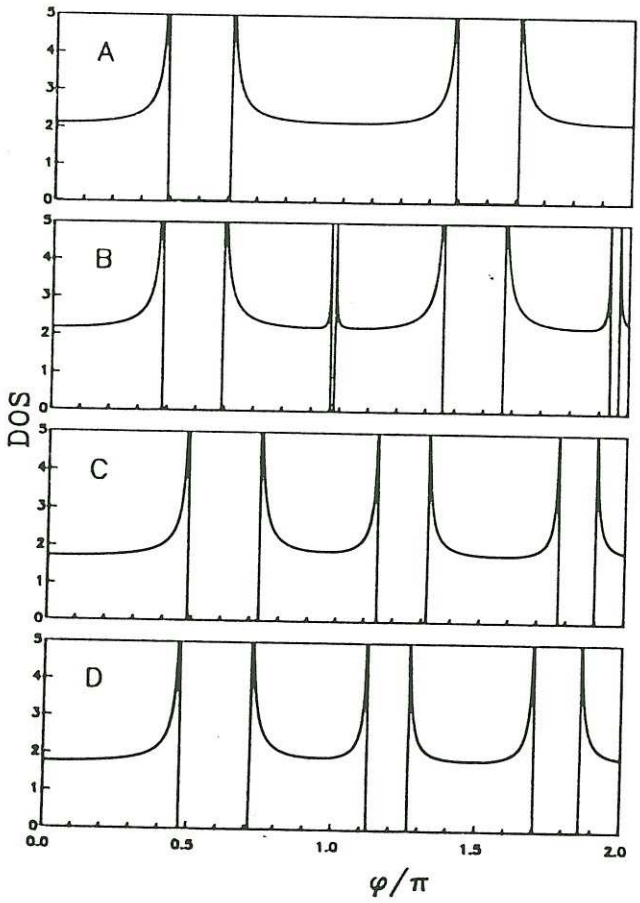

FIG. 6. Density of states, per SL period, of tuned and detuned regular superlattices vs phase shift φ of the wave inside the barrier layer. In all graphs $c_n=2$. *A*, $c_\varphi=1$; *B*, $c_\varphi=1.05$; *C*, $c_\varphi=0.63$; and *D*, $c_\varphi=0.68$.

l between two consecutive gaps in these two cases. There is, nevertheless, a fundamental difference in the gap structure of the two corresponding regular SL's in the first two zones. This difference is illustrated in Fig. 6, with graphs of the density of states[13] versus φ for regular SL's with $c_\varphi=1$, graph *A*, and $c_\varphi=1.05$, graph *B*.

We observe that the small deviation from $c_\varphi=1$ creates a third narrow photonic gap just below $\varphi=\pi$ (and $\varphi=2\pi$). A similar gap above $\varphi=\pi$ appears for c_φ slightly lower than 1. Disorder creates a random detuning around $c_\varphi=1$ that is responsible for the plateau close to $\varphi=\pi$ in Fig. 3. On the contrary, small deviations from $c_\varphi=0.63$ do not result in the creation of any gap around $\varphi=\pi$, as one can see by comparing graphs *C* and *D* of Fig. 6. The energy dependence of l close to $\varphi=\pi$ for $c_\varphi=0.63$ (Fig. 5), reflects only the creation of tails on the edges of the gaps.

V. THE ROLE OF ABSORPTION

The formalism and computational method we have used are not restricted to real refractive indices. The combined effect of disorder and absorption can be readily investigated without simplifying assumptions. We have

performed a series of calculations with a nonzero imaginary part for n_w covering many phases of φ outside the gaps of the corresponding regular. The imaginary part of n_w, in each case, was chosen in such a way that the decay length inside the corresponding regular in the presence of absorption (the inelastic l without disorder: $l_{0,i}$), was not very different from l, the decay length of the random SL in the absence of absorption. The inelastic decay constant l_i in the random SL, as well as $l_{0,i}$, was computed in exactly the same manner as previously described for l. In order to test the interdependence of disorder and absorption, we have computed in each case a localization length l_c using the formula

$$\frac{1}{l_c}=\frac{1}{l_i}-\frac{1}{l_{0,i}} , \tag{18}$$

which, applied to l's that are of the same order of magnitude, should yield a value close to the localization length, if disorder and absorption are independent.

We have considered the random well case with $\sigma_w=1/60$ and $\sigma_w=10/60$. The values of decay constants were obtained by averaging over 20 SL's differing only in the random-thickness sequence used. Several values of φ in the first zone were tested. The relative difference $|l-l_c|/l$ we have found in all cases was less than 15% and, more often, lower than 5%.

VI. CONCLUSIONS

A series of numerical calculations of the localization length l in various, random-thickness, multilayer structures with two types of layers has been performed. The picture emerging from these calculations, when disorder is weak, is that the variation of the localization length with photon energy closely relates to the gap structure of the corresponding regular superlattices. A finite localization length is found at all nonzero photon energies, with the exception of multilayers having rigorously constant thickness for one type of layer and random for the other. There are frequencies, then, at which the wave propagates freely no matter how strong the thickness fluctuations are. The trends in the frequency dependence of l we have found for large disorder are in good qualitative agreement with previous studies of randomly layered systems with different types of disorder. Finally, it was shown that absorption and disorder have independent effects on wave attenuation in the structures studied.

ACKNOWLEDGMENT

The authors are grateful to Professor E. N. Economou for valuable discussions throughout the progress of the work presented here.

[1]E. Sendler and D. G. Steel, J. Opt. Am. B **5**, 1636 (1988).
[2]M. P. van Albada, M. B. van der Mark, and A. Lagendijk, Phys. Rev. Lett. **58**, 361 (1987).
[3]M. M. Sigalas and E. N. Economou (unpublished).
[4]E. N. Economou and C. M. Soukoulis, Phys. Rev. B **40**, 7977 (1989).
[5]K. M. Ho, C. T. Chan, and C. M. Soukoulis, Phys. Rev. Lett. **65**, 3152 (1990).
[6]J. Igarashi, J. Phys. Soc. Jpn. **57**, 3391 (1988).
[7]*Scattering and Localization of Classical Waves in Random Media*, edited by P. Sheng (World Scientific, Singapore, 1990).
[8]A. Kondilis and P. Tzanetakis, Philos. Mag. Lett. **62**, 299 (1990).
[9]S. Nitta, T. Itoh, S. Nonomura, H. Ohta, and K. Morigaki, Philos. Mag. B **60**, 119 (1989).
[10]T. Itoh, S. Nitta, and S. Nonomura, J. Non-Cryst. Solids **114**, 723 (1989).
[11]S. Nitta, S. Takeuchi, K. Ogawa, T. Furukawa, T. Itoh, and S. Nonomura, J. Non-Cryst. Solids **137&138**, 1095 (1991).
[12]Z. Knittl, *Optics of Thin Films* (Wiley, New York, 1976).
[13]The density of states is calculated using Bloch's theorem, in a way analogous to that of the one-dimensional electronic case of the Kronig-Penney model.

Chapter 3

LIGHT PROPAGATION AND LOCALIZATION IN DISORDERED BINARY MULTILAYER FILMS : AN APPROXIMATE ANALYTICAL SOLUTION

ABSTRACT

An approximate calculation method for light propagation in random multilayer films is presented. It is applied to a particular structure consisting of alternating lower and higher refractive index materials with one type of layer having random thickness. An analytical expression for the localization length is derived. It is found to be in excellent agreement, over a very broad wavelength range, with numerical calculations performed using the transfer matrix formalism without any simplifying assumptions. Furthermore, this approximation accounts very well for anomalous reflectance effects that have been reported in experimental studies of amorphous silicon/silicon nitride multilayer films with random thickness layers. Within the approximation presented, one can identify separate terms responsible for localization and for anomalous reflectance. This separation is helpful in clarifying the origin of both effects.

3.1 Introduction

Interesting and potentially useful effects are observed in the reflectance spectra of random thickness, binary multilayer (ML) films. Nitta et al[1] have fabricated structures of this type using hydrogenated amorphous silicon (a-Si:H) and silicon nitride (a-Si_xN_{1-x} :H) layers. The thickness of a-Si_xN_{1-x}:H layers, referred to as barrier layers, was kept constant at $40\mathring{A}$. The a-Si:H, the well layers, had variable thickness chosen randomly from a Gaussian distribution around $20\mathring{A}$. In this case, the disorder parameter is the standard deviation of the thickness distribution. By reducing the standard deviation to zero, one obtains the corresponding periodic multilayer whose reflectance spectrum is similar to that of a conventional single layer film, in the wavelength region of the experimental spectra. This is not true for the random thickness MLs. Their reflectance spectra, when compared to those of the corresponding periodic, show a distortion of the fringe pattern and a broad peak in the transition region between low and high absorption. Using classical wave propagation theory and the transfer matrix (TM) method, we have obtained, in a previous publication[2] , computed spectra that show all the effects observed experimentally. The same numerical method has been applied to the study of light localization in random binary multilayers we have performed[3] , covering a very broad wavelength range, including optical gaps of the corresponding periodic structures.

The purpose of this paper is to present an approximate analytical approach we have developed in dealing with light propagation in this type of MLs. The approximate analytical formula derived gives surprisingly good results for the localization length l, when compared to the TM numerical calculations[3] . The transfer matrix calculations contain no simplifying assumptions and can be considered as the "exact" solution of wave propagation in the system we study.

In a recent publication, Nitta et al[4] suggested that the effects they have observed

in the reflectance spectra are related to disorder induced light localization. We discuss this point in the light of the approximation we have mentioned above, based on the fact that it accounts for these effects as well as the TM calculation does. This approximation allows for a qualitative separation of disorder induced anomalous reflectance from the light localization effect. In this paper, the term *localization* is used to denote an exponential attenuation of wave amplitude, versus distance from the entrance surface, that is not due to absorption of wave energy by the medium.

3.2 Spatial dependence of wave amplitude inside the multilayer

We consider a system similar to the one studied experimentally[1] . It is composed of cells of two layers: barrier and well, the former having fixed thickness and the latter having randomly chosen thickness. We define $E_{0,j}(N)$ as the ratio of the electric field amplitude at the end of cell N, in a given ML labeled by the index j, to that at the exit surface. Numbering of cells starts from the exit surface, i.e. the interface between the substrate and the ML. We assume normal incidence of light and a semi-infinite substrate. We calculate $ln(E_{0,j}(N))$ for a large ensemble of different random sequences ($j = 1, 2, ...10000$) with the same number of cells N. We use the transfer matrix formalism[2] and a representative set of layer parameters. The probability distribution of $ln(E_{0,j})$ is plotted in Fig.1, in the form of histograms, for three values of N: 100,500 and 1000. Large deviations of $ln(E_{0,j}(N))$ from their ensemble average are observed. The solid lines correspond to Gaussian distribution functions of the form:

$$P_N(lnE_0) = \frac{1}{\sqrt{2\pi}\,\sigma}\, exp\left[-\left(\frac{lnE_0 - < lnE_0 >}{\sqrt{2}\,\sigma}\right)^2\right] \qquad (3.1)$$

where $< lnE_0 >$ is the ensemble average and σ the standard deviation of the computed data for N cells.

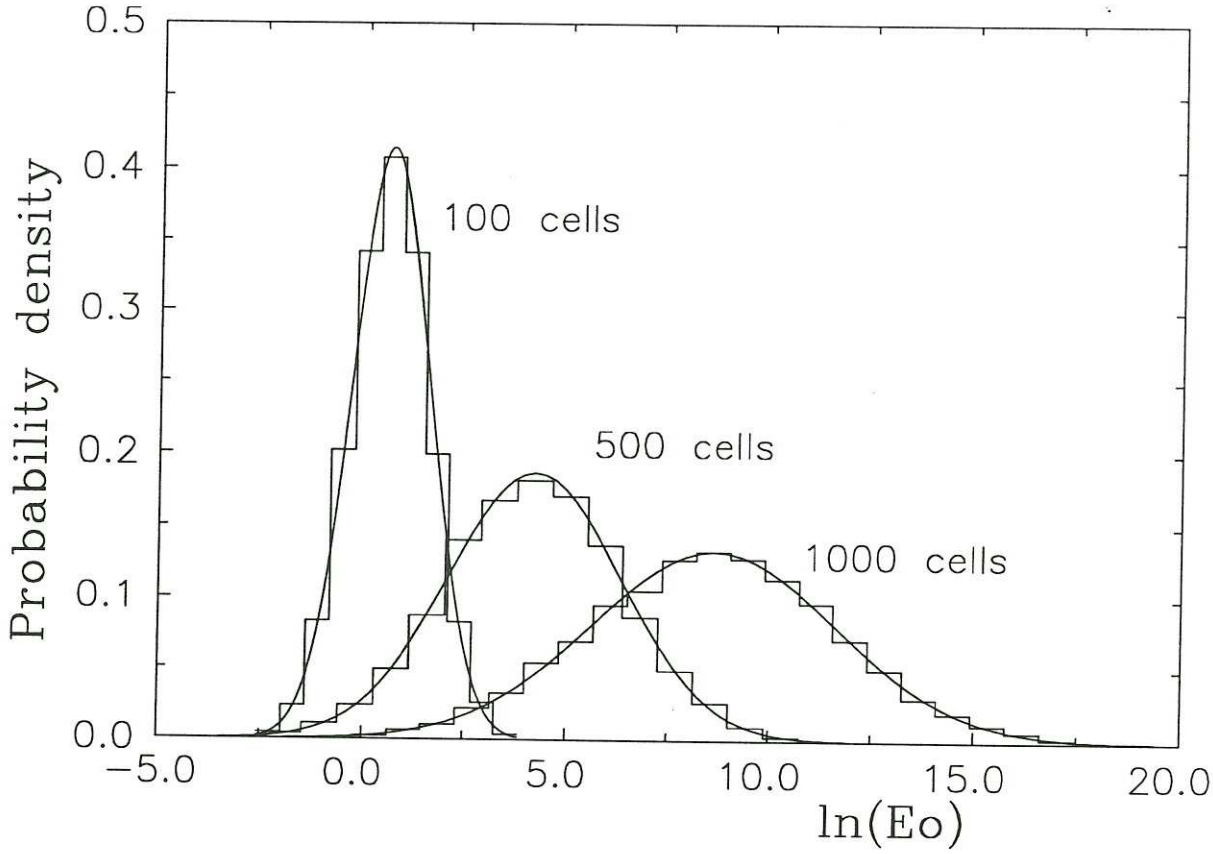

FIG.1. *Probability density functions of $ln(E_0)$ for ML's of 100,500 and 1000 cells. Solid lines are Gaussian distribution functions fitted to the data points. A set of 10000 random sequences is used in each case. E_0 is computed by the transfer matrix method. The optical path in the barrier layer is equal to that in the average thickness well layer. The random thickness of the well layers obeys a Gaussian distribution. The standard deviation σ_w of the well layer thickness is expressed in units of average cell thickness is taken equal to 10/60. $c_n = 2$ and $\phi = 0.2\pi$ (see text for symbols).*

It is evident that $lnE_{0,j}$ values for a given number of cells do follow very well a Gaussian distribution. The symmetry of the distribution guarantees that the average

value is equal to the most probable one. We find in all numerical calculations that the normalized standard deviation σ_r varies with $< lnE_0 >$ according to :

$$\sigma_r = \frac{\sigma}{< lnE_0 >} = \frac{1}{\sqrt{< lnE_0 >}} \tag{3.2}$$

This relation is also derived analytically within the approximation presented in section 3.3. As $< lnE_0 >$ increases, either by increasing N or by approaching a photonic gap of the corresponding periodic multilayer, σ_r decreases. On the other hand large relative deviations, σ_r , are expected for small $< lnE_0 >$.

The abscissa of the distribution peak increases linearly with the number of cells N, which is essentially the distance travelled by the wave divided by the average cell thickness. This is the localization effect. Based on the numerical results presented above we define, following a common practice in localization theory, a localization length l for this system through the relation:

$$l^{-1} = \frac{< lnE_0(N) >}{N} \tag{3.3}$$

where l is expressed in units of average cell thickness.

Relations (3.2) and (3.3) imply that l can be determined, with reasonable accuracy from a single multilayer, only when the ratio E_0 is several orders of magnitude[3]. When E_0 is small, i.e. when N is not much larger than l, ensemble averaging over several random sequences must be used in order to find the localization length.

We calculate by the TM method $< ln(E_0) >$ as a function of N using the same layer parameter set as for the curves of Fig.1. The results are shown in Fig.2.

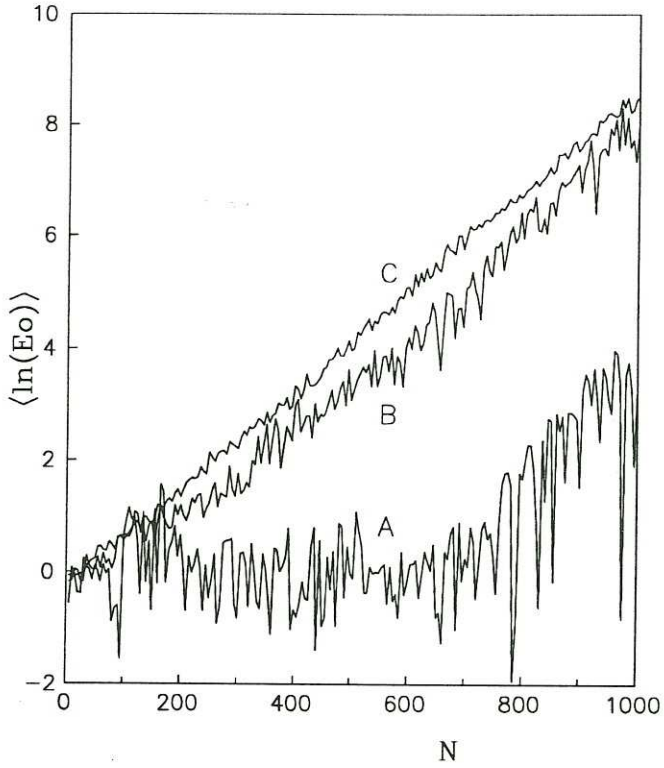

FIG.2. *Ensemble average of* $ln(E_0)$ *plotted vs the number of cells N. Curve A corresponds to 1 random sequence. Curves B and C correspond to ensembles of 10 and 100 sequences, respectively. All other parameters are identical to those of Fig.1.*

Curve A is the plot of $lnE_0(N)$ for only one random sequence. Curves B and C correspond to averages over ensembles of 10 and 100 random sequences, respectively. Curve C can be fitted very well by a straight line. The inverse of its slope is the localization length. The value of l is 113 cells. Despite the fact that the number of cells in the single multilayer of curve A is 1000, one order of magnitude larger than l, it is evident that no straight line can be fitted to it. On the other hand averaging over 10 sequences (curve B) is enough to yield l with reasonable accuracy even when the total thickness of the ML is of the order of l.

In the numerical calculations presented in ref.[3], a single multilayer for each l data point was used. A large lnE_0 is then necessary and no restriction was placed to N

until a ratio E_0 of 10^8 is reached. Significant fluctuations of l versus wavelength were found and averaging of l's at each wavelength, for several different sequences, is used in order to obtain a smoother curve. The definition of l (3.3) we use in the present paper gives an alternative and easier way to calculate its value in all cases. As far as we have checked, we have found no meaningful difference between the localization lengths computed by these methods. We shall, therefore, use the results of ref.[3] in order to to check the validity of the analytical formula for l, derived in the following.

3.3 Approximate analytical expression for the wavelenght dependence of the localization lenght. Comparison with exact numerical calculations

In the study of light propagation in layered media, a simple approximation is often used and is referred to as Vector Approximation (VA)[5]. In the VA, the reflection coefficient for a ML with N layers, deposited on a semi-infinite substrate is given by:

$$r_V = \sum_{j=1}^{N+1} r_j \, exp(-2i \sum_{k=1}^{j} \Phi_{k-1}) \tag{3.4}$$

with $\Phi_0 = 0$.

r_j is the Fresnel reflection coefficient at the boundary j and Φ_k is the phase shift inside layer k. Indexing in (3.4) starts from the free surface of the ML.

The expansion of the exact formula for the reflection coefficient[5] in a series of Fresnel Reflection Coefficients (FRC's) takes the general form:

$$r = O_1(r_j) + O_3(r_j r_k r_m) + ... \tag{3.5}$$

The term $O_1(r_j)$ is equal to the VA of r, a sum of first order terms with respect to FRC's. $O_3(r_j r_k r_m)$ stands for a sum of third order terms. Noticing that no terms with products of even number of FRC's appear in (3.5), we conclude that the VA has the validity of second order approximation. If $|r|^2$ is lower than approximately .3, one can neglect O_3 and higher order terms without significant error. In order to compute the localization length l, we consider the spatial evolution of wave amplitude inside the ML. In the absence of absorption, the time-averaged Poynting vector is conserved throughout the medium. Therefore:

$$E_0(N) = \sqrt{\frac{n_s}{n_b}} \frac{|1+r_N|}{\sqrt{1-|r_N|^2}} \quad , \tag{3.6}$$

where n_s is the substrate index, n_b is the barrier layer index and r_N is the reflection coefficient of part of the actual ML comprising cells up to N included, assuming that the next (barrier) layer extends to infinity. The subscript j of E_0 , introduced in the previous paragraph to label a particular ML, is omitted for simplicity.

Our numerical results indicate that the linear dependence of $< lnE_0 >$ on N, holds at small N, lower than the localization length. An example is illustrated by curve C of Fig.2. At these values of N, at wavelengths outside the gap region, it is expected that $|r_N|$ is sufficiently small to satisfy the condition of validity of the VA. Based on these considerations, one is tempted to calculate $< lnE_0 >$ in the framework of the vector approximation , expecting that the latter accounds for a significant part of the overall linear dependence of $< lnE_0 >$ on N. We expand lnE_0 in a series in r_N and we keep up to second order terms :

$$lnE_0(N) = \frac{1}{2} ln\frac{n_s}{n_b} + Re(r_N) + \frac{1}{2}(|r_N|^2 - Re(r_N^2)) \tag{3.7}$$

Since, as we mentioned above, only odd type terms appear in relation (3.5), we can use the VA of r_N in relation (3.7) without losing the validity of second order approximation with respect to FRC's. With the assumption of statistical independence of the well layer thicknesses, we take the ensemble average of $lnE_0(N)$. Using (3.3), and neglecting all terms decaying with N, we find :

$$l = \frac{|l-X|^2}{2\,r_0^2\,sin^2\phi(\,1-|X|^2\,)} \tag{3.8}$$

where

$$X = exp(-2i\phi) < exp(-2i\phi_{w,j}) > . \tag{3.9}$$

r_0 is the FRC at a barrier/well interface and is given by

$$r_0 = \frac{1 - c_n}{1 + c_n} \tag{3.10}$$

c_n is the ratio of the refractive index of barrier layers to that of the well layers. The quantity ϕ is the phase shift inside any barrier layer and $\phi_{w,j}$ is the phase shift inside well layer j. The derivation of (3.8) is tedious but straightforward. It can be seen that only the term $|r_N|^2$ of (3.7) contributes to the localization length l . It is also easy to derive relation (3.2) within the vector approximation. Assuming a Gaussian distribution of well layer thicknesses in (3.9), we obtain:

$$l = \frac{1 + exp(-4\sigma_{\phi w}^2) - 2exp(-2\sigma_{\phi w}^2)cos2\phi_c}{(2r_0^2 sin^2\phi)\,(1 - exp(-4\sigma_{\phi w}^2))} \tag{3.11}$$

$$\phi_c = \phi + < \phi_{w,j} >$$

$\sigma_{\phi w}$ is the standard deviation of the distribution of well layer phase shifts.

Relation (3.8) is not limited to normal incidence. It can be directly applied to oblique incidence as well, provided that the FRC's, phases and σ_ϕ's are taken properly for the non-zero angle of incidence and for the polarization state. At the Brewster angle r_0 becomes zero for p-polarized light, resulting in infinite l according to (3.8) at that angle. This effect is known and is discussed in ref.[6] .

Let us now compare the values of l given by (3.11) with the results of the TM numerical calculation[3] . A typical example is illustrated in Fig.3.

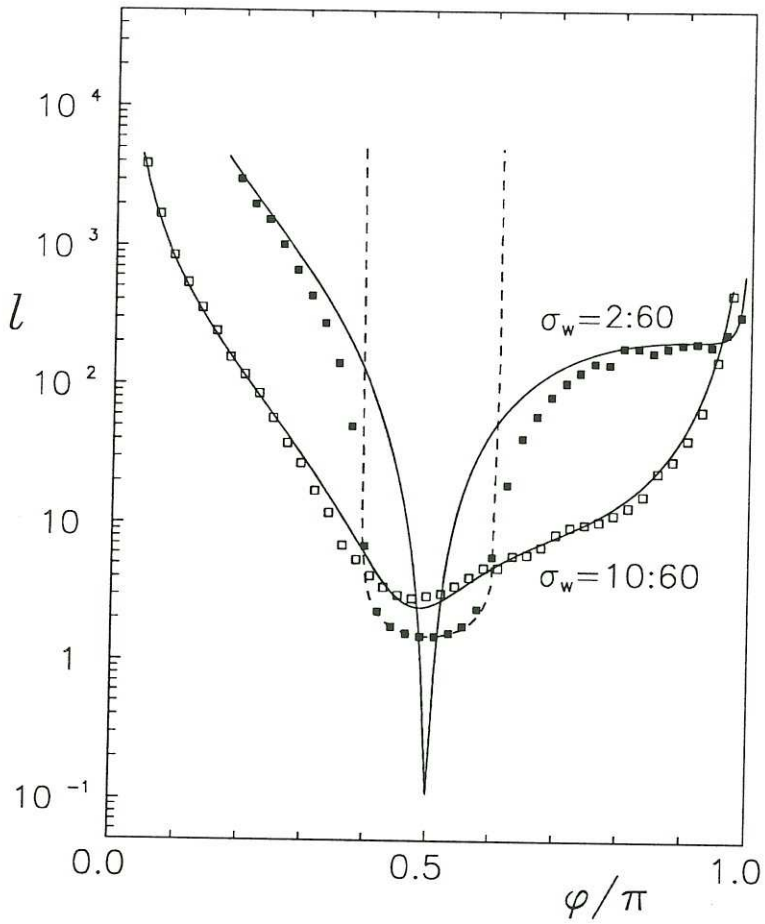

FIG.3. *Localization length l in units of average cell thickness, plotted as a function of the phase shift inside a barrier layer. Squares correspond to exact numerical calculations and solid lines to the results of expression (3.11). The optical path in the barrier layers is equal to that in the average thickness well layer. The corresponding* σ_w*'s are shown with each curve.* $c_n = 2$.

The corresponding periodic ML belongs to the so called tuned type. A tuned ML is one for which the ratio of optical paths in the two types of layers is a small integer. We have considered the simplest case with equal optical paths. This ML has photonic gaps centered at $\phi = \pi/2 + m\pi$ (m : integer). The dashed line shows the extinction

length of the periodic ML. The extinction length is infinite outside the gap region that extends from $\phi = 0.4\pi$ to 0.6π approximately. We obtain surprisingly good results. Except for the region of the gap, the agreement is excellent for both weak and strong disorder. In the latter case relation (3.11) accounts very well for the complex variation of l over the entire phase range. It is important to note that there are no adjustable parameters in (3.11). We have chosen to present this example because of the complexity of features involved. The poor agreement of (3.11) with the numerical results in the gap, when disorder is weak, has a simple explanation. With little disorder, l inside the gap must be similar to that of the periodic structure. It is well known that the photonic gap of a periodic ML is determined by *multiple* reflections while the vector approximation, used to derive (3.11), takes into account only single reflections. The comparison of results obtained for strong and weak disorder indicates that the contribution to the localization length of terms neglected by the VA diminishes with increasing disorder.

A peculiar behavior of l versus ϕ close to π is manifested by the creation of an antigap. When ϕ is precisely π , the wave amplitude does not change upon crossing a barrier layer. We can then think of the ML as consisting entirely of well material. As a consequence, l is infinite at $\phi = \pi$ no matter how strong the disorder of the well layer thickness is. This effect and the behavior of l in the vicinity of $\phi = \pi$ are discussed in detail in ref.[3]. An interesting observation is that inside a small ϕ range, close to π , l increases with increasing disorder. This effect is due to a disorder induced broadening of the antigap.

3.4 Approximate calculation of reflectance spectra

Let us try now to calculate reflectance spectra in the vector approximation and compare the results with the TM numerical calculations of reflectance[2] for MLs similar to those studied experimentally[1] . As mentioned above, VA is a good approximation if $|r|^2$ is lower than approximately .3. This condition does not necessarily hold for the multilayer we consider because of the high FRC at the free surface. In order to avoid this problem, we separate the contribution of the free surface as follows. We start with the exact formula for the reflection coefficient:

$$r = \frac{r_1 + r' exp(-2i\phi_1)}{1 + r_1 r' exp(-2i\phi_1)} \tag{3.12}$$

where r_1 stands for the FRC at the free surface, ϕ_1 is the phase shift inside the first layer and r' is the reflection coefficient of a virtual ML formed from the original one by extending to infinity its first layer. Indexing in (3.12) starts from the free surface. Since $|r'|^2$ satisfies the condition of applicability of VA mentioned above, we use the VA of r' in (3.12) and we calculate the reflectance R through:

$$R = |r|^2 \ . \tag{3.13}$$

In accordance to the experimental study[1] , we take the first and last layers to be of barrier type. We assume normal incidence and a semi-infinite substrate. The reflectance spectrum of graph I of Fig.4 is the result of TM calculation for a given ML. Graph II of Fig.4 shows the same spectrum in the VA calculation. The two curves are almost identical. All characteristic features associated with thickness randomness are reproduced with great accuracy. Based on the success of VA in interpreting the disorder induced anomalous reflectance effects,

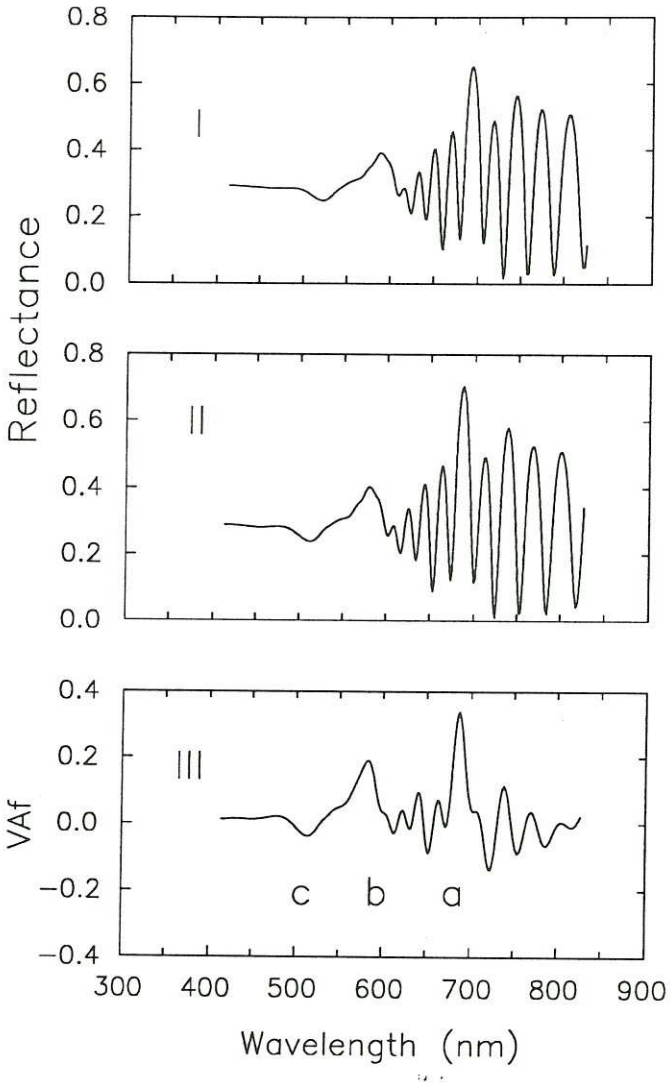

FIG.4. *Reflectance spectra and vector approximation function vs wavelength of light for a random-well thickness ML consisting of 400 well layers alternating with 401 barrier ones. Graph I shows reflectance in the exact numerical calculation. The reflectance spectrum in the vector approximation is shown in graph II. In graph III the vector approximation function is plotted vs. wavelength. All barrier layers have the same thickness (40*$\circ$*A). Well layer thicknesses have been randomly chosen from a Gaussian distribution centered at 20* $\circ$*A and having 10*$\circ$*A standard deviation. The complex refractive indices for the two types of layers are given in reference [2]. These functions are very close to the actual ones of the a-Si:H , a-*$Si_{1-x}Nx$ *:H films studied experimentally*[1] .

we proceed in an attempt to extract from this approximation the main term responsible for these effects. In the wavelength region of interest, the imaginary part of the barrier refractive index can be neglected in comparison to the much larger real part. One can then obtain, keeping only the first order terms with respect to the FRC's of the virtual ML in the expansion of (3.13), the following approximate formula for the reflectivity:

$$R = \left[\frac{(1-n_b)^2}{(1+n_b)^2} + \frac{8n_b(1-n_b)(n_b-n_s)}{(1+n_b)^3(n_b+n_s)} Re(exp(-2i < k > L)) \right] +$$

$$+ \frac{8n_b(n_b-1)}{(1+n_b)^3} r_{V0} \qquad (3.14)$$

where

$$r_{V0} = -Re\left(r_V \, exp(-2i\, k_0\, n_b\, d_b) \right) \qquad (3.15)$$

L is the total thickness of the ML and $< k >$ is the average wavevector defined by:

$$< k >= \frac{k_0}{L} \int_0^L n(\xi) d\xi \qquad (3.16)$$

k_0 is the vacuum wavevector of light and $n(\xi)$ is the refractive index.

It is easy to verify that r_V is the VA of the reflection coefficient of a virtual ML formed from the original one by extending to infinity its first and last layers, both of barrier type.

As can be seen in relation (3.14), randomness does not affect the term in brackets. It has only an effect on r_{V0} through r_V. We call r_{V0} *vector approximation function* (VAF). Its variation with wavelength is shown in graph III of Fig.4 for the same ML used for the computations of the other graphs in Fig.4. All randomness induced effects observed in the entire wavelength region studied, are accounted for by the vector approximation function. These include peaks a and b as well as the minimum c.

It is important to notice that the disorder induced effects on the reflectance spectra can be well accounted for by keeping only the first order terms with respect to the FRC's. On the contrary it is easy to verify that first order terms give a null contribution to the localization length. This fact provides a clear qualitative separation between the anomalous reflectance effects and localization. The link attempted by Nitta et al[4] between these two effects is by no means justified in our opinion.

REFERENCES

[1]. S. Nitta, T. Itoh, S. Nonomura, H. Ohta, and K. Morigaki, Phil. Mag.B60, 119 (1989)

[2]. A. Kondilis, and P. Tzanetakis, Phil. Mag. Lett.62, 299 (1990)

[3]. A. Kondilis, and P. Tzanetakis, Phys. Rev. B46(23), 15426 (1992)

[4]. S. Nitta, S. Takeuchi, K. Ogawa, T. Furukawa, T. Itoh, and S. Nonomura, J. Non-Cryst. Solids **137&138**, 1095 (1991)

[5]. Z. Knittl, Optics of thin films (Wiley, New York, 1976)

[6]. J. E. Sipe, P. Sheng, B. S. White, and M. H. Cohen, Phys.Rev.Lett.60, 108 (1986)